QCD and scattering amplitudes in the high-energy regime

Candidate number: [redacted]

University of Oxford

A dissertation submitted for the degree of

Master of Mathematical and Theoretical Physics

Trinity 2022

Aan papa, mama,
Mees, en Wybe.

Abstract

Perturbative calculations can be used to gain important insight into the all-order structures of QCD in special kinematic configurations. We consider elastic $2 \to 2$ scattering amplitudes in the high-energy 'Regge' limit. In this limit, perturbation theory naturally organises itself into a tower of large logarithms of the dimensionless variable $-t/s$, where t and s are the standard Mandelstam variables. From first principles, we re-derive the leading-logarithmic behaviour of these amplitudes in QCD. Using recent results, we verify that the Regge factorisation for elastic $2 \to 2$ scattering amplitudes works up next-to-leading logarithmic order, and extract the gluon Regge trajectory and impact factor up to two loops at higher orders in the dimensional regularisation parameter ϵ. We observe that at next-to-next-to-leading logarithmic order, Regge factorisation breaks down as a more complicated colour structure emerges. We proceed by developing a colour formalism to help disentangle this structure, and use it to extract the leading-colour contribution to the gluon Regge trajectory at three loops.

Contents

1 Introduction

Studying scattering amplitudes in Quantum Chromodynamics (QCD) is essential to describing the dynamics of high-energy collision events taking place at the Large Hadron Collider (LHC) at CERN. Determining these amplitudes to higher loop orders is important for making increasingly precise predictions for Standard Model (SM) processes, and helps with the search for New Physics beyond the SM. Very interestingly, these perturbative calculations can also be used to gain insight into all-order QCD structures that appear in special kinematic limits. One such example is the Regge limit, in which the centre-of-mass energy is assumed to be much greater than the typical momentum transfer [1]. In this limit, perturbation theory organises itself into a tower of large logarithms of the dimensionless variable $-t/s$, where s and t are the standard Mandelstam variables. More concretely, a scattering amplitude f can be written as

$$f \sim f_{\mathrm{LL}}(\alpha_s L) + \alpha_s f_{\mathrm{NLL}}(\alpha_s L) + \alpha_s^2 f_{\mathrm{NNLL}}(\alpha_s L) + \dots \tag{1.1}$$

where $L = \ln(-t/s)$ is the large logarithm and α_s is the strong coupling constant. The contributions in equation (1.1) are referred to as the leading logarithm (LL), next-to-leading logarithm (NLL), next-to-next-to-leading logarithm (NNLL), and so forth.

This dissertation has multiple goals. Firstly, to re-derive from first principles the LL behaviour of elastic scattering amplitudes in the Regge limit. To prepare for the more complicated case of QCD, we first see how the LL behaviour emerges in a simpler scalar field theory. This is done in section 2, following the treatment in [2]. We observe that the logarithms can be re-summed into an exponent. Next, we proceed to QCD in section 3. Here, the all-order resummation of the tower of logarithms can be interpreted as the exchange of a so-called *Reggeised gluon* or *Reggeon*.

Next, we set up the formalism of so-called *Regge poles* and *Regge cuts* in section 4. The single Reggeon exchange that we derived from first principles emerges due to a simple Regge pole. If one assumes that, under higher order corrections, we retain this Regge pole structure, it is possible to factorise the amplitude in a particular way. This is called *Regge factorisation*, and it can be shown to hold up to NLL [3]. We use recent results for gluon scattering in QCD [4] to verify that, indeed, Regge factorisation works up to 3 loops at NLL level. In the process, we derive the so-called *Regge trajectory* up to two loops, and verify its consistency.

It is known that Regge factorisation breaks down at NNLL as Regge cuts start to play a more prominent role, and a non-trivial colour structure emerges [5–8]. That is, the picture of a single Reggeon exchange can only be consistently interpreted up to NLL, and at NNLL we have a complicated interplay between contributions from multiple Regge poles which gives rise to Regge cuts. Interestingly, the Regge pole and

Regge cut contributions have different colour structures. We finish the dissertation by setting up a colour formalism that can be used to disentangle the contributions from the Regge poles and cuts. As a first application, we use this formalism to derive the leading-colour (LC) contribution to the gluon Regge trajectory at three loops, agreeing with recent results [4].

2 High-energy elastic scattering in a scalar field theory

We start by studying the Regge limit in a simpler scalar field theory [2]. This is useful because it will equip us with some of the machinery required to tackle the case of full QCD. The type of scattering we consider is (the toy-model analogue of) $qq \to qq$ scattering via the exchange of a colour singlet. That is, the initial quarks have different flavours, but emerge with the same colours in the final state. We consider the Regge limit $s/|t| \gg 1$, and keep only LL terms – these are corrections of the order $\mathcal{O}\left((g^2(\ln s))^n\right)$ with respect to the leading-order contribution. At LL order, we will see that the infinite sum of logarithms exponentiates into a power:

$$\mathcal{A} \propto s^{\alpha(t)}.$$

We will show that in this simple theory only certain classes of diagrams contribute – namely genuine, uncrossed ladder diagrams.

2.1 Introducing the model

We consider a model where the "quarks" are represented by a massless complex scalar field ϕ, and the "gluons" by a scalar field χ. To avoid infrared divergences, we give the gluons a mass m, but treat it as negligible compared to any other energy scale. The quarks are massless. To create an analogue of QCD, we need a triple gluon self-interaction proportional to the structure constant of the colour group. In a first naïve guess, we would assign one adjoint colour-index to the χ-fields, i.e.

$$-\frac{gm}{3!} f_{abc} \chi^a \chi^b \chi^c, \tag{2.1}$$

where f_{abc} are the structure constants of SU(N) and g is a dimensionless coupling. However, the (bosonic) χ-field is symmetric under exchange of two gluons, and the structure constant is completely antisymmetric. We are therefore forced to add an additional colour index – a complication not present in QCD. Thus our gluon fields carry two adjoint indices $\chi^{a,r}$ with $a, r = 1, \ldots, N^2 - 1$. The quark fields transform under two copies of the fundamental, i.e. $\phi_{i,l}$ with $i, l = 1, \ldots, N$. We arrive at the following Lagrangian:

$$\begin{aligned} \mathcal{L} = {} & \partial^\mu \bar{\phi}^{i,l} \partial_\mu \phi_{i,l} + \frac{1}{2} \partial^\mu \chi_{a,r} \partial_\mu \chi^{a,r} - \frac{m^2}{2} \chi_{a,r} \chi^{a,r} \\ & - gm \bar{\phi}^{i,l} (T^a)^j_i (T^r)^m_l \phi_{j,m} \chi_{a,r} - \frac{gm}{3!} f_{abc} f_{rst} \chi^{a,r} \chi^{b,s} \chi^{c,t}, \end{aligned} \tag{2.2}$$

where $(T^a)^j_i$ are the generators of SU(N) in the fundamental representation, as detailed in appendix B containing our colour algebra conventions. Note that we have not introduced an analogue of a quartic gluon self-interaction, since in QCD it will turn out that diagrams with these vertices are sub-leading in the LL approximation.

The Feynman rules for our scalar theory are listed in appendix A.1. Before we proceed with finding the leading-order contributions to our elastic $qq \to qq$ scattering, we begin with a discussion of general properties of the S-matrix. This will allow us to employ a powerful *dispersive* approach to calculating multi-loop amplitudes. For the scalar theory case, this is arguably overkill – however, it will prepare us for elastic scattering in full QCD.

2.2 Unitarity and analyticity of the S-matrix

In principle, for our simpler scalar theory, we could directly inspect the loop diagrams to extract the LL contributions and then re-sum them to all orders. However, to prepare for the more complicated case of QCD, we employ a more refined approach.

The logic is roughly as follows. We treat the S-matrix as an analytic function of Lorentz invariants (say, s and t) with only those singularities required by physical thresholds; this is known as the *Landau principle*. Of course, S-matrix elements are technically only defined for external particles with real momenta – however, we can get around this by instead defining the S-matrix by the Feynman rules of the theory, which allows for the analytic continuation of our Lorentz invariants. Unitarity of the S-matrix then allows us to relate the imaginary part of a scattering amplitudes to products of other amplitudes – this is the well-known *optical theorem*, that we review in appendix C for completeness. At the level of an individual Feynman diagram, this can be done through a set of Cutkosky *cutting rules*. Finally, full amplitude is reconstructed from the imaginary part through a *dispersion relation*. We will show how this can help extracting LL contributions in what follows.

2.2.1 Dispersion relations

We define the S-matrix by the Feynman rules, thus treating scattering amplitude $\mathcal{A}(s,t)$ as an analytic function of complex variables s and t. Consider for the moment the physical kinematic region $s > 0$ and $t, u < 0$. Let $s_{th} (= s_{th}^{+} > 0)$ be the threshold for the production of the lightest possible multi-particle intermediate state. It follows from the optical theorem that for $s < s_{th}$ along the $\mathrm{Re}(s)$ axis, the phase space of intermediate states vanishes, and thus $\mathrm{Im}\big(\mathcal{A}(s,t)\big) = 0$. Since the amplitude is real for some portion of the real s axis (i.e. the part below threshold), it satisfies the *Schwarz reflection-principle* throughout its domain of analyticity:

$$\mathcal{A}(s^*,t)^* = \mathcal{A}(s,t). \tag{2.3}$$

From this, we can deduce that

$$\mathrm{Im}\big(\mathcal{A}(s > s_{th},t)\big) = \Delta_s(s,t), \tag{2.4}$$

where

$$\Delta_s(s,t) \equiv \frac{1}{2i} \lim_{\epsilon \to 0} [\mathcal{A}(s+i\epsilon,t) - \mathcal{A}(s-i\epsilon,t)] \tag{2.5}$$

is the s-channel *discontinuity function*, taken across all the cuts. Thus, for $\mathcal{A}$ to have an imaginary part above threshold, we need a branch cut along the real axis with a branch point at the threshold energy. This is true because we assumed the lightest possible intermediate state has more than one particle. If we had a single particle, we would have a pole at $s = m^2$. However such poles need not be considered for our purposes.

Through the analytic continuation of our Lorentz invariants s and t, we can also access the kinematic region $s, t < 0$. This corresponds to the u-channel process, which has an associated physical threshold $u = u_{th} > 0$ (we treat t as fixed). This implies that $\mathcal{A}(s,t)$ must also have a branch cut along the negative real s-axis, with a branch point at $s = s_{th}^- = \sum_i m_i^2 - t - u_{th}$. This singularity structure is shown on the complex s-plane in figure 1.

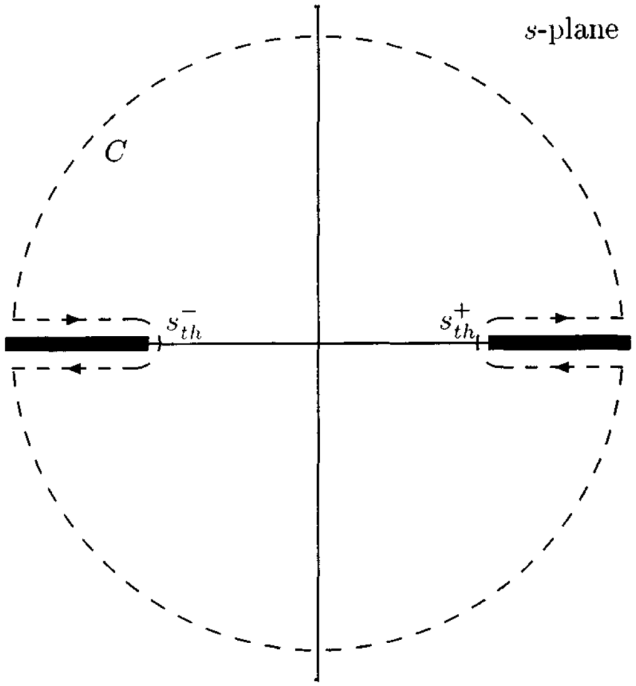

Figure 1: Complex s-plane and its branch cut singularities, with branch points corresponding to physical thresholds. Diagram borrowed from [2].

We can use the analyticity of scattering amplitudes to reconstruct the full amplitude from its imaginary part. The idea of dispersion relations is to use Cauchy's integral formula to express the scattering amplitude as

$$\mathcal{A}(s,t) = \frac{1}{2\pi i} \oint_{\mathcal{C}} d\hat{s} \frac{\mathcal{A}(\hat{s},t)}{\hat{s} - s}, \tag{2.6}$$

with $\mathcal{C}$ is any closed anti-clockwise contour in the complex s-plane enclosing the point s such that $\mathcal{A}$ is analytic inside and along the contour. Next, we deform the contour

such that it encloses the branch cuts as shown in figure 1. Then, if $|\mathcal{A}(s,t)| \to 0$ fast enough for $s \to \infty$, we are left with

$$\begin{aligned}\mathcal{A}(s,t) &= \frac{1}{\pi}\int_{s_{th}}^{\infty}\frac{d\hat{s}}{\hat{s}-s}\Delta_s(\hat{s},t) + \frac{1}{\pi}\int_{u_{th}}^{\infty}\frac{d\hat{u}}{\hat{u}-u}\Delta_u(\hat{u},t)\\ &= \frac{1}{\pi}\int_{s_{th}^{+}}^{\infty}\frac{d\hat{s}}{\hat{s}-s}\mathrm{Im}\big(\mathcal{A}(\hat{s},t)\big) + \frac{1}{\pi}\int_{-\infty}^{s_{th}^{-}}\frac{d\hat{s}}{\hat{s}-s}\mathrm{Im}\big(\mathcal{A}(\hat{s},t)\big).\end{aligned} \tag{2.7}$$

The second integral is the imaginary part associated with the amplitude for $s < s_{th}^{-}$, obtained from the Cutkosky rules applied to the u-channel process. This means:

$$\mathrm{Im}\big(\mathcal{A}(s < s_{th}^{-},t)\big) = -\Delta_u(s,t). \tag{2.8}$$

If $\mathcal{A}(s,t)$ does not vanish at $|s| \to \infty$, then we need to perform subtractions. Below, we make one subtraction at the point $s = s_0$. Note that these points are arbitrary; one needs to divide the amplitude a sufficient number of times by a factor of $s - s_i$ until it vanishes at infinity.

$$\begin{aligned}\mathcal{A}(s,t) = \mathcal{A}(s_0,t) &+ \frac{s-s_0}{\pi}\int_{s_{th}^{+}}^{\infty}\frac{d\hat{s}}{(\hat{s}-s)(\hat{s}-s_0)}\mathrm{Im}\big(\mathcal{A}(\hat{s},t)\big)\\ &+ \frac{s-s_0}{\pi}\int_{-\infty}^{s_{th}^{-}}\frac{d\hat{s}}{(\hat{s}-s)(\hat{s}-s_0)}\mathrm{Im}\big(\mathcal{A}(\hat{s},t)\big).\end{aligned} \tag{2.9}$$

So far, the discussion of dispersion relations has been generic (apart from ignoring single-particle states). For our purposes, we are interested in the first integral on the second line of equation (2.7). We obtain the u-channel contribution to the full amplitude through the crossing symmetry $s \leftrightarrow u$, and using the fact that $s \approx -u$ in the Regge limit. We also do not have an s-channel threshold, $s_{th}^{+} = 0$. Thus, our 'master formula' to reconstruct the full amplitude from the imaginary part is as follows:

$$\mathcal{A}(s,t) = \frac{1}{\pi}\int_{0}^{\infty}\frac{d\hat{s}}{\hat{s}-s}\mathrm{Im}\big(\mathcal{A}(\hat{s},t)\big) + s \leftrightarrow u. \tag{2.10}$$

A useful example in our case is to reconstruct a function whose imaginary part is given by $C(\ln s)^n$. We require one subtraction since $(\ln s)^n/s \to 0$ as $s \to \infty$. Choose $s_0 = 1$ as a subtraction point. Then

$$\begin{aligned}\mathcal{A}(s,t) &= \frac{s-1}{\pi}\int_{0}^{\infty}d\hat{s}\frac{C(\ln s')^n}{(\hat{s}-s)(\hat{s}-1)} + \mathcal{A}(s_0,t)\\ &\overset{!}{=} -C\frac{\big(\ln(-s)\big)^{n+1}}{(n+1)\pi} \overset{!}{=} -C\frac{(\ln s)^{n+1}}{(n+1)\pi},\end{aligned} \tag{2.11}$$

where $\overset{!}{=}$ denotes a step where we have dropped sub-leading terms in the LL approximation. In the last line we also used the fact that, according to the Feynman

prescription, $\ln(-s-i\epsilon) = \ln(s) - i\pi$. We therefore find that to LL order this function is purely real.

We will now show how to reconstruct the full LL tower in our model using a dispersive approach.

2.3 Leading-order contributions

Let us write the perturbative expansion of the amplitude as follows:

$$\mathcal{A} = \mathcal{A}^{(0)} + \mathcal{A}^{(1)} + \cdots + \mathcal{A}^{(n)} + \ldots \tag{2.12}$$

where $\mathcal{A}^{(n)} \sim \mathcal{O}\left(g^{2n}\right)$ denotes the amplitude at n-loops.

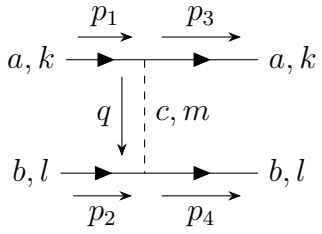

Figure 2: Elastic $qq \to qq$ scattering at tree-level.

We start by considering elastic $qq \to qq$ scattering at tree-level, shown in figure 2. In the diagram, we have defined the momentum transfer $q = p_1 - p_3$, such that $q^2 = t$. We will keep this definition throughout this dissertation. Under the exchange of a colour singlet, the tree-level contribution actually vanishes since the SU(N) generators are traceless. Explicitly, the colour-factor of the tree-level diagram is given by

$$\mathcal{A}^{(0)}_{\text{colour}} = \text{Tr}(T^c)\text{Tr}(T^c)\text{Tr}(T^m)\text{Tr}(T^m) = 0, \tag{2.13}$$

where T^a are the SU(N) generators in the fundamental representation. Thus our leading-order contributions for colour-singlet exchange are one-loop Feynman diagrams. These are shown shown in figure 3.

(a) $\mathcal{A}_{\text{box}}$ (b) $\mathcal{A}_{\text{crossed}}$

Figure 3: Leading-order contributions to elastic $qq \to qq$ scattering in our toy model.

The diagrams in figure 3 are all we need to consider at one-loop:[1]

$$\mathcal{A}^{(1)} = \mathcal{A}_{\text{box}} + \mathcal{A}_{\text{crossed}}. \tag{2.14}$$

For now, consider the diagram in figure 3a. The colour factor is given by:

$$\mathcal{A}^{\text{colour}}_{\text{box}} = \frac{1}{N^4}\text{Tr}(T^a T^b)\text{Tr}(T^a T^b)\text{Tr}(T^c T^d)\text{Tr}(T^c T^d) = \frac{(N^2-1)^2}{16N^4}. \tag{2.15}$$

It is identical for the crossed diagram in the u-channel:

$$\mathcal{A}^{\text{colour}}_{\text{crossed}} = \frac{(N^2-1)^2}{16N^4}. \tag{2.16}$$

We can exploit the symmetry between the two diagrams, by noting that we can map $\mathcal{A}_{\text{box}}$ to $\mathcal{A}_{\text{crossed}}$ by exchanging $p_4 \leftrightarrow -p_2$. Inspecting our Mandelstam variables s and u,

$$\begin{aligned} s &= (p_1+p_2)^2 = 2p_1\cdot p_2, \\ u &= (p_1-p_4)^2 = -2p_1\cdot p_4, \end{aligned} \tag{2.17}$$

we can see that this is the same as exchanging $s \leftrightarrow u$. Therefore, it is sufficient to calculate $\mathcal{A}_{\text{box}}$, and obtain $\mathcal{A}_{\text{crossed}}$ through this symmetry.

We could use Feynman parametrisation to compute the box diagram, and extract the leading logarithmic behaviour from there. However, it will prove much more powerful to employ the dispersive technique introduced in section 2.2. The only cut we can make through diagram 3a such that our intermediate state can be put on-shell is one through the two quark propagators, shown in 4.

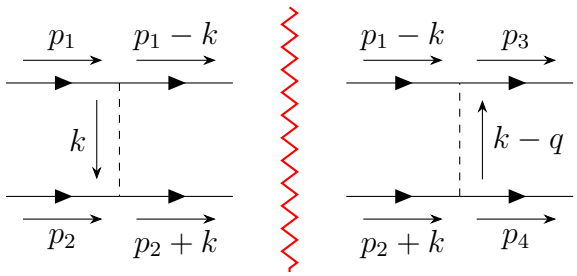

Figure 4: Left- and right-hand side of the Cutkosky-cut through the diagram 3a.

From the optical theorem, we can therefore relate the imaginary part of the box amplitude to these two tree-level amplitudes. This yields the integral:

$$\text{Im}\big(\mathcal{A}_{\text{box}}\big) = \frac{(-igm)^4}{2}\sum_f \int d\Pi_f \left(\frac{i}{k^2-m^2+i\epsilon}\right)\left(\frac{i}{(k-q)^2-m^2+i\epsilon}\right)^*, \tag{2.18}$$

[1] We have not included vertex- or self-energy corrections, since those give sub-leading contributions in the LL approximation, as will be argued later.

where we have suppressed the colour factor for brevity. The integral over intermediate states is given by:

$$\sum_f \int d\Pi_f = \int \frac{d^4k}{(2\pi)^4}(2\pi)^2\delta((p_1-k)^2)\delta((p_2+k)^2). \tag{2.19}$$

Note that we suppress any notion of m in the on-shell conditions, for we treat it as smaller than any energy scale. Recall that it was only added to avoid infrared divergences.

In the centre-of-mass frame, we can write the kinematics of our incoming state as follows:

$$\begin{aligned} p_1 &= \frac{\sqrt{s}}{2}(1,0,0,1), \\ p_2 &= \frac{\sqrt{s}}{2}(1,0,0,-1). \end{aligned} \tag{2.20}$$

We can use p_1 and p_2 as two basis vectors for a general 4-momentum, and complete the basis with a transverse component. This is known as a *Sudakov decomposition*. Using this basis for the momentum k, we write:

$$k = \rho p_1 + \lambda p_2 + k_\perp, \tag{2.21}$$

where $k_\perp = (0, \mathbf{k}_\perp, 0)$ is the transverse component, and ρ and λ are the *Sudakov parameters*. We would like to change variables in equation (2.18). The Jacobian is readily computed:

$$d^4k = \frac{sd\rho d\lambda d^2\mathbf{k}_\perp}{2}. \tag{2.22}$$

Also, we note that:

$$\begin{aligned} (p_1-k)^2 &= -s(1-\rho)\lambda - \mathbf{k}_\perp^2, \\ (p_2+k)^2 &= s(1+\lambda)\rho - \mathbf{k}_\perp^2. \end{aligned} \tag{2.23}$$

This allows us to write our phase space integral (2.19) over the two-quark intermediate state as:

$$\sum_f \int d\Pi_f = \frac{1}{8\pi^2}\int sd\rho d\lambda d^2\mathbf{k}_\perp \delta(-s(1-\rho)\lambda - \mathbf{k}_\perp^2)\delta(s(1+\lambda)\rho - \mathbf{k}_\perp^2). \tag{2.24}$$

As a result, the imaginary part of diagram 3a can be written:

$$\begin{aligned} \mathrm{Im}\big(\mathcal{A}_{\mathrm{box}}\big) = \frac{(gm)^4}{16\pi^2}\int sd\rho d\lambda d^2\mathbf{k}_\perp \delta(-s(1-\rho)\lambda - \mathbf{k}_\perp^2)\delta(s(1+\lambda)\rho - \mathbf{k}_\perp^2) \\ \times \frac{1}{k^2-m^2+i\epsilon}\frac{1}{(k-q)^2-m^2+i\epsilon}. \end{aligned} \tag{2.25}$$

Note also that from the on-shell conditions we have that $\rho = -\lambda$. Hence we can put a further constraint on ρ:

$$s(1-\rho)\rho - \mathbf{k}_\perp^2 = 0 \implies 0 < \rho < 1 \text{ and } \rho \sim \mathbf{k}_\perp^2/s. \tag{2.26}$$

So far, the calculation has been exact. We are interested in finding the dominant contribution in the Regge limit $s \gg |t|$. In this limit, we have:

$$t = q^2 \approx -\mathbf{q}_\perp^2. \tag{2.27}$$

The dominant contributions come from the region of integration where the denominators in (2.25) are as on-shell as possible. With respect to the energy scale of our system, this means

$$-k^2/s = \mathbf{k}_\perp^2/s - \lambda\rho \ll 1. \tag{2.28}$$

Hence, we can summarise our kinematic regime as

$$\begin{aligned} &0 < \rho \ll 1, \\ &\rho = -\lambda \sim \mathbf{k}_\perp^2/s. \end{aligned} \tag{2.29}$$

This identifies the *Regge kinematics* of our system. From here, we also deduce that

$$\begin{aligned} k^2 &\approx -\mathbf{k}_\perp^2, \\ (k-q)^2 &\approx -(\mathbf{k}_\perp - \mathbf{q}_\perp)^2. \end{aligned} \tag{2.30}$$

Using this and the Regge kinematics, (2.25) becomes

$$\begin{aligned} \mathrm{Im}\big(\mathcal{A}_{\text{box}}\big) = \frac{(gm)^4}{16\pi^2} \int s d\rho d\lambda d^2\mathbf{k}_\perp \delta(-s\lambda - \mathbf{k}_\perp^2)\delta(s\rho - \mathbf{k}_\perp^2) \\ \times \frac{1}{\mathbf{k}_\perp^2 + m^2} \frac{1}{(\mathbf{k}_\perp - \mathbf{q}_\perp)^2 + m^2}. \end{aligned} \tag{2.31}$$

Integrating out ρ and λ and reinstating the colour factor, we obtain

$$\begin{aligned} \mathrm{Im}\big(\mathcal{A}_{\text{box}}\big) &= \left[\frac{(N^2-1)^2}{16N^4}\frac{(gm)^4}{16\pi^2}\int d^2\mathbf{k}_\perp \frac{1}{\mathbf{k}_\perp^2 + m^2}\frac{1}{(\mathbf{k}_\perp - \mathbf{q}_\perp)^2 + m^2}\right]\frac{1}{s} \\ &\equiv \left[\frac{(N^2-1)^2}{16N^4}\frac{(gm)^4}{16\pi^2}\int d^2\mathbf{k}_\perp f_0(\mathbf{k}_\perp, \mathbf{q}_\perp)\right]\frac{1}{s}. \end{aligned} \tag{2.32}$$

Using (2.11) we can construct the full amplitude from the imaginary part to LL order. Alternatively, we can just notice that

$$\ln(s/t) = \ln(-s/t) - i\pi \tag{2.33}$$

since $s/t < 0$ in the physical kinematic regime for (2.25). This means

$$\begin{aligned}\mathcal{A}_{\text{box}} &= -\frac{\text{Im}\big(\mathcal{A}_{\text{box}}\big)}{\pi}\ln(s/t) \\ &= -\left[\frac{(N^2-1)^2}{16N^4}\frac{(gm)^4}{16\pi^3}\int d^2\mathbf{k}_\perp f_0(\mathbf{k}_\perp,\mathbf{q}_\perp)\right]\frac{1}{s}\ln(s/t).\end{aligned} \tag{2.34}$$

We obtain the contribution from the crossed diagram 3b via $s \leftrightarrow u$:

$$\mathcal{A}_{\text{crossed}}(s,t) = \mathcal{A}_{\text{box}}(u,t) = -\left[\frac{(N^2-1)^2}{16N^4}\frac{(gm)^4}{16\pi^3}\int d^2\mathbf{k}_\perp f_0(\mathbf{k}_\perp,\mathbf{q}_\perp)\right]\frac{1}{u}\ln(u/t). \tag{2.35}$$

Using $s \approx -u$, we have that our total one-loop amplitude is given by

$$\begin{aligned}\mathcal{A}^{(1)}(s,t) &= \mathcal{A}_{\text{box}} + \mathcal{A}_{\text{crossed}} \\ &= -\left[\frac{(N^2-1)^2}{16N^4}\frac{(gm)^4}{16\pi^3}\int d^2\mathbf{k}_\perp f_0(\mathbf{k}_\perp,\mathbf{q}_\perp)\right]\frac{1}{s}\left(\ln(s/t) - \ln(-s/t)\right).\end{aligned} \tag{2.36}$$

Then, using (2.33) we see that the logarithms cancel and that we are left with just the imaginary part from diagram 3b.

$$\boxed{\mathcal{A}^{(1)}(s,t) = i\frac{(N^2-1)^2}{16N^4}\frac{(gm)^4}{16\pi^2 s}\int d^2\mathbf{k}_\perp f_0(\mathbf{k}_\perp,\mathbf{q}_\perp).} \tag{2.37}$$

Before accepting this as the one-loop amplitude in the LL approximation, we have to justify why vertex corrections and self-energy corrections do not contribute. Representative diagrams for such processes at one-loop order are shown in figure 5.

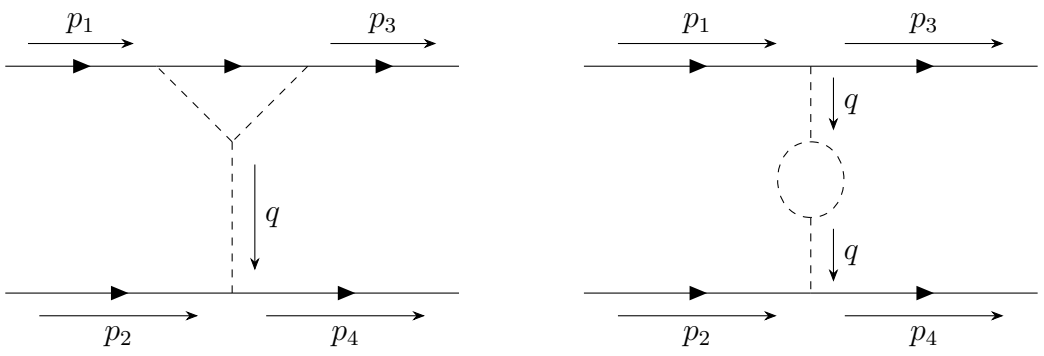

(a) (b)

Figure 5: Representative diagrams for (a) vertex corrections and (b) self-energy corrections at one-loop.

Consider first the vertex correction 5a. The result of any loop integral within the vertex correction must be some function of Lorentz invariants constructed from

the momenta flowing into the vertex. We can construct p_1^2, p_3^2, q^2, $p_1 \cdot p_3$, $p_1 \cdot q$, or $p_3 \cdot q$. All of these either vanish or are of the order $\sim t$ in the Regge limit. We observe that none of them have any s dependence, so the vertex correction cannot possibly generate a logarithm. Therefore the contribution is sub-leading. An identical train of thought shows that the self energy correction in 5b cannot generate a leading logarithm either, for the momentum flowing into the loop is $q^2 = t$. We conclude that, indeed, (2.37) is the one-loop amplitude correct to LL-order. Now we want to consider multi-loop diagrams.

2.4 $\mathcal{O}\left(g^{2n} \ln^n(s)\right)$ corrections

It turns out that the $\mathcal{O}\left(g^{2n} \ln^n(s)\right)$ corrections to the leading-order contributions are given by uncrossed ladder diagrams with n horizontal rungs, shown in figure 6. We will first show that, indeed, these diagrams give such corrections, and delay for now the justification for why other classes of diagrams are sub-leading at LL order.

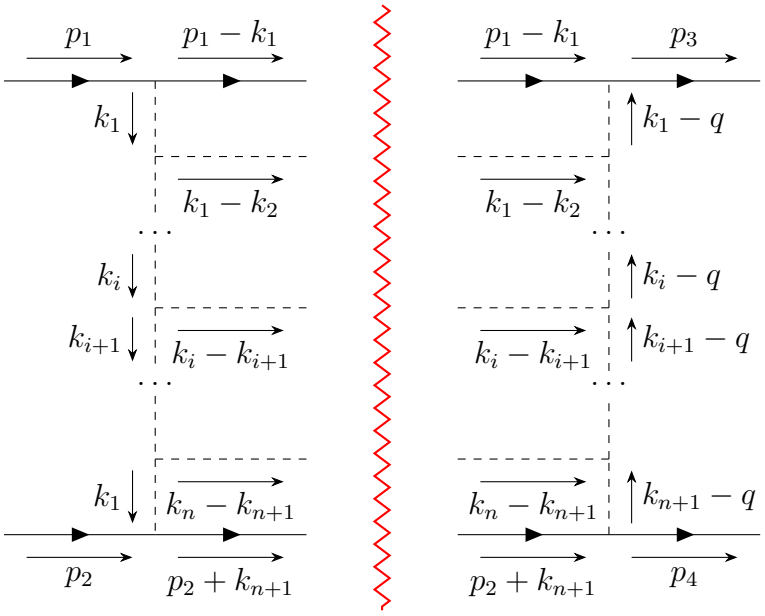

Figure 6: Left- and right-hand side of the cut through the n-rung ladder diagram.

Let us start by finding the colour factor. This is straightforward to do by forming a recurrence relation. First, we can write down:

$$\begin{aligned}\mathcal{A}_{n\text{-rung}}^{\text{colour}} &= \mathrm{Tr}(T^{a_1}T^{c_1})\mathrm{Tr}(T^{b_1}T^{d_1})\mathrm{Tr}(T^{a_{n+1}}T^{c_{n+1}})\mathrm{Tr}(T^{b_{n+1}}T^{d_{n+1}}) \\ &\quad \times f_{a_1 e_1 a_2} f_{b_1 f_1 b_2} f_{c_1 e_1 c_2} f_{d_1 f_1 d_2} \cdots f_{a_n e_n a_{n+1}} f_{b_n f_n b_{n+1}} f_{c_n e_n c_{n+1}} f_{d_n f_n d_{n+1}}.\end{aligned} \tag{2.38}$$

Here, (a_i, b_i) are the adjoint colour indices of the virtual gluons on the left-hand side of the ladder; (c_i, d_i) are those on the right. The indices (e_i, f_i) are those of the ith

horizontal gluon in the intermediate state. This becomes:

$$\mathcal{A}^{\text{colour}}_{n\text{-rung}} = C_A^2 \mathcal{A}^{\text{colour}}_{n-1\text{-rung}} = N^{2n} \frac{(N^2-1)^2}{16N^4} \tag{2.39}$$

where we used the colour factor at one-loop $\mathcal{A}^{\text{colour}}_{\text{box}}$ in the last step. We thus observe that we obtain an extra factor N^2 for each additional rung in the ladder.

Using the optical theorem, we can write the imaginary part of the amplitude (suppressing the colour factor for brevity):

$$\text{Im}(\mathcal{A}_{n\text{-rung}}) = \frac{1}{2}(gm)^{4+2n} \sum_f \int d\Pi_f \prod_{i=1}^{n+1} \frac{1}{k_i^2 - m^2} \frac{1}{(k_i - q)^2 - m^2}, \tag{2.40}$$

where the momentum assignment is consistent with figure 6.

The integral over the phase space of intermediate states is given by:

$$\begin{aligned} \sum_f \int d\Pi_f = &\left(\prod_{i=1}^{n+1} \frac{s}{2} \int \frac{d\rho_i d\lambda_i d^2\mathbf{k}_{i\perp}}{(2\pi)^4} \right) \left(\prod_{j=1}^{n} 2\pi\delta((k_j - k_{j+1})^2 - m^2) \right) \\ &\times 2\pi\delta\left((p_1 - k_1)^2\right) 2\pi\delta\left((p_2 + k_{n+1})^2\right). \end{aligned} \tag{2.41}$$

As before, we perform a Sudakov parametrisation for the transverse momenta:

$$k_i = \rho_i p_1 + \lambda_i p_2 + k_{i\perp}, \tag{2.42}$$

with $k_{i\perp} = (0, \mathbf{k}_{i\perp}, 0)$. The phase space in (2.41) becomes:

$$\begin{aligned} \sum_f \int d\Pi_f = &\left(\prod_{i=1}^{n+1} \frac{s}{2} \int \frac{d\rho_i d\lambda_i d^2\mathbf{k}_{i\perp}}{(2\pi)^4} \right) \\ &\times \left(\prod_{j=1}^{n} 2\pi\delta\left(s(\rho_j - \rho_{j+1})(\lambda_j - \lambda_{j+1}) - (\mathbf{k}_{j\perp} - \mathbf{k}_{j+1\perp})^2\right) \right) \\ &\times 2\pi\delta\left(-s(1-\rho_1)\lambda_1 - \mathbf{k}_{i\perp}^2\right) 2\pi\delta\left(s(1+\lambda_{n+1})\rho_{n+1} - \mathbf{k}_{n+1\perp}^2\right). \end{aligned} \tag{2.43}$$

Now, we claim that the Sudakov components follow a *kinematic ordering*:

$$\begin{aligned} 1 > \rho_1 > \rho_2 > \cdots > \rho_{n+1} > 0; \\ -1 < \lambda_{n+1} < \cdots < \lambda_2 < \lambda_1 < 0. \end{aligned} \tag{2.44}$$

This follows from the on-shell conditions of the intermediate state, together with the requirement that the time-component of the 4-momenta of the horizontal rungs must be greater than 0. Consider the ith horizontal gluon rung:

$$\begin{aligned} E > 0: &\quad (k_i - k_{i+1})_0 = \frac{\sqrt{s}}{2}(\lambda_i - \lambda_{i+1} + \rho_i - \rho_{i+1}) > 0; \\ \text{On-shell}: &\quad s(\rho_j - \rho_{j+1})(\lambda_j - \lambda_{j+1}) - (\mathbf{k}_{j\perp} - \mathbf{k}_{j+1\perp})^2 = 0. \end{aligned} \tag{2.45}$$

The only way this can be accomplished is indeed $\rho_i > \rho_{i+1}$ and $\lambda_i > \lambda_{i+1}$. Doing the same for the the intermediate quark lines, we get $\lambda_1 < 0$ and $\rho_1 < 1$ at the top of the ladder and $\lambda_{n+1} > -1$ and $\rho_{n+1} > 0$ at the bottom of the ladder. Thus we have proved the kinematic ordering in equation (2.44).

So far, our calculations have been generic – but we want to isolate the leading logarithmic contribution to this imaginary part. First, we integrate out $\lambda_1, \ldots, \lambda_{n+1}$ from the phase space integral (2.43):

$$\begin{aligned}\sum_f \int d\Pi_f =& \frac{s^{n+1}}{2^{n+1}(2\pi)^{3n+2}} \left(\prod_{i=1}^{n+1} \int d\rho_i d^2\mathbf{k}_{i\perp}\right) \left(\prod_{j=1}^{n} \frac{1}{s(\rho_i - \rho_{i+1})}\right) \\ &\times \frac{1}{s(1-\rho_1)} \delta\left(s(1+\lambda_{n+1})\rho_{n+1} - \mathbf{k}^2_{n+1\perp}\right),\end{aligned} \tag{2.46}$$

where we have kept a λ_{n+1} in the last δ-function for ease of notation, but this must be replaced by the value obtained by the value dictated by the integral over the other δ-functions.

The large logarithms come from the integration region where the Sudakov components are *strongly ordered*:

$$\begin{aligned}&1 \gg \rho_1 \gg \cdots \gg \rho_{n+1}, \\ &1 \gg |\lambda_{n+1}| \gg \cdots \gg |\lambda_1|,\end{aligned} \tag{2.47}$$

such that the ρ-part of the phase space integral (2.46) becomes:

$$\left(\prod_{i=1}^{n} \int_{\rho_{i+1}}^{1} \frac{d\rho_i}{\rho_i - \rho_{i+1}}\right) \int_0^1 \frac{d\rho_{n+1}}{1-\rho_1} \longrightarrow \left(\prod_{i=1}^{n} \int_{\rho_{i+1}}^{1} \frac{d\rho_i}{\rho_i}\right) \int_0^1 d\rho_{n+1}. \tag{2.48}$$

In this kinematic region we can identify a 'logarithmic term' of:

$$\int_x^1 \frac{dx_1}{x_1} \int_{x_1}^1 \frac{dx_2}{x_2} \cdots \int_{x_{n-1}}^1 \frac{dx_n}{x_n} = \frac{1}{n!} \left(\ln(1/x)\right)^n. \tag{2.49}$$

Note that, while this not explicit here, the strong ordering for λ in the second line of (2.47) is obtained if, instead of λ, we would have integrated out ρ using the on-shell conditions.

Let us examine what the strong ordering implies for the transverse gluon momenta. From the δ-functions in (2.43), we identify:

$$\begin{aligned}&|\lambda_1| \sim \frac{\mathbf{k}^2_{1\perp}}{s}, \quad \rho_{n+1} \sim \frac{\mathbf{k}^2_{n+1\perp}}{s}, \\ &\rho_j \lambda_{j+1} \sim \frac{-(\mathbf{k}_{j\perp} - \mathbf{k}_{j+1\perp})^2}{s} \implies \mathbf{k}^2_{j\perp} \sim \mathbf{k}^2_{j+1\perp}.\end{aligned} \tag{2.50}$$

Hence, we can summarise our kinematic regime as follows:

$$\boxed{\begin{aligned}&1 \gg \rho_1 \gg \cdots \gg \rho_{n+1} \sim \mathbf{k}^2_\perp/s, \\ &1 \gg |\lambda_{n+1}| \gg \cdots \gg |\lambda_1| \sim \mathbf{k}^2_\perp/s, \\ &\mathbf{k}^2_{1\perp} \sim \mathbf{k}^2_{2\perp} \sim \cdots \sim \mathbf{k}^2_{n+1\perp} \sim \mathbf{k}^2_\perp.\end{aligned}} \tag{2.51}$$

This defines the so-called *multi-Regge kinematics*. We have introduced $\mathbf{k}_\perp$ as a 'typical' transverse momentum scale, since we have shown that the virtual gluons have transverse momenta of the same order – all are much smaller in magnitude compared to the centre-of-mass energy $\sqrt{s}$.

From (2.51), it also follows that

$$k_i^2 \approx -\mathbf{k}_{i\perp}^2, \tag{2.52}$$

and

$$(k_i - q)^2 \approx -(\mathbf{k}_{i\perp} - \mathbf{q}_\perp)^2, \tag{2.53}$$

allowing us to write the denominators in (2.40) in terms of the transverse momenta of our system only, which yields (up to a colour factor):

$$\mathrm{Im}(\mathcal{A}_{n\text{-rung}}) = \frac{(gm)^{4+2n}}{2} \sum_f \int d\Pi_f \prod_{i=1}^{n+1} \frac{1}{\mathbf{k}_{i\perp}^2 + m^2} \frac{1}{(\mathbf{k}_{i\perp} - \mathbf{q}_\perp)^2 + m^2}. \tag{2.54}$$

The integral over intermediate states is given by

$$\sum_f \int d\Pi_f = \frac{1}{2^{4n+3}\pi^{3n+2}} \left(\prod_{i=1}^{n} \int_{\rho_{i+1}}^1 \frac{d\rho_i}{\rho_i} \right) \int_0^1 d\rho_{n+1} \left(\prod_{j=1}^{n+1} d^2\mathbf{k}_{j\perp} \right) \delta\left(s\rho_{n+1} - \mathbf{k}_{n+1\perp}^2 \right). \tag{2.55}$$

The range of integration warrants further discussion. We have just argued that the logarithms are generated in the strongly ordered kinematic region, and hence made simplifications to our integrand. Yet, we have kept the entire range of integration – clearly this is inconsistent. However, we are justified in keeping it, because the contributions outside from outside the strongly ordered region do not produce leading logarithms. To see this, we split up the range of integration:

$$\int_{\rho_{i+1}}^1 \frac{d\rho_i}{\rho_i} \xrightarrow{\rho_{i+1} \sim \mathbf{k}_\perp^2/s} \int_{\mathbf{k}_\perp/s}^1 \frac{d\rho_i}{\rho_i} = \left[\int_{\mathbf{k}_\perp/s}^{\mathbf{k}_\perp/s\epsilon_1} + \int_{\mathbf{k}_\perp/s\epsilon_1}^{\epsilon_2} + \int_{\epsilon_2}^1 \right] \frac{d\rho_i}{\rho_i}, \tag{2.56}$$

where ϵ_1 and ϵ_2 have been introduced such that $\mathbf{k}_\perp/s \ll \epsilon_1, \epsilon_2 \ll 1$. This produces the following logarithms:

$$\left[\int_{\mathbf{k}_\perp/s}^{\mathbf{k}_\perp/s\epsilon_1} + \int_{\mathbf{k}_\perp/s\epsilon_1}^{\epsilon_2} + \int_{\epsilon_2}^1 \right] \frac{d\rho_i}{\rho_i} = \ln(1/\epsilon_1) + \ln(\epsilon_1\epsilon_2) + \ln(s/\mathbf{k}_\perp^2) + \ln(1/\epsilon_2). \tag{2.57}$$

The leading logarithm $\ln(s/\mathbf{k}_\perp^2)$ is produced in the region $1 \gg \rho_i \gg \mathbf{k}_\perp$. In the LL approximation, only this term survives. This is because $1/\epsilon_1,\ 1/\epsilon_2 \ll s/\mathbf{k}_\perp^2$. Therefore, in the formal limit of $s \to \infty$, the $\ln(s/\mathbf{k}_\perp^2)$ term will always overcome the $\ln(1/\epsilon_1)$ and $\ln(1/\epsilon_2)$ terms.

In the next section, we will study in detail equation (2.54) and show that a very simple all-order structure emerges.

2.5 All-order resummation

Consistent with the one-loop case, we write equation (2.54) in the following form:

$$\mathrm{Im}(\mathcal{A}_{n\text{-rung}}) = \frac{(N^2-1)^2}{16N^4}\frac{g^4m^4}{16\pi^2 s}\int d^2\mathbf{k}_{1\perp} f_n(s,\mathbf{k}_{1\perp},\mathbf{q}_\perp), \tag{2.58}$$

where

$$\begin{aligned} f_n(s,\mathbf{k}_{1\perp},\mathbf{q}_\perp) = &\left(\frac{g^2m^2N^2}{2(2\pi)^3}\right)^n \left(\prod_{i=1}^{n}\int_{\rho_{i+1}}^{1}\frac{d\rho_i}{\rho_i}\right)\int_0^1 d\rho_{n+1}\left(\prod_{j=2}^{n+1}d^2\mathbf{k}_{j\perp}\right) \\ &\times\left(\prod_{l=1}^{n+1}\frac{1}{\mathbf{k}_{l\perp}^2+m^2}\frac{1}{(\mathbf{k}_{l\perp}-\mathbf{q}_\perp)^2+m^2}\right) s\,\delta\left(s\rho_{n+1}-\mathbf{k}_{n+1\perp}^2\right). \end{aligned} \tag{2.59}$$

This form will facilitate taking the sum over all n later on. Note that we have now incorporated the colour factor in equation (2.39) into the amplitude.

To deal with the ρ-integrals, it is convenient to take the *Mellin transform* of our result. We define the Mellin transform $\mathcal{M}$ of a function $f(s)$ as:

$$\mathcal{F}(\omega) = \mathcal{M}\{f\}(\omega) = \int_1^\infty d\left(\frac{s}{\mathbf{k}_\perp^2}\right)\left(\frac{s}{\mathbf{k}_\perp^2}\right)^{-\omega-1} f(s), \tag{2.60}$$

with the inverse transform given by:

$$f(s) = \frac{1}{2\pi i}\int_{\mathcal{C}} d\omega\left(\frac{s}{\mathbf{k}_\perp^2}\right)^{\omega}\mathcal{F}(\omega), \tag{2.61}$$

where $\mathcal{C}$ is a contour to the right of all the singularities of $\mathcal{F}(\omega)$ on the ω-plane. We refer the reader to appendix D for a brief account of its connection to the Laplace transform, as well as an overview of some of its useful properties. To compute the Mellin transform of equation (2.39), we start by writing

$$\int_1^\infty d\left(\frac{s}{\mathbf{k}_\perp}\right)\left(\frac{s}{\mathbf{k}_\perp}\right)^{-\omega-1} s\,\delta\left(s\rho_{n+1}-\mathbf{k}_{n+1\perp}^2\right) = \rho_{n+1}^{\omega-1}\left(\frac{\mathbf{k}_{n+1\perp}^2}{\mathbf{k}_\perp^2}\right)^{\omega} \approx \rho_{n+1}^{\omega-1}, \tag{2.62}$$

where in the last step we have dropped drop the fraction of transverse momenta, since (as we will see later) it is the pole at $\omega = 0$ that generates the leading logarithms.

Defining $\mathcal{F}_n \equiv \mathcal{M}\{f_n\}$ and using the above result, we obtain:

$$\begin{aligned} \mathcal{F}_n(\omega,\mathbf{k}_{1\perp},\mathbf{q}_\perp) = &\left(\frac{g^2m^2N^2}{2(2\pi)^3}\right)^n \left(\prod_{i=1}^{n}\int_{\rho_{i+1}}^{1}\frac{d\rho_i}{\rho_i}\right)\int_0^1 d\rho_{n+1}\left(\prod_{j=2}^{n+1}d^2\mathbf{k}_{j\perp}\right) \\ &\times\left(\prod_{l=1}^{n+1}\frac{1}{\mathbf{k}_{l\perp}^2+m^2}\frac{1}{(\mathbf{k}_{l\perp}-\mathbf{q}_\perp)^2+m^2}\right)\rho_{n+1}^{\omega-1}. \end{aligned} \tag{2.63}$$

To solve the integrals over ρ_i, we can perform a particularly convenient change of variables. Define:

$$\tau_i \equiv \frac{\rho_i}{\rho_{i-1}}, \quad \tau_i \in [0,1], \tag{2.64}$$

where we take $\rho_0 = 1$. The Jacobian of this transformation is:

$$|J| = \epsilon_{i_1 \dots i_{n+1}} \left(\frac{\partial \tau_1}{\partial \rho_{i_1}} \dots \frac{\partial \tau_{n+1}}{\partial \rho_{i_{n+1}}} \right). \tag{2.65}$$

Using the fact that

$$\frac{\partial \tau_i}{\partial \rho_j} = \frac{1}{\rho_{i-1}} \delta_{ij} - \frac{\rho_i}{\rho_{i-1}^2} \delta_{i-1\, j}, \tag{2.66}$$

we get

$$\begin{aligned} |J| &= \epsilon_{i_1 \dots i_{n+1}} \delta_{1\, i_1} \left(\delta_{2\, i_2} \frac{1}{\rho_1} - \delta_{1\, i_2} \frac{\rho_2}{\rho_1^2} \right) \dots \left(\delta_{n+1\, i_{n+1}} \frac{1}{\rho_n} - \delta_{n\, i_{n+1}} \frac{\rho_{n+1}}{\rho_n^2} \right) \\ &= \epsilon_{i_1 \dots i_{n+1}} \delta_{1\, i} \dots \delta_{n+1\, i_{n+1}} \left(\frac{1}{\rho_1} \dots \frac{1}{\rho_n} \right) = \frac{1}{\rho_1} \dots \frac{1}{\rho_n}, \end{aligned} \tag{2.67}$$

and

$$d\tau_1 \dots d\tau_{n+1} = \frac{d\rho_1 \dots d\rho_{n+1}}{\rho_1 \dots \rho_n}. \tag{2.68}$$

This means that:

$$\left(\prod_{i=1}^{n} \frac{d\rho_i}{\rho_i} \right) d\rho_{n+1} = \prod_{i=1}^{n+1} d\tau_i. \tag{2.69}$$

Furthermore, from the definition (2.64) we have:

$$\rho_{n+1} = \prod_{i=1}^{n+1} \tau_i. \tag{2.70}$$

Using (2.69) and (2.70) in (2.63), and performing the integrals over τ_i, we finally obtain:

$$\begin{aligned} \omega^{n+1} \mathcal{F}_n(\omega, \mathbf{k}_{1\perp}, \mathbf{q}_\perp) = \left(\frac{g^2 m^2 N^2}{2(2\pi)^3} \right)^n \left[\int d^2\mathbf{k} \frac{1}{\mathbf{k}^2 + m^2} \frac{1}{(\mathbf{k} - \mathbf{q}_\perp)^2 + m^2} \right]^n \\ \times \frac{1}{\mathbf{k}_{1\perp}^2 + m^2} \frac{1}{(\mathbf{k}_{1\perp} - \mathbf{q}_\perp)^2 + m^2}. \end{aligned} \tag{2.71}$$

The leading logarithms are generated by the pole at $\omega = 0$, with the factor $1/\omega^{n+1}$ being the Mellin transform of $(\ln s/\mathbf{k}_\perp)^n/n!$.

We can now perform an all-order summation, by seeing that the sum:

$$\mathcal{F}(\omega, \mathbf{k}_\perp, \mathbf{q}_\perp) = \sum_{n=0}^{\infty} \mathcal{F}_n(\omega, \mathbf{k}_\perp, \mathbf{q}_\perp) \tag{2.72}$$

is a geometric series with a common ratio of

$$\left(\frac{g^2m^2N^2}{2(2\pi)^3}\right)\frac{1}{\omega}\int d^2\mathbf{k}\frac{1}{\mathbf{k}^2+m^2}\frac{1}{(\mathbf{k}-\mathbf{q}_\perp)^2+m^2}. \tag{2.73}$$

Performing the infinite sum (2.72), we obtain:

$$\mathcal{F}(\omega,\mathbf{k}_\perp,\mathbf{q}_\perp)=\left(\frac{1}{\mathbf{k}_\perp^2+m^2}\frac{1}{(\mathbf{k}_\perp-\mathbf{q}_\perp)^2+m^2}\right)\frac{1}{\omega-\epsilon_g(t)}, \tag{2.74}$$

where we have defined:

$$\epsilon_g(t)=\left(\frac{g^2m^2N^2}{2(2\pi)^3}\right)\int d^2\mathbf{k}\frac{1}{\mathbf{k}^2+m^2}\frac{1}{(\mathbf{k}-\mathbf{q}_\perp)^2+m^2}\qquad(\mathbf{q}_\perp^2=-t). \tag{2.75}$$

We can compute the integral in (2.75) by Feynman parametrisation:

$$\int d^2\boldsymbol{\ell}\int_0^1\frac{dx}{\left(\boldsymbol{\ell}^2+M^2\right)^2}=\pi\int_0^1\frac{dx}{M^2}, \tag{2.76}$$

where $\boldsymbol{\ell}=\mathbf{k}-x\mathbf{q}_\perp$ and $M^2=m^2+x\mathbf{q}_\perp^2(1-x)$. Using $-\mathbf{q}_\perp^2=t$ and Taylor expanding around $|t|\ll m^2$, we get:

$$\begin{aligned}\pi\int_0^1\frac{dx}{M^2}=\pi\int_0^1\frac{dx}{m^2-x(1-x)t}&=\pi\int_0^1\frac{dx}{m^2}\left(1+x(1-x)\frac{t}{m^2}+\dots\right)\\&=\frac{\pi}{m^2}\left(1+\frac{t}{6m^2}+\dots\right).\end{aligned} \tag{2.77}$$

And so for small $|t|$ we have:

$$\epsilon_g(t)\approx\frac{g^2N^2}{16\pi^2}\left(1+\frac{t}{6m^2}+\dots\right). \tag{2.78}$$

Let us write the complete amplitude, summed to all orders, as

$$\mathcal{A}(s,t)=\sum_{n=0}^{\infty}\left(\mathcal{A}_{n\text{-rung}}(s,t)+\mathcal{A}_{n\text{-rung}}(u,t)\right), \tag{2.79}$$

where the second term in the sum accounts for the contribution from crossing symmetry – we drop this for now, and add it back at the end. From equation (2.58) we have:

$$\mathrm{Im}\big(\mathcal{A}(s,t)\big)=\frac{(N^2-1)^2}{16N^4}\frac{g^4m^4}{16\pi^2s}\int d^2\mathbf{k}_{1\perp}f(s,\mathbf{k}_{1\perp},\mathbf{q}_\perp), \tag{2.80}$$

where $f=\mathcal{M}^{-1}\{\mathcal{F}\}$. Thus, taking the inverse Mellin transform of (2.74) we obtain

$$\begin{aligned}\mathrm{Im}(\mathcal{A}(s,t))&=\left[\frac{(N^2-1)^2}{16N^4}\frac{g^4m^4}{16\pi^2s}\int d^2\mathbf{k}_\perp\frac{1}{\mathbf{k}_\perp^2+m^2}\frac{1}{(\mathbf{k}_\perp-\mathbf{q}_\perp)^2+m^2}\right]\left(\frac{-s}{t}\right)^{\epsilon_g(t)}\\&=-i\mathcal{A}^{(1)}(s,t)\left(\frac{-s}{t}\right)^{\epsilon_g(t)},\end{aligned} \tag{2.81}$$

where we substituted $\mathbf{k}_\perp^2 \to -t$ for the normalisation of s inside the leading logarithms. Recall also that $\mathcal{A}^{(1)}(s,t)$ is purely imaginary, see equation (2.37).

Reconstructing the full amplitude using the dispersion relations, we obtain:

$$\begin{aligned}\mathcal{A}(s,t) &= \left(\frac{s}{t}\right)^{\epsilon_g(t)} \frac{-i\mathcal{A}^{(1)}(s,t)}{\sin(\pi\epsilon_g(t))} \\ &\approx \left(\frac{s}{t}\right)^{\epsilon_g(t)} \frac{-i\mathcal{A}^{(1)}(s,t)}{\pi\epsilon_g(t)},\end{aligned} \tag{2.82}$$

where we used the fact that $\epsilon_g(t) \sim \mathcal{O}(g^2)$, so it can be treated as a small parameter. Adding contribution from the crossing symmetry $s \leftrightarrow u$ we get:

$$\mathcal{A}(s,t) = \left(\frac{s}{t}\right)^{\epsilon_g(t)} \frac{-i\mathcal{A}^{(1)}(s,t)}{\pi\epsilon_g(t)} + \left(\frac{u}{t}\right)^{\epsilon_g(t)} \frac{-i\mathcal{A}^{(1)}(u,t)}{\pi\epsilon_g(t)}. \tag{2.83}$$

Using $s \approx u$, we observe that the real parts cancel, and we are left with the purely imaginary amplitude

$$\boxed{\mathcal{A}(s,t) = \mathcal{A}^{(1)}(s,t)\left(\frac{-s}{t}\right)^{\epsilon_g(t)}}. \tag{2.84}$$

Our leftover task is to justify why all other diagrams, apart from the genuine ladder diagram, are suppressed in the LL approximation. These include crossed ladder diagrams, triple gluon exchange, vertex corrections, and self-energy corrections. We refer the reader to appendix E.1 to see the discussion for this.

This concludes our LL analysis in the toy model. In the next section, we will move on to QCD. We will find that a very similar, albeit more complicated, structure emerges. We will see that in the QCD case the all-order summation of elastic $2 \to 2$ scattering due to colour octet exchange at LL order can be interpreted as the exchange of a single particle known as the *Reggeised gluon*.

3 High-energy elastic scattering in QCD

In our ϕ^3 theory, the scattering was dominated by uncrossed ladder-type diagrams. Unfortunately, this is no longer true in QCD. However, we will still be able to organise the scattering amplitude in terms of 'effective' ladder-type diagrams. For definiteness, here we consider the scattering of two quarks of different flavours $qq' \to qq'$. For simplicity, we will drop the prime index in what follows since there is no room for ambiguity. Working in the Feynman gauge, and in the Regge limit $-t/s \ll 1$, we keep only the LL contributions of the form $\alpha_s^n (\ln s)^{n-1}$ and drop all sub-leading terms. We expand the full amplitude $\mathcal{A}$ as:

$$\mathcal{A}(s,t) = \mathcal{A}^{(0)} + \mathcal{A}^{(1)} + \mathcal{A}^{(2)} + \dots, \tag{3.1}$$

with $\mathcal{A}^{(n)}$ the amplitude at n loops.

It will turn out that at LL level, this infinite sum exponentiates in a similar fashion to the scalar field theory example. As such, we will see that the full amplitude can be described by the exchange of a single *Reggeised gluon*, or *Reggeon*.

3.1 Eikonal approximation

For this discussion it is convenient to work in *light-cone coordinates*. A general 4-momentum $p^\mu = (p^0, \mathbf{p}_\perp, p^3)$ in these coordinates is written as

$$p^\mu = (p_0 + p_3, p_0 - p_3, \mathbf{p}_\perp) \equiv (p^+, p^-, \mathbf{p}_\perp). \tag{3.2}$$

The inner product between two 4-vectors p and q is given by

$$p \cdot q = \frac{1}{2}(p^+ q^- + p^- q^+) - \mathbf{p}_\perp \cdot \mathbf{q}_\perp. \tag{3.3}$$

The kinematics of our incoming state (2.20) can be written as

$$\begin{aligned} p_1^\mu &= (\sqrt{s} \equiv P^+, 0, \mathbf{0}_\perp), \\ p_2^\mu &= (0, \sqrt{s} \equiv P^-, \mathbf{0}_\perp). \end{aligned} \tag{3.4}$$

In the Regge limit, P^+ and P^- are the largest momentum scales of our system, with all others assumed to be sub-leading. This is the *Eikonal approximation* for Regge kinematics [9].

Consider an incoming particle with momentum $p = (P^+, 0, \mathbf{0}_\perp)$ that emits a gluon with with a momentum q. We assume that every component of q sub-leading compared to P^+. We will now show that this gluon couples the same way to $q\bar{q}$ as it does to gg.

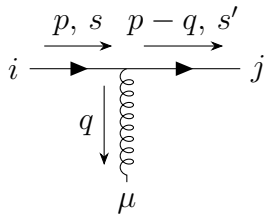

Figure 7: $gq\bar{q}$ vertex in the Eikonal approximation.

3.1.1 $gq\bar{q}$ vertex

From the QCD Feynman rules, we obtain:

$$igT^a_{ij}\bar{u}^{s'}(p-q)\gamma^\mu u^s(p). \tag{3.5}$$

Since q is sub-leading in every component with respect to the centre of mass energy, we can write:

$$\simeq igT^a_{ij}\bar{u}^{s'}(p)\gamma^\mu u^s(p). \tag{3.6}$$

We can simplify this further. If we normalise the eigenspinors as follows:

$$u^{s'}(p)^\dagger u^s(p) = 2E_{\mathbf{p}}\delta_{ss'}, \tag{3.7}$$

we have that:

$$\bar{u}^{s'}(p)\gamma^\mu u^s(p) = 2p^\mu\delta_{ss'}. \tag{3.8}$$

To see this, consider the fact that under Lorentz transformations

$$\bar{\psi}\gamma^\mu\psi \to \Lambda^\mu_\nu\bar{\psi}\gamma^\nu\psi, \tag{3.9}$$

where ψ is a Dirac spinor. This is straightforward to show by considering an infinitesimal Lorentz transformation. As a result, we must have that

$$\bar{u}^{s'}(p)\gamma^\mu u^s(p) \propto p^\mu, \tag{3.10}$$

since this is the only covariant object it can depend on. We can fix the constant of proportionality by considering the $\mu = 0$ case of (3.10), which corresponds to the normalisation condition (3.7).

Therefore, in the Eikonal approximation, our vertex rule is:

$$\boxed{-2igT^a_{ji}p^\mu\delta_{ss'}.} \tag{3.11}$$

3.1.2 ggg vertex

From the QCD Feynman rules, we have

$$gf^{abc}\left((2p-q)^\mu g^{\alpha\beta} + (2q-p)^\alpha g^{\beta\mu} - (q+p)^\beta g^{\mu\alpha}\right)\epsilon_{\alpha\,\lambda}(p)\epsilon^*_{\beta\,\lambda'}(p-q) \tag{3.12}$$

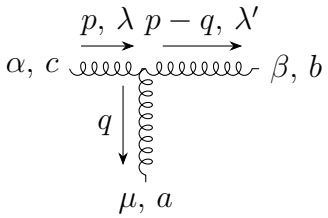

Figure 8: ggg vertex in the Eikonal approximation.

which, in our approximation, becomes:

$$\simeq g f^{abc} \left(2p^\mu g^{\alpha\beta} - p^\alpha g^{\beta\mu} - p^\beta g^{\mu\alpha}\right) \epsilon_{\alpha\,\lambda}(p)\epsilon^*_{\beta\,\lambda'}(p). \tag{3.13}$$

If we now use the fact that the gluon polarisations are orthogonal to the gluon momenta:

$$p \cdot \epsilon_\lambda(p) = p \cdot \epsilon^*_{\lambda'}(p) = 0, \tag{3.14}$$

and also that:

$$\epsilon_\lambda(p) \cdot \epsilon^*_{\lambda'}(p) = \delta_{\lambda\lambda'}, \tag{3.15}$$

we obtain the vertex rule:

$$\boxed{2g f^{abc} p^\mu \delta_{\lambda\lambda'}.} \tag{3.16}$$

Comparing (3.11) and (3.16), we find that (up to a colour factor) the soft transverse gluon couples in an identical way to the $q\bar{q}$ as it does to gg, just like we foreshadowed. Furthermore, notice in both cases how the spins or helicities of the particles no longer play a role.

3.1.3 Propagators of longitudinal momenta

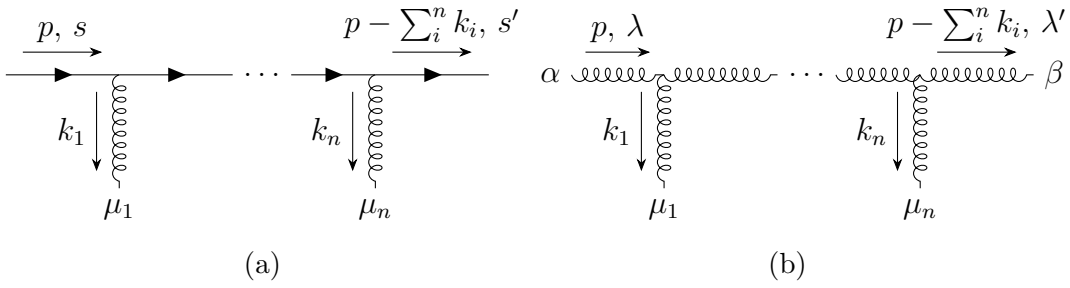

Figure 9: n consecutive Eikonal vertices

In our analysis, we will encounter diagrams that contain the sub-structures shown in figure 9. This is a generalisation of the Eikonal vertices discussed above. Here, like before, p is a longitudinal momentum with a dominant light-cone component P^+. All n emitted gluons have a momentum k_i that has all components sub-leading compared to P^+. It seems that we cannot directly use the Eikonal vertex rules, since we now

also have fermion and gluon propagators in the upper line. However, we actually can, under the prescription that we exchange the fermion or gluon propagators with scalar propagators. Intuitively, this quite a logical extension because we have just shown in the case of simple 3-point vertices vertices that the spins of the particles become irrelevant.

Consider the diagram 9a. From the QCD Feynman rules, we obtain:[2]

$$\begin{aligned}(-ig)^n \bar{u}^{s'}\big(p-\sum_{i=1}^{n} k_i\big)\frac{\gamma^{\alpha_n} i\big(\not{p}-\sum_{j=1}^{n-1}\not{k}_j\big)\gamma^{\alpha_{n-1}}\dots i(\not{p}-\not{k}_1)\gamma^{\alpha_1}}{\prod_{m=1}^{n-1}(p-k_m)^2}u^s(p)\\ \approx (-ig)^n \bar{u}^{s'}(p)\frac{\gamma^{\alpha_n} i\not{p}\gamma^{\alpha_{n-1}}\dots i\not{p}\gamma^{\alpha_1}}{\prod_{m=1}^{n-1}(p-k_m)^2}u^s(p),\end{aligned} \tag{3.17}$$

where in the second line we have dropped sub-leading contributions. Now we use the fact that $\gamma^\mu\not{p} = 2p^\mu - \not{p}\gamma^\mu$, which also implies that for massless quarks $\not{p}^2 = 0$. Further, in the massless case, we have the eigenspinor equation $\not{p}u^s(p) = 0$. This yields:

$$= \underbrace{\left(\prod_{i=1}^{n} -2igp^{\alpha_i}\right)\delta_{ss'}}_{n \text{ Eikonal vertices}}\underbrace{\left(\prod_{j=1}^{n-1}\frac{i}{(p-\sum_{m=1}^{j}k_m)^2}\right)}_{n-1 \text{ scalar propagators}}. \tag{3.18}$$

Indeed, we recognise the term in the first pair of brackets as n Eikonal vertices, and we interpret the term in the second pair of brackets as the fermion propagators that have turned into scalar propagators. One can also verify that the same holds for gluons, i.e. figure 9b.

3.2 General tree-level elastic scattering in the Regge limit

(a) $\mathcal{A}^{(0)}_{qq\to qq}$ (b) $\mathcal{A}^{(0)}_{gg\to gg}$

Figure 10: t-channel diagrams for (a) $qq \to qq$ and (b) $gg \to gg$.

Consider the t-channel contributions shown in figure 10a. Using the Feynman rules for Eikonal vertices in section 3.1, we can immediately write down the ampli-

[2]We have dropped the colour factors for brevity.

tudes:

$$\begin{aligned} i\mathcal{A}^{(0)}_{qq\to qq} &= (-2igp_1^\mu \delta_{s_1 s_3})\,(-2igp_2^\nu \delta_{s_2 s_4})\,\frac{-ig_{\mu\nu}}{q^2} T^a_{ji} T^a_{lk} \\ &= \frac{8\pi i\alpha_s s}{t} \delta_{s_1 s_3}\delta_{s_2 s_4} T^a_{ji} T^a_{lk}, \end{aligned} \tag{3.19}$$

where we have used $2p_1 \cdot p_2 = s$ and $q^2 = t$, and introduced the strong coupling $\alpha_s = g^2/4\pi$. Similarly, for figure 10b:

$$\begin{aligned} i\mathcal{A}^{(0)}_{gg\to gg} &= (2gp_1^\alpha \delta_{\lambda_1\lambda_3})\left(2gp_2^\beta \delta_{\lambda_2\lambda_4}\right)\frac{-ig_{\alpha\beta}}{q^2}(-f^{abe}f^{cde}) \\ &= \frac{8\pi i\alpha_s s}{t}\delta_{\lambda_1\lambda_3}\delta_{\lambda_2\lambda_4} f^{abe}f^{cde}. \end{aligned} \tag{3.20}$$

We observe that, in both cases, the t-channel amplitudes scale with our kinematics like $\sim s/t$. Other contributions at tree-level are obviously sub-leading. To see this, consider the s-channel for $gg \to gg$, for which we get a factor of $1/s$ from the propagator. Kinematics dependencies from the two vertices can only enter the numerator as $\sim s$ or $\sim t$. The same applies to the u-channels of $qq \to qq$ and $gg \to gg$, where we get a factor of $1/u$ from the propagator (note that $s \simeq -u$ in our kinematic limit). Therefore the s- and u-channels are sub-leading. Finally, at tree-level we also have contributions from the $gggg$-vertex for $gg \to gg$. However, this vertex carries no momentum dependence and as a result this diagram does not scale with the kinematics. We conclude that in these two cases, all other tree-level diagrams are sub-leading to the t-channel contributions.

Of course we can come up with other configurations of elastic scattering ($qg \to qg$, $q\bar{q} \to q\bar{q}$, $\bar{q}g \to \bar{q}g$) and these will differ from the above only by a colour factor, by virtue of the universality of the Eikonal vertex. Thus, in the Regge limit, we can write the structure of the general tree-level amplitude of elastic scattering in QCD as follows:

$$i\mathcal{A}^{(0)}_{ij\to ij} = \frac{8\pi i\alpha_s s}{t}(T^b_i)_{a_3a_1}(T^b_j)_{a_4a_2}\delta_{\lambda_1\lambda_3}\delta_{\lambda_2\lambda_4}, \tag{3.21}$$

with

$$(T^b_i)_{a_3a_1} = \begin{cases} T^b_{a_3a_1} & \text{for quarks} \\ -T^b_{a_1a_3} & \text{for antiquarks} \\ -if^{ba_1a_3} & \text{for gluons.} \end{cases}$$

For the sake of clarity, in what follows, we will consider the $qq \to qq$ case – however the results will be easy to generalise with a suitable change of the colour part.

3.3 $\mathcal{O}(\alpha_s \ln(s))$ corrections

In the LL approximation, we do not get contributions from vertex- or self-energy corrections, as we will see later. Thus at leading-order, the diagrams we need to

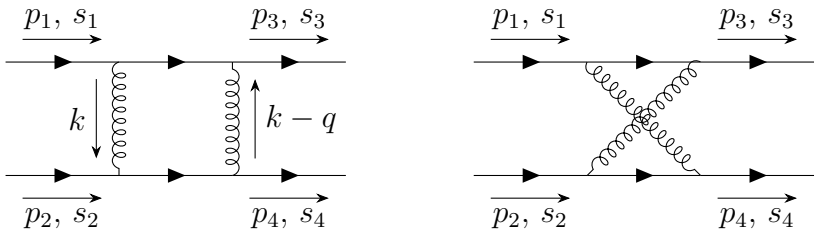

(a) $\mathcal{A}_{\text{box}}$ (b) $\mathcal{A}_{\text{crossed}}$

Figure 11: One-loop contributions in the LL approximation.

consider (analogously to the scalar field theory) are the 'box' and 'crossed' diagrams shown in figure 11. These will generate contributions $\sim \alpha_s^2 \ln s$.

Using our result at tree-level, we can write down (up to a colour factor):

$$\text{Im}\big(\mathcal{A}_{\text{box}}\big) = \frac{64\pi^2\alpha_s^2}{2}\sum_f \int d\Pi_f \left(\frac{s}{k^2}\right)\left(\frac{s}{(k-q)^2}\right)\delta_{s_1 s_3}\delta_{s_2 s_4}. \tag{3.22}$$

The integral over intermediate states is given by

$$\begin{aligned}\sum_f \int d\Pi_f &= \int \frac{d^4k}{(2\pi)^4}\delta\big((p_1-k)^2\big)\delta\big((p_2+k)^2\big)(2\pi)^2 \\ &= \frac{s}{8\pi^2}\int d\rho d\lambda d^2\mathbf{k}_\perp \delta(-s(1-\rho)\lambda - \mathbf{k}_\perp^2)\delta(s(1+\lambda)\rho - \mathbf{k}_\perp),\end{aligned} \tag{3.23}$$

where in the last term we have as per usual performed the Sudakov decomposition $k = \rho p_1 + \lambda p_2 + k_\perp$. In complete analogy with the ϕ^3-theory case, the LL terms are generated in the strongly-ordered region:

$$\begin{aligned}1 &\gg \rho \sim \mathbf{k}_\perp^2/s, \\ 1 &\gg |\lambda| \sim \mathbf{k}_\perp^2/s.\end{aligned} \tag{3.24}$$

We now use the fact that in this limit we have

$$\begin{aligned}k^2 &\approx -\mathbf{k}_\perp^2, \\ (k-q)^2 &\approx -(\mathbf{k}_\perp - \mathbf{q}_\perp)^2,\end{aligned} \tag{3.25}$$

and we integrate out λ and ρ using the δ-functions in (3.23). This becomes:

$$\text{Im}\big(\mathcal{A}_{\text{box}}\big) = 4\alpha_s^2 s \int d^2\mathbf{k}_\perp \frac{1}{\mathbf{k}_\perp^2(\mathbf{k}_\perp - \mathbf{q}_\perp)^2}\delta_{s_1 s_3}\delta_{s_2 s_4}. \tag{3.26}$$

Next, we reconstruct the full amplitude using the dispersion relations (or, from equation (2.11) by inspection). At LL-order, the contribution from the box diagram is purely real and given by:

$$\mathcal{A}_{\text{box}} = \frac{-4\alpha_s^2 s}{\pi}\left[\int d^2\mathbf{k}\frac{1}{\mathbf{k}^2(\mathbf{k}-\mathbf{q}_\perp)^2}\right]\ln\left(s/\mathbf{k}_\perp^2\right)\delta_{s_1 s_3}\delta_{s_2 s_4}. \tag{3.27}$$

We obtain the contribution from the crossed diagram in figure 11b by exchanging $s \leftrightarrow u$. The contribution at LL-order is given by:

$$\mathcal{A}_{\text{crossed}} = \frac{-4\alpha_s^2 u}{\pi}\left[\int d^2\mathbf{k}\frac{1}{\mathbf{k}^2(\mathbf{k}-\mathbf{q}_\perp)^2}\right]\ln\left(-u/\mathbf{k}_\perp^2\right)\delta_{s_1s_3}\delta_{s_2s_4}, \tag{3.28}$$

In the Regge limit, $s \approx -u$ so:

$$= \frac{4\alpha_s^2 s}{\pi}\left[\int d^2\mathbf{k}\frac{1}{\mathbf{k}^2(\mathbf{k}-\mathbf{q}_\perp)^2}\right]\ln\left(s/\mathbf{k}_\perp^2\right)\delta_{s_1s_3}\delta_{s_2s_4}. \tag{3.29}$$

It appears that, like in the case of the $\sim g^4 \ln s$ contribution in the ϕ^3-theory, the contributions (3.27) and (3.29) cancel. However, here they do not. The total contribution, including colour factors, is given by:

$$\mathcal{A}^{(1)} = \mathcal{A}_{\text{box}} + \mathcal{A}_{\text{crossed}} = (\mathcal{A}^{\text{colour}}_{\text{crossed}} - \mathcal{A}^{\text{colour}}_{\text{box}})\frac{4\alpha_s^2 s}{\pi}\left[\int d^2\mathbf{k}\frac{1}{\mathbf{k}^2(\mathbf{k}-\mathbf{q}_\perp)^2}\right] \ln\left(s/\mathbf{k}_\perp^2\right)\delta_{s_1s_3}\delta_{s_2s_4}, \tag{3.30}$$

where

$$\begin{aligned}\mathcal{A}^{\text{colour}}_{\text{crossed}} - \mathcal{A}^{\text{colour}}_{\text{box}} &= (T^bT^a)_{ji}(T^aT^b)_{lk} - (T^bT^a)_{ji}(T^bT^a)_{lk} \\ &= if^{abc}(T^bT^a)_{ji}T^c_{lk} = \frac{1}{2}if^{abc}(T^bT^a - T^aT^b)_{ji}T^c_{lk} \\ &= \frac{1}{2}f^{abc}f^{abd}T^d_{ji}T^c_{lk} = \frac{N}{2}T^c_{ji}T^c_{lk}.\end{aligned} \tag{3.31}$$

Hence,

$$\mathcal{A}^{(1)} = \frac{N}{2}\frac{4\alpha_s^2 s}{\pi}\left[\int d^2\mathbf{k}\frac{1}{\mathbf{k}^2(\mathbf{k}-\mathbf{q}_\perp)^2}\right]\ln\left(s/\mathbf{k}_\perp^2\right)T^a_{ji}T^a_{lk}\delta_{s_1s_3}\delta_{s_2s_4}. \tag{3.32}$$

Recalling (3.19), we can write as:

$$\boxed{\mathcal{A}^{(1)} = \mathcal{A}^{(0)}\epsilon_g(t)\ln\left(s/\mathbf{k}_\perp^2\right).} \tag{3.33}$$

where

$$\epsilon_g(t) = \frac{N\alpha_s}{4\pi^2}\int d^2\mathbf{k}\frac{t}{\mathbf{k}^2(\mathbf{k}-\mathbf{q}_\perp)^2} \qquad (t=-\mathbf{q}_\perp^2). \tag{3.34}$$

Note that this integral is IR divergent, and has to be regulated. We use *dimensional regularisation* in the 't Hooft-Veltman scheme [10], with loop momenta taken to be $d = 4-2\epsilon$ dimensional, to evaluate this integral in the standard way. Doing so, we obtain[3]:

$$\begin{aligned}\epsilon_g(t) &= \frac{\alpha_s}{4\pi}\frac{2N}{\epsilon}\left[e^{\epsilon\gamma_E}\frac{\Gamma(1-\epsilon)^2\Gamma(1+\epsilon)}{\Gamma(1-2\epsilon)}\right]\left(\frac{-t}{\mu^2}\right)^{-\epsilon} \\ &\overset{\mu^2\to-t}{\approx} \frac{\alpha_s}{4\pi}\left[\frac{2N}{\epsilon} - N\zeta_2\epsilon - \frac{14N}{3}\zeta_3\epsilon^2 + \mathcal{O}(\epsilon^3)\right],\end{aligned} \tag{3.35}$$

[3]Later, we will interpret $\epsilon_g(t) \equiv \frac{\alpha_s}{4\pi}\alpha_g^{(1)}(t)$ as the leading-order gluon Regge trajectory.

We note that equation (3.35) does not depend on t when we choose our normalisation scale such that $\mu^2 = -t$ [6]. If this is not the case, then terms of the form $\ln(-\mu^2/t)$ will enter $\epsilon_g(t)$.

This completes the calculation up to one loop in QCD.

3.4 $\mathcal{O}\left((\alpha_s^2 \ln^2(s)\right)$ corrections

Now we will go one order higher. We will consider corrections to the box diagram in section 3.3, and obtain the corresponding corrections to the crossed diagrams from symmetry $s \leftrightarrow u$. To begin with, we consider the case where the Cutkosky cut passes through a virtual gluon, putting it on-shell. We are therefore interested in the tree-level amplitude for $qq \to qq + g$, denoted by $\mathcal{A}_{2\to3}$.

3.4.1 Tree-level $qq \to qq + g$

The contributions to $\mathcal{A}_{2\to3}$ are shown in figure 12. We will consider each diagram separately.

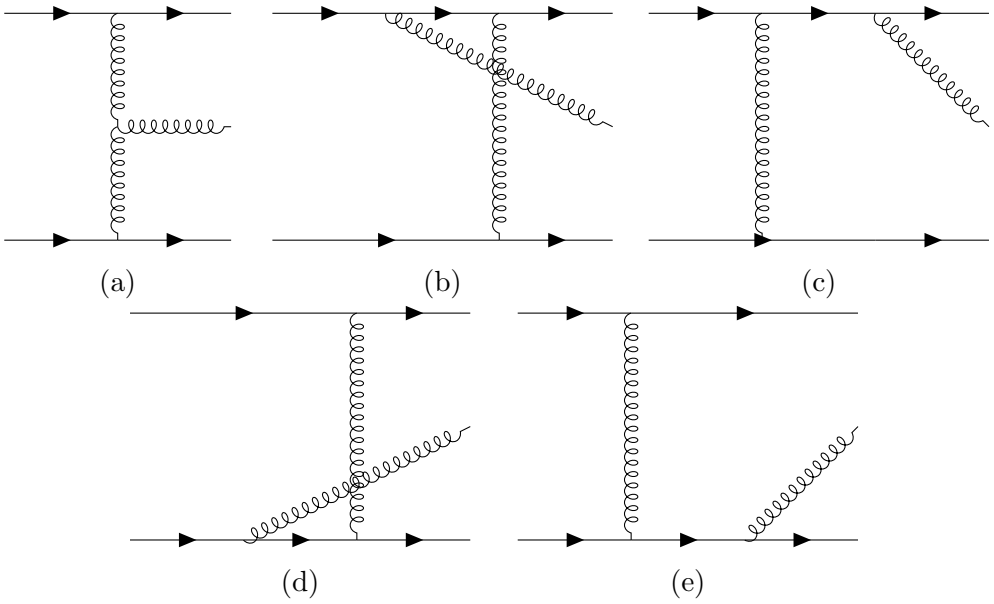

Figure 12: Tree-level diagrams for the process $qq \to qq + g$.

As per usual, we perform a Sudakov decomposition on the transverse momenta $k_i = \rho_i p_1 + \lambda_i p_2 + k_{i\perp}$ and work in the strongly-ordered region

$$\begin{aligned} 1 \gg \rho_1 \gg \rho_2 \sim \mathbf{k}_\perp^2/s, \\ 1 \gg |\lambda_2| \gg |\lambda_1| \sim \mathbf{k}_\perp^2/s, \end{aligned} \tag{3.36}$$

with $\mathbf{k}_\perp$ a typical transverse momentum.

Figure 12a has one Eikonal vertex on the top and bottom quark lines. Using the Eikonal vertex rules we can write down its contribution:

$$
\begin{aligned}
iA^{\sigma\,(a)}_{2\to3} &= \left(-2igp_{1\alpha}T^a_{ji}\right)\left(-2igp_{2\beta}T^b_{lk}\right)\frac{(-i)^2}{k_1^2k_2^2}\delta_{s_1s_1'}\delta_{s_2s_2'} \\
&\times gf_{abc}\left[(2k_1-k_2)^\beta g^{\alpha\sigma}+(2k_2-k_1)^\alpha g^{\sigma\beta}-(k_1+k_2)^\sigma_\perp g^{\alpha\beta}\right] \\
&\approx 2g^3 s\left[\rho_1 p_1^\sigma+\lambda_2 p_2^\sigma-(k_1+k_2)^\sigma_\perp\right]\frac{f_{abc}T^a_{ji}T^b_{lk}}{\mathbf{k}_{1\perp}^2\mathbf{k}_{2\perp}^2}\delta_{s_1s_1'}\delta_{s_2s_2'},
\end{aligned}
\tag{3.37}
$$

,

where we have used the strong ordering to drop sub-leading terms in the square brackets.

The figure 12b has one Eikonal vertex in the bottom quark line, and two in the upper quark line. Using the results in section 3.1.3, we can use the Eikonal vertex rules on the upper quark line under the prescription that we replace the fermion propagator with a scalar propagator. This allows us to immediately write down

$$
\begin{aligned}
iA^{\sigma\,(b)}_{2\to3} &\approx 4ig^3\frac{s}{k_2^2}p_1^\sigma\left[\frac{(T^bT^c)_{ji}T^b_{lk}}{(p_1-k_1+k_2)^2}\right]\delta_{s_1s_1'}\delta_{s_2s_2'} \\
&\approx -4ig^3\frac{s}{\mathbf{k}_{2\perp}^2}p_1^\sigma\left[\frac{(T^bT^c)_{ji}T^b_{lk}}{s\lambda_2}\right]\delta_{s_1s_1'}\delta_{s_2s_2'},
\end{aligned}
\tag{3.38}
$$

where in the last step we used the fact that $k_2^2\approx-\mathbf{k}_{2\perp}^2$ and $(p_1-k_1+k_2)^2\approx\lambda_2 s$. Similarly:

$$
\begin{aligned}
iA^{\sigma\,(c)}_{2\to3} &\approx 4ig^3p_1^\sigma\frac{s}{k_2^2}\frac{(T^cT^b)_{ji}T^b_{lk}}{(p_1-k_2)^2}\delta_{s_1s_1'}\delta_{s_2s_2'} \\
&\approx 4ig^3p_1^\sigma\frac{s}{\mathbf{k}_{2\perp}^2}\frac{(T^cT^b)_{ji}T^b_{lk}}{s\lambda_2}\delta_{s_1s_1'}\delta_{s_2s_2'},
\end{aligned}
\tag{3.39}
$$

where we substituted $(p_1-k_2)^2\approx-s\lambda_2$ and $k_2^2\approx-\mathbf{k}_{2\perp}^2$. Notice that:

$$
iA^{\sigma\,(b)}_{2\to3}+iA^{\sigma\,(c)}_{2\to3}=4g^3p_1^\sigma\frac{1}{\mathbf{k}_{2\perp}^2\lambda_2}f_{abc}T^a_{ji}T^b_{lk}\delta_{s_1s_1'}\delta_{s_2s_2'}. \tag{3.40}
$$

It is interesting to note that the sum of diagrams 12b and 12c would vanish in an Abelian theory such as QED, given the dependence of the above on the structure constant. The physical interpretation of this is that, in the Regge limit, the upper quark line moves along its light cone with very little recoil; it does not acquire any acceleration. In the case of an electron, the absence of acquired acceleration or deceleration then also implies it cannot radiate. In the non-Abelian theory of QCD the radiation is not only caused by acceleration, but also colour rotation – thus despite the absence of recoil or acquired acceleration, the quarks can still radiate (see e.g. [9] for further discussion).

By symmetry, we can then write down

$$iA^{\sigma\,(d)}_{2\to3} + iA^{\sigma\,(e)}_{2\to3} = 4g^3 p_2^\sigma \frac{1}{\mathbf{k}_{1\perp}^2 \rho_1} f_{abc} T^a_{ji} T^b_{lk} \delta_{s_1 s_1'} \delta_{s_2 s_2'}. \tag{3.41}$$

Summing all contributions in figure 12, i.e. equations (3.37), (3.40), and (3.41), we obtain

$$i\mathcal{A}^\sigma_{2\to3} = \frac{4g^3 p_1^\mu p_2^\nu}{\mathbf{k}_{1\perp}^2 \mathbf{k}_{2\perp}^2} \delta_{s_1 s_1'} \delta_{s_2 s_2'} f^{abc} T^a_{ji} T^b_{lk} \Gamma^\sigma_{\mu\nu}(k_1, k_2), \tag{3.42}$$

where

$$\Gamma^\sigma_{\mu\nu}(k_1, k_2) = \frac{2p_{2\mu} p_{1\nu}}{s} \left[\left(\rho_1 + \frac{2\mathbf{k}_{1\perp}^2}{\lambda_2 s} \right) p_1^\sigma + \left(\lambda_2 + \frac{2\mathbf{k}_{2\perp}^2}{\rho_1 s} \right) p_2^\sigma - (k_1 + k_2)^\sigma_\perp \right] \tag{3.43}$$

defines an *effective* non-local vertex, as shown in figure 13a. It is non-local, because it also encodes the quark propagators on the top and bottom quark line of diagrams 12b – 12e.

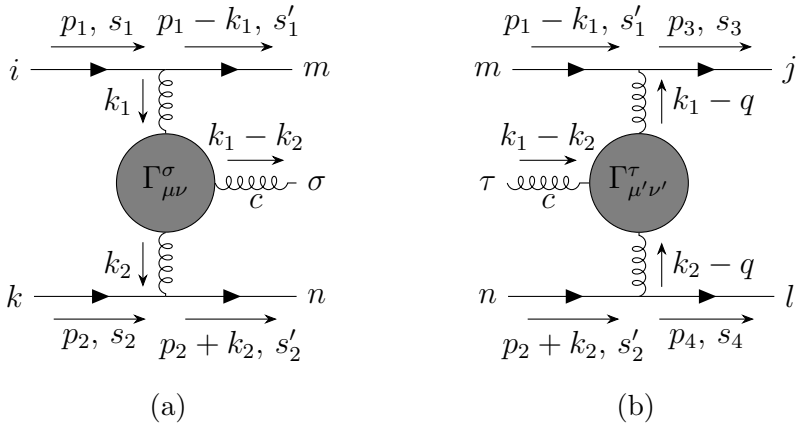

Figure 13: (a) 'Effective' non-local vertex $\Gamma^\sigma_{\mu\nu}(k_1, k_2)$ for the tree-level process $qq \to qq + g$ and (b) the corresponding right side of the cut.

Note that, at the order at which we are working, the effective vertex obeys the Ward identity:

$$\begin{aligned}(k_1 - k_2)_\sigma \Gamma^\sigma_{\mu\nu}(k_1, k_2) = p_{2\mu} p_{1\nu} \Bigg[& \left(\rho_1 + \frac{2\mathbf{k}_{1\perp}^2}{\lambda_2 s} \right) (\lambda_1 - \lambda_2) \\ & + \left(\lambda_2 + \frac{2\mathbf{k}_{2\perp}^2}{\rho_1 s} \right) (\rho_1 - \rho_2) + \frac{2}{s} \left(\mathbf{k}_{1\perp}^2 - \mathbf{k}_{2\perp}^2 \right) \Bigg] \\ \approx p_{2\mu} p_{1\nu} \Big[& - \rho_1 \lambda_2 + \rho_1 \lambda_2 \Big] = 0,\end{aligned} \tag{3.44}$$

where we have used the strong ordering (3.36) in the second equality. This implies that $\mathcal{A}_{2\to3}$ is, in fact, gauge invariant.

We have succeeded in deriving the effective vertex by considering all tree-level contributions to the $qq \to qq + g$ amplitude. However, we can exploit the gauge invariance of the effective vertex in a very powerful way, yielding the same result for $\mathcal{A}_{2\to3}$ but reducing the effective ladder graph to a genuine ladder graph. This is discussed in the next section.

3.4.2 Exploiting the gauge-invariance of the effective vertex

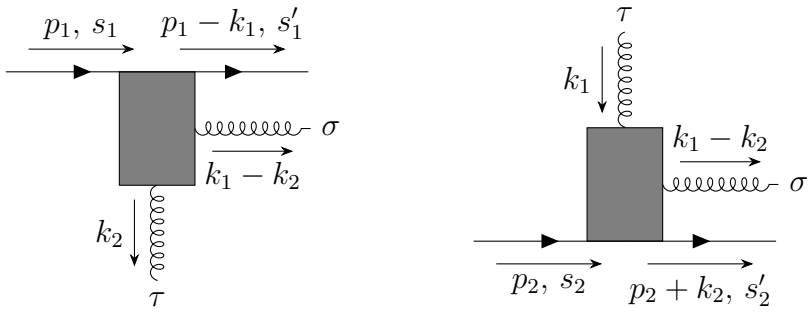

(a) $\mathcal{M}_\tau^\sigma$ (b) $\mathcal{N}_\tau^\sigma$

Figure 14: Tree-level $qq \to qq + g$ amplitudes from figure 12 with (a) the lower quark line removed and (b) the upper quark line removed.

Consider the tree-level diagrams 12a, 12b, and 12c with the lower quark line removed. Call this amplitude $\mathcal{M}_\tau^\sigma(k_1, k_2)$, as shown in figure 14a. From the Eikonal vertex rule, we know that

$$i\mathcal{A}_{2\to3}^{(a)} + i\mathcal{A}_{2\to3}^{(b)} + i\mathcal{A}_{2\to3}^{(c)} \propto p_2^\tau \mathcal{M}_\tau^\sigma. \tag{3.45}$$

Since all but the bottom gluon are on-shell, $\mathcal{M}_\tau^\sigma$ must satisfy the Ward identity:

$$k_2^\tau \mathcal{M}_\tau^\sigma = (\rho_2 p_1^\tau + \lambda_2 p_2^\tau + k_{2\perp}^\tau)\mathcal{M}_\tau^\sigma = 0. \tag{3.46}$$

For the upper part, the dominant energy scale is the positive light-cone component of the quark line, so we expect that in our approximation $\mathcal{M}_\tau^\sigma \mathrel{\tilde{\propto}} p_{1\tau}$. This means that we can neglect the $\rho_2 p_1^\tau$ part in equation (3.46), and obtain:

$$p_2^\tau \mathcal{M}_\tau^\sigma = -\frac{k_{2\perp}^\tau}{\lambda_2}\mathcal{M}_\tau^\sigma, \tag{3.47}$$

and

$$i\mathcal{A}_{2\to3}^{(a)} + i\mathcal{A}_{2\to3}^{(b)} + i\mathcal{A}_{2\to3}^{(c)} \propto -\frac{k_{2\perp}^\tau}{\lambda_2}\mathcal{M}_\tau^\sigma. \tag{3.48}$$

However, it is straightforward to see that in the Eikonal approximation $\mathcal{M}_\tau^\sigma$ receives no transverse contribution from diagrams 12b and 12c. Thus in this construction, the diagram 12a dominates.

We can perform the same procedure with the lower quark line removed. Together, the diagrams 12a, 12d, and 12e form amplitude $\mathcal{N}_\tau^\sigma$, as shown in figure 14b. We have $\mathcal{N}_\tau \mathrel{\tilde{\propto}} p_{2\tau}$, and then from $k_1^\tau \mathcal{N}_\tau^\sigma = 0$ we get:

$$i\mathcal{A}_{2\to3}^{(a)} + i\mathcal{A}_{2\to3}^{(d)} + i\mathcal{A}_{2\to3}^{(e)} \propto -\frac{k_{1\perp}^\tau}{\rho_1}\mathcal{N}_\tau^\sigma. \tag{3.49}$$

Again, only diagram 12a provides the transverse contribution and is dominant. Our amplitude therefore reduces to that of a genuine ladder type graph, with the replacements $p_1 \to -k_{1\perp}/\rho_1$ and $p_2 \to -k_{2\perp}/\lambda_2$ for the Eikonal vertices on the top and bottom quark line, respectively. This yields:

$$\begin{aligned} i\mathcal{A}_{2\to3} = {} & \frac{4g^3}{\mathbf{k}_{1\perp}^2\mathbf{k}_{2\perp}^2}\frac{k_{1\perp}^\mu k_{2\perp}^\nu}{\rho_1\lambda_2}\delta_{s_1s_1'}\delta_{s_2s_2'}f^{abc}T_{ji}^a T_{lk}^b \\ & \times \left[-g_{\mu\nu}(k_1+k_2)^\sigma + g_\nu^\sigma(2k_2-k_1)_\mu + g_\mu^\sigma(2k_1-k_2)_\nu\right]. \end{aligned} \tag{3.50}$$

Making use of the strong ordering (3.36), we can write this as:

$$\begin{aligned} & = -\frac{2g^3}{\mathbf{k}_{1\perp}^2\mathbf{k}_{2\perp}^2}\frac{1}{\rho_1\lambda_2}\delta_{s_1s_1'}\delta_{s_2s_2'}f^{abc}T_{ji}^a T_{lk}^b \\ & \times \Bigg[\left((\mathbf{k}_{1\perp}-\mathbf{k}_{2\perp})^2 - 2\mathbf{k}_{1\perp}^2\right)\rho_1 p_1^\sigma + \left((\mathbf{k}_{1\perp}-\mathbf{k}_{2\perp})^2 - 2\mathbf{k}_{2\perp}^2\right)\lambda_2 p_2^\sigma \\ & + (\mathbf{k}_{1\perp}^2 - \mathbf{k}_{2\perp}^2)\left((\rho_1-\rho_2)p_1^\sigma + (\lambda_1-\lambda_2)p_2^\sigma + (k_1-k_2)_\perp^\sigma\right)\Bigg]. \end{aligned} \tag{3.51}$$

The term in the third line is proportional to $(k_1-k_2)^\sigma$, which we can drop because it is orthogonal to the polarisation vector of the on-shell gluon. Next, we use the fact that $(\mathbf{k}_{1\perp}-\mathbf{k}_{2\perp})^2 = -\rho_1\lambda_2 s$ from the on-shell condition of the intermediate gluon. Doing this, we obtain:

$$i\mathcal{A}_{2\to3}^\sigma = \frac{4g^3 p_1^\mu p_2^\nu}{\mathbf{k}_{1\perp}^2\mathbf{k}_{2\perp}^2}\delta_{s_1s_1'}\delta_{s_2s_2'}f^{abc}T_{ji}^a T_{lk}^b \Gamma_{\mu\nu}^\sigma(k_1,k_2), \tag{3.52}$$

i.e. precisely equation (3.42). From arguments of gauge invariance, we have reduced the tree-level $qq \to qq + g$ amplitudes from an 'effective' ladder to a genuine ladder graph, and successfully re-derived the effective vertex rule.

3.4.3 Dispersive calculation of two-loop contributions

We would now like to calculate the contributions of all diagrams for which the Cutkosky-cut passes through two quarks and one intermediate gluon. These contributions are shown in figure 13, with an effective vertex on the left and right side of the cut. Using the optical theorem we can write down:

$$\mathrm{Im}\big(\mathcal{A}^{(2)}\big) = \frac{1}{2}\underbrace{\sum_\lambda \epsilon_{\lambda,\sigma}(k_1-k_2)\epsilon_{\lambda,\tau}^*(k_1-k_2)}_{\to -g_{\sigma\tau},\ \text{by Ward identity}}\sum_f \int d\Pi_f A_{2\to3}^\sigma(k_1,k_2)A_{2\to3}^{\tau\dagger}(k_1-q,k_2-q). \tag{3.53}$$

First consider the colour factor. This is given by:

$$f^{abc}T^a_{mi}T^b_{nk}f^{dce}T^d_{jm}T^e_{ln} = -f^{abc}f^{dec}(T^aT^d)_{ji}(T^bT^e)_{lk}. \tag{3.54}$$

Next we perform a convenient manipulation. Anticipating that the contribution from the $s \leftrightarrow u$ amplitude will be equal and opposite (up to the colour factor), we will add the colour factor from the u-channel now. This is in analogy with the one-loop case (see e.g. equation (3.30)). We also include a factor of $1/2$, such that the colour factor is equally 'shared' between the s- and u-channel. Noting that the u-channel has $b \leftrightarrow e$, our colour factor becomes:

$$\begin{aligned} -f^{abc}f^{dec}(T^aT^d)_{ji}(T^bT^e)_{lk} &\to -\frac{1}{2}f^{abc}f^{dec}(T^aT^d)_{ji}\left[(T^bT^e)_{lk} - (T^eT^b)_{lk}\right] \\ &= -\frac{1}{2}\left(f^{abc}f^{dec} - f^{aec}f^{dbc}\right)(T^aT^d)_{ji}(T^bT^e)_{lk} \\ &= \frac{1}{8}f^{adc}f^{cbe}f^{adf}f^{gbe}T^f_{ji}T^g_{lk} = \frac{N^2}{8}T^a_{ji}T^a_{lk}, \end{aligned} \tag{3.55}$$

where in the third step we have made use of the Jacobi identity (see appendix B). Our integrand is therefore

$$\begin{aligned} -\frac{1}{2}\mathcal{A}^{\sigma}_{2\to 3}(k_1,k_2)\mathcal{A}_{2\to 3\sigma}(k_1-q,k_2-q) &= -\frac{g^6N^2}{16}T^a_{ji}T^a_{lk}\delta_{s_1s_1'}\delta_{s_2s_2'} \\ &\times \frac{16p_1^{\mu}p_2^{\nu}p_1^{\mu'}p_2^{\nu'}}{\mathbf{k}_{1\perp}^2\mathbf{k}_{2\perp}^2(\mathbf{k}_{1\perp}-\mathbf{q}_{\perp})^2(\mathbf{k}_{2\perp}-\mathbf{q}_{\perp})^2} \\ &\times g_{\sigma\tau}\Gamma^{\sigma}_{\mu\nu}(k_1,k_2)\Gamma^{\tau}_{\mu'\nu'}(-(k_1-q),-(k_2-1)). \end{aligned} \tag{3.56}$$

Performing the contractions, this becomes:

$$\begin{aligned} &= -g^4\frac{N^2s}{4}\mathcal{A}^{(0)}\mathbf{q}_{\perp}^2\left\{\frac{\mathbf{q}_{\perp}^2}{\mathbf{k}_{1\perp}^2\mathbf{k}_{2\perp}^2(\mathbf{k}_{1\perp}-\mathbf{q}_{\perp})^2(\mathbf{k}_{2\perp}-\mathbf{q}_{\perp})^2}\right. \\ &\left. - \frac{1}{\mathbf{k}_{1\perp}^2(\mathbf{k}_{1\perp}-\mathbf{k}_{2\perp})^2(\mathbf{k}_{2\perp}-\mathbf{q}_{\perp})^2} - \frac{1}{\mathbf{k}_{2\perp}^2(\mathbf{k}_{1\perp}-\mathbf{k}_{2\perp})^2(\mathbf{k}_{1\perp}-\mathbf{q}_{\perp})^2}\right\}, \end{aligned} \tag{3.57}$$

where we have used $\rho_1\lambda_2 s \to -(\mathbf{k}_{1\perp}-\mathbf{k}_{2\perp})^2$ from the on-shell condition of the intermediate gluon.

From (2.46) we can write down the two-body phase space integral, which after integrating out λ_1, λ_2, and ρ_2, becomes:

$$\sum_f \int d\Pi_f = \frac{1}{(2\pi)^5}\frac{1}{4s}\int \frac{d\rho_1}{\rho_1}d^2\mathbf{k}_{1\perp}d^2\mathbf{k}_{2\perp}. \tag{3.58}$$

Hence, we obtain:

$$\begin{aligned} \mathrm{Im}\big(\mathcal{A}^{(2)}\big) = -\frac{N^2\alpha_s^2}{32\pi^3}\mathcal{A}^{(0)}\mathbf{q}_{\perp}^2\int\frac{d\rho_1}{\rho_1}d^2\mathbf{k}_{1\perp}d^2\mathbf{k}_{2\perp}\left\{\frac{\mathbf{q}_{\perp}^2}{\mathbf{k}_{1\perp}^2\mathbf{k}_{2\perp}^2(\mathbf{k}_{1\perp}-\mathbf{q}_{\perp})^2(\mathbf{k}_{2\perp}-\mathbf{q}_{\perp})^2}\right. \\ \left. - \frac{1}{\mathbf{k}_{1\perp}^2(\mathbf{k}_{1\perp}-\mathbf{k}_{2\perp})^2(\mathbf{k}_{2\perp}-\mathbf{q}_{\perp})^2} - \frac{1}{\mathbf{k}_{2\perp}^2(\mathbf{k}_{1\perp}-\mathbf{k}_{2\perp})^2(\mathbf{k}_{1\perp}-\mathbf{q}_{\perp})^2}\right\}. \end{aligned} \tag{3.59}$$

However, we have more contributions we need to consider – these correspond to the cases where the Cutkosky-cut does not pass through the middle gluon, but only through two quark lines. Two cases, with a tree-level t-channel amplitude on the right of the cut, are shown in figure 15. We also need to consider the two cases where the one gluon is exchanged on the left of the cut, though we can get those contributions from symmetry, by exchanging $\mathbf{k}_{1\perp} \leftrightarrow \mathbf{k}_{2\perp}$.

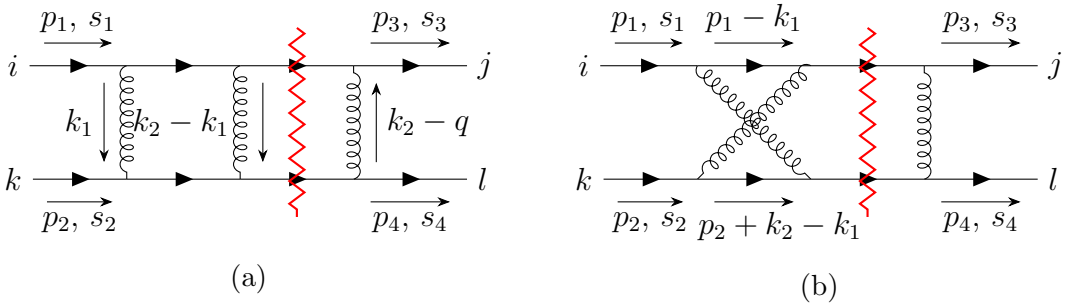

Figure 15: Two-loop diagrams with the Cutkosky cut passing through two intermediate quarks.

Adapting our result at tree-level (see section 3.2, equation (3.19)) and our result at one-loop (see section 3.3, equation (3.33)), we can write down the contribution from the diagrams in 15.

$$\frac{1}{2}\sum_f \int d\Pi_f \mathcal{A}^{(1)}(s,k_2^2)\mathcal{A}^{(0)\dagger}(s,(k_2-q)^2) = \frac{1}{2}\sum_f \int d\Pi_f \frac{8\pi\alpha_s s}{-\mathbf{k}_{2\perp}^2}\epsilon_g(k_2^2)\ln(s/\mathbf{k}_\perp^2) \times \left[-8\pi\alpha_s \frac{s}{(\mathbf{k}_{2\perp}\mathbf{q}_\perp)^2}\right](T^bT^a)_{ji}(T^bT^a)_{lk}\delta_{s_1s_3}\delta_{s_2s_4}. \tag{3.60}$$

We perform a similar manipulation with the colour factor as before. Anticipating the equal and opposite contribution from the u-channel, we can share the combined colour factor equally between the s- and u-channels:

$$\begin{aligned}(T^bT^a)_{ji}(T^bT^a)_{lk} \to \frac{1}{2}(T^bT^a)_{ji}\left[(T^bT^a)_{lk} - (T^aT^b)_{lk}\right] &= \frac{1}{2}if^{bac}(T^bT^a)_{ji}T^c_{lk} \\ = -\frac{1}{4}f^{bac}f^{bad} &= -\frac{N}{4}T^a_{ji}T^a_{lk}.\end{aligned} \tag{3.61}$$

Thus we can write the total contribution from the diagrams in figure 15 as

$$-\frac{4g^4}{2}\frac{N}{4}\sum_f \int d\Pi_f \frac{s^2}{\mathbf{k}_{2\perp}^2(\mathbf{k}_{2\perp}-\mathbf{q}_\perp)^2}\epsilon_g(k_2^2)\ln(s/\mathbf{k}_\perp^2)T^a_{ji}T^a_{lk}\delta_{s_1s_3}\delta_{s_2s_4}. \tag{3.62}$$

Here our phase space integral is given by:

$$\begin{aligned}\sum_f \int d\Pi_f &= \frac{s}{8\pi^2}\int d\rho d\lambda d^2\mathbf{k}_{2\perp}\delta(-s\lambda-\mathbf{k}_{2\perp}^2)\delta(s\rho-\mathbf{k}_{2\perp}^2)\\ &\stackrel{!}{=}\frac{1}{8\pi^2 s}\int d^2\mathbf{k}_{2\perp},\end{aligned} \tag{3.63}$$

where in the last step we have integrated out ρ and λ using the δ-functions, since our integrand is independent of them. Equation (3.62) becomes

$$-\frac{N^2\alpha_s^2}{32\pi^3}\mathcal{A}^{(0)}\mathbf{q}_\perp^2\int d^2\mathbf{k}_{1\perp}d^2\mathbf{k}_{2\perp}\frac{1}{\mathbf{k}_{1\perp}^2(\mathbf{k}_{1\perp}-\mathbf{k}_{2\perp})^2(\mathbf{k}_{2\perp}-\mathbf{q}_\perp)^2}\ln(s/\mathbf{k}_\perp^2). \tag{3.64}$$

The corresponding contribution with the single gluon exchanged on the left of the cut is

$$-\frac{N^2\alpha_s^2}{32\pi^3}\mathcal{A}^{(0)}\mathbf{q}_\perp^2\int d^2\mathbf{k}_{1\perp}d^2\mathbf{k}_{2\perp}\frac{1}{\mathbf{k}_{2\perp}^2(\mathbf{k}_{1\perp}-\mathbf{k}_{2\perp})^2(\mathbf{k}_{1\perp}-\mathbf{q}_\perp)^2}\ln(s/\mathbf{k}_\perp^2). \tag{3.65}$$

Evidently, contributions (3.64) and (3.65) completely cancel the last two terms in equation (3.59). We are left with

$$\begin{aligned}\mathrm{Im}\big(\mathcal{A}^{(2)}\big) &= -\frac{N^2\alpha_s^2}{32\pi^3}\mathcal{A}^{(0)}\mathbf{q}_\perp^2\int d^2\mathbf{k}_{1\perp}d^2\mathbf{k}_{2\perp}\frac{\mathbf{q}_\perp^2}{\mathbf{k}_{1\perp}^2\mathbf{k}_{2\perp}^2(\mathbf{k}_{1\perp}-\mathbf{q}_\perp)^2(\mathbf{k}_{2\perp}-\mathbf{q}_\perp)^2}\ln(s/\mathbf{k}_\perp^2)\\ &= -\frac{1}{2}\epsilon_G^2(t)\pi\ln(s/\mathbf{k}_\perp^2)\mathcal{A}^{(0)}\end{aligned} \tag{3.66}$$

From our dispersion relations, we deduce that to LL-order, the full amplitude at two loops is given by:

$$\begin{aligned}\mathcal{A}^{(2)} &= \frac{1}{4}\epsilon_G^2(t)\ln^2(s/\mathbf{k}_\perp^2)\mathcal{A}^{(0)}+s\leftrightarrow u\\ &\stackrel{!}{=}\frac{1}{2}\epsilon_G^2(t)\ln^2(s/\mathbf{k}_\perp^2)\mathcal{A}^{(0)},\end{aligned} \tag{3.67}$$

where in the second line we have included the u-channel contribution and dropped sub-leading terms.

Let us recall what we have found so far. The $qq\to qq$ amplitude in the Regge limit, to the first three terms in the LL expansion, is given by

$$\mathcal{A}(s,t)=\mathcal{A}^{(0)}(s,t)\left(1+\epsilon_g(t)\ln(s/\mathbf{k}_\perp^2)+\frac{1}{2}\epsilon_g^2(t)\ln^2(s/\mathbf{k}_\perp^2)+\dots\right), \tag{3.68}$$

which looks very suggestively like an expansion of

$$\mathcal{A}(s,t)\stackrel{?}{=}\mathcal{A}^{(0)}(s,t)\left(\frac{s}{\mathbf{k}_\perp^2}\right)^{\epsilon_g(t)}. \tag{3.69}$$

This will turn out to be the case. To see this, we need to go to all orders in the LL expansion, which we will start to do in the next section. We will prove this inductively by making the ansatz that the sum of all leading $\ln s$ corrections to the single gluon exchange amplitude is given by equation (3.69), which can be interpreted as the exchange of a single *Reggeised gluon* or *Reggeon*. Then we proceed to show its self-consistency, which together with the results from the first orders in perturbation theory serves as an inductive proof for the Reggeisation of the gluon.

3.5 Tree-level $qq \to qq + n \times g$

We showed that, in the Eikonal approximation, the spin of the particle with the large light-cone component compared to the emitted gluon is irrelevant. As such, we can also apply the non-local effective vertex if we replace the quark lines with gluons, with an appropriate adjustment of the colour factor.

Consider an effective vertex inside a general ladder diagram – this is shown in figure 16. Recalling the Sudakov decomposition $k_i = \rho_i p_1 + \lambda_i p_2 + k_{i\perp}$, we can see that the strong ordering $\rho_i \gg \rho_{i+1}$ ensures that $k_i^+ \gg k_{i+1}^+$ for the upper gluon line. Similarly, for the lower gluon line, we have $k_{i+2}^- \gg k_{i+1}^-$ by virtue of $|\lambda_{i+2}| \gg |\lambda_{i+1}|$. As such, the Eikonal approximation is still valid, and we are justified to put effective vertices in the ladder. The effective vertex has the effect of adding a gluon line with momentum $k_i - k_{i+1}$ to all the gluon lines in figure 16. This is shown in figure 17.

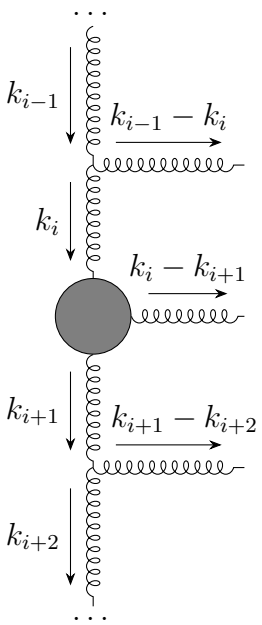

Figure 16: Effective vertex inside a ladder section.

We want to form the general tree-level scattering amplitude for two quarks scattering to two quarks and n gluons. To do so, we use the same gauge technique we used in the two-loop case. Consider the general case of such a process, with a

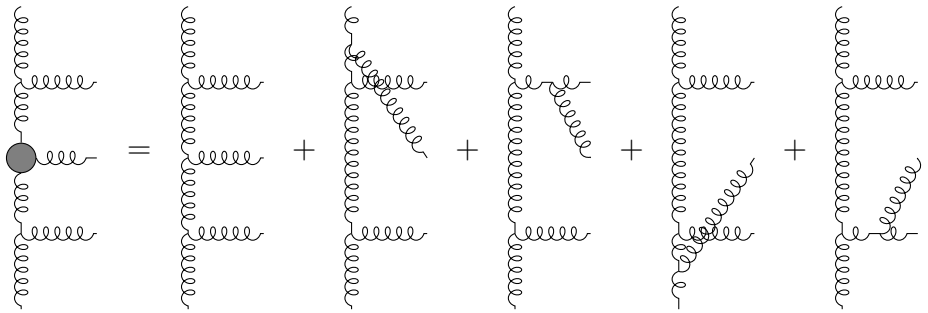

Figure 17: Interpretation of the effective vertex inside the ladder section.

cut through the ith vertical gluon. This is shown in figure 18. This separates the amplitude into an upper and a lower part, which we call $\mathcal{M}_\mu$ and $\mathcal{N}_\nu$ respectively (suppressing the free σ_i indices).

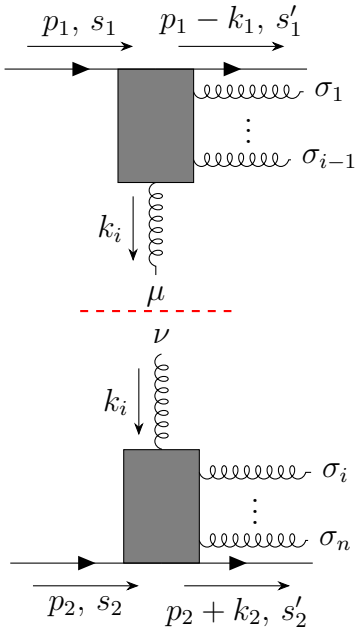

Figure 18: Amplitude separated into an upper and lower part by cutting through the ith vertical gluon.

Given the on-shell conditions for all but the cut gluon line, the upper and lower parts of the amplitude obey the Ward identity

$$\begin{aligned} k_i^\mu \mathcal{M}_\mu(p_1, k_1, \ldots, k_i) &= 0, \\ k_i^\nu \mathcal{N}_\nu(p_2, k_i, \ldots, k_{n+1}) &= 0. \end{aligned} \tag{3.70}$$

In our approximation we are interested in the dominant light-cone components $P^\pm$, which come from the upper and lower quark lines respectively. As such, we expect

that to leading order $\mathcal{M}^\mu \mathrel{\widetilde{\propto}} p_1^\mu$ and $\mathcal{N}^\nu \mathrel{\widetilde{\propto}} p_2^\nu$. This, paired with the Ward identity (3.70), means that

$$\begin{aligned} k_{i\perp}^\mu \mathcal{M}_\mu(p_1, k_1, \ldots, k_i) &\approx -\lambda_i p_2^\mu \mathcal{M}_\mu(p_1, k_1, \ldots, k_i), \\ k_{i\perp}^\mu \mathcal{N}_\nu(p_1, k_i, \ldots, k_n) &\approx -\rho_i p_1^\nu \mathcal{N}_\nu(p_2, k_i, \ldots, k_n). \end{aligned} \tag{3.71}$$

To 'glue' the two pieces back together and recover the full amplitude, we must contract the upper and lower parts using the propagator of the ith vertical gluon:

$$\mathcal{A}_{2\to 2+n} \propto \mathcal{M}_\mu \mathcal{N}_\nu g^{\mu\nu}. \tag{3.72}$$

However, using the fact that $s = 2p_1 \cdot p_2$ together with (3.71), the respective replacements

$$\begin{aligned} \mathcal{M}^\mu &\to -\frac{2k_{i\perp}^\mu}{s\lambda_i} p_{2\alpha} \mathcal{M}^\alpha, \\ \mathcal{N}^\nu &\to -\frac{2k_{i\perp}^\nu}{s\rho_i} p_{1\alpha} \mathcal{N}^\alpha, \end{aligned} \tag{3.73}$$

do not change $\mathcal{A}_{2\to 2+n}$ in our approximation. Making both replacements at the same time yields:

$$\mathcal{A}_{2\to 2+n} \propto \mathcal{M}_\mu \mathcal{N}_\nu g^{\mu\nu} \to \mathcal{M}_\mu \mathcal{N}_\nu \frac{2k_{i\perp}^\mu k_{i\perp}^\nu}{s\lambda_i\rho_i}. \tag{3.74}$$

The net effect is that we can replace all vertical gluon propagators by

$$\frac{ig^{\mu\nu}}{\mathbf{k}_{i\perp}^2} \to \frac{i}{\mathbf{k}_{i\perp}^2} \frac{2k_{i\perp}^\mu k_{i\perp}^\nu}{s\lambda_i\rho_i}. \tag{3.75}$$

For ease of notation, associate

$$\sqrt{\frac{2}{s}} \frac{k_{i\perp}^\mu}{\lambda_i}$$

to the top part of the ith vertical gluon, and

$$\sqrt{\frac{2}{s}} \frac{k_{i\perp}^\mu}{\rho_i}$$

to the bottom part.

It turns out that using this gauge technique, analogously to the two-loop case, the amplitude reduces down to (the left half of) a genuine uncrossed ladder diagram. All diagrams that are *not* uncrossed ladders are suppressed under this prescription. For now, consider the amplitude associated with the left half of an uncrossed ladder diagram:

$$\begin{aligned} &(-2igp_1^{\mu_1})(-2igp_2^{\nu_n}) \left(\prod_{i=1}^{n} f_{a_1 a_{i+1} b_i}\right) T_{ji}^{a_1} T_{lk}^{a_{n+1}} \left(\prod_{l=1}^{n+1} \frac{ig^{\mu_l \nu_{l-1}}}{\mathbf{k}_{l\perp}^2}\right) \delta_{s_1 s_1'} \delta_{s_2 s_2'} \\ &\times \prod_{j=1}^{n} \left\{ -g \left[g_{\mu_j \nu_j} (-k_i - k_{i+1})^{\sigma_j} + g_{\mu_j}^{\sigma_j} (2k_j - k_{j+1})_{\nu_j} + g_{\nu_j}^{\sigma_j} (2k_{j+1} - k_j)_{\mu_j} \right] \right\}. \end{aligned} \tag{3.76}$$

Under replacement of the gluon propagators, this becomes:

$$\boxed{\begin{aligned}\mathcal{A}^{\sigma_1\ldots\sigma_n}_{2\to(n+2)} &= i2sg^{n+2}\delta_{s_1s_1'}\delta_{s_2s_2'}\frac{i}{\mathbf{k}^2_{1\perp}}\left(\prod_{j=1}^{n} f_{a_j a_{j+1} b_j}\right)T^{a_1}_{ji}T^{a_{n+1}}_{lk} \\ &\times\prod_{i=1}^{n}\left[\frac{2p_1^{\mu_i}p_2^{\nu_{i+1}}}{s}\Gamma^{\sigma_i}_{\mu_i\nu_{i+1}}(k_i,k_{i+1})\frac{i}{\mathbf{k}^2_{i+1\perp}}\right].\end{aligned}} \tag{3.77}$$

In equation (3.77) we have used the fact that

$$\begin{aligned}&\frac{2k_{i\perp}^{\mu_i}k_{i+1\perp}^{\nu_i}}{\lambda_{i+1}\rho_i s}\left[g_{\mu_i\nu_i}(-k_i-k_{i+1})^{\sigma_i}+g^{\sigma_i}_{\mu_i}(2k_i-k_{i+1})_{\nu_i}+g^{\sigma_i}_{\nu_i}(2k_{i+1}-k_i)_{\mu_i}\right] \\ &\qquad=\frac{2p_2^{\mu_i}p_1^{\nu_i}}{s}\Gamma^{\sigma_i}_{\mu_i\nu_i}(k_i,k_{i+1}),\end{aligned} \tag{3.78}$$

which we showed in section 3.4.2. Notice how this can be interpreted as an uncrossed genuine ladder diagram with the vertices at each horizontal rung replaced by effective vertices – this is shown in figure 19.

Again, our only leftover task is to show that *using this gauge technique*, all but the uncrossed ladders are sub-leading at LL order. We refer the interested reader to appendix E.2 where this is done.

3.6 The Reggeised gluon

We have just derived the tree-level amplitude for two quarks to scatter to two quarks and n gluons. Next, we want to consider loop corrections. We saw that in the two-loop case, we had also had to consider the diagrams in figure 15. The 'sub'-graphs on the left side of the cut can be interpreted as the start of another ladder diagram developing. The effect of this recursive structure is to 'Reggeise' the gluons in the vertical lines of diagram 19, i.e. that the t-channel gluon propagators can be replaced by the effective propagators in equation (3.79).

We begin by assuming that equation (3.69) is true. As such, the propagator of the ith vertical Reggeised gluon is given by

$$D_{\mu\nu}(\hat{s}_i,k_i^2)=\frac{ig_{\mu\nu}}{\mathbf{k}^2_{i\perp}}\left(\frac{\hat{s}_i}{\mathbf{k}^2_{\perp}}\right)^{\epsilon_g(k_i^2)}, \tag{3.79}$$

where $\hat{s}_i$ is the centre-of-mass energy flowing into the section. Since

$$\hat{s}_i=(k_{i-1}-k_{i+1})^2\approx-\rho_{i-1}\lambda_{i+1}s=\frac{\rho_{i-1}}{\rho_i}(\mathbf{k}_{i\perp}-\mathbf{k}_{i+1\perp})^2\sim\frac{\rho_{i-1}}{\rho_i}\mathbf{k}^2_{\perp}, \tag{3.80}$$

we can also write this as

$$D_{\mu\nu}(\hat{s}_i,k_i^2)=\frac{ig_{\mu\nu}}{\mathbf{k}^2_{i\perp}}\left(\frac{\rho_{i-1}}{\rho_i}\right)^{\epsilon_g(k_i^2)}. \tag{3.81}$$

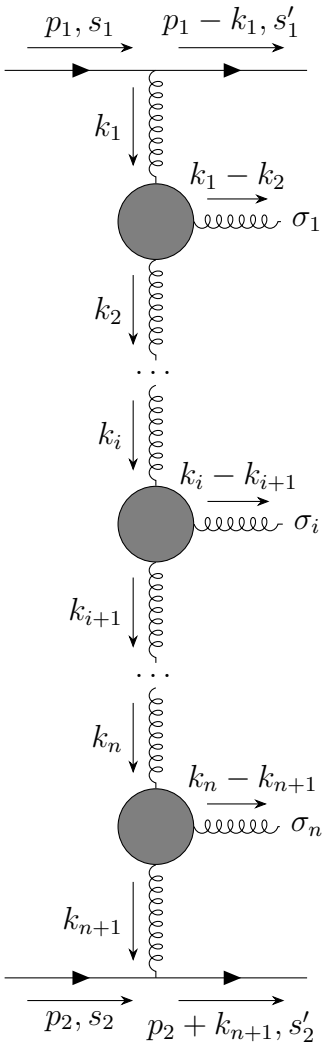

Figure 19: $qq \to qq + n \times g$ at tree-level.

We will now proceed by induction. Assuming the Reggeisation ansatz is true, the imaginary part of the colour octet exchange amplitude is given by:

$$\begin{aligned}\mathrm{Im}\big(\mathcal{A}(s,t)\big) = \frac{1}{2}\sum_{n=0}^{\infty}(-1)^n \sum_f \int d\Pi_f \mathcal{A}^{\sigma_1\ldots\sigma_n}_{2\to(n+2)}(k_1,\ldots,k_{n+1}) \\ \times \mathcal{A}^{\dagger}_{2\to(n+2)\sigma_1\ldots\sigma_n}(k_1-q,\ldots,k_{n+1}-q),\end{aligned} \tag{3.82}$$

with the phase space integral given by equation (2.55), but repeated here:

$$\sum_f \int d\Pi_f = \frac{1}{2^{4n+3}\pi^{3n+2}}\left(\prod_{i=1}^{n}\int_{\rho_{i+1}}^{1}\frac{d\rho_i}{\rho_i}\right)\int_0^1 d\rho_{n+1}\left(\prod_{j=1}^{n+1} d^2\mathbf{k}_{\perp j}\right)\delta(s\rho_{n+1} - \mathbf{k}^2_{\perp n+1}). \tag{3.83}$$

The amplitude on the left side of the cut is that of equation (3.77), but with the vertical gluons replaced with Reggeised gluons:

$$\begin{aligned}\mathcal{A}^{\sigma_1\dots\sigma_n}_{2\to(n+2)} = i2sg^{n+2}\delta_{s_1s_3}\delta_{s_2s_4}\frac{i}{\mathbf{k}^2_{1\perp}}\left(\frac{1}{\rho_1}\right)^{\epsilon_g(k_1^2)}\left(\prod_{j=1}^{n} f_{a_ja_{j+1}b_j}\right)T^{a_1}_{ji}T^{a_{n+1}}_{lk} \\ \times\prod_{i=1}^{n}\left[\frac{2p_1^{\mu_i}p_2^{\nu_{i+1}}}{s}\Gamma^{\sigma_i}_{\mu_i\nu_{i+1}}(k_i,k_{i+1})\frac{i}{\mathbf{k}^2_{i+1\perp}}\left(\frac{\rho_i}{\rho_{i+1}}\right)^{\epsilon_g(k^2_{i+1})}\right].\end{aligned} \tag{3.84}$$

Let us begin by considering the colour factor:

$$\left(\prod_{j=1}^{n} f_{a_ja_{j+1}b_j}\right)T^{a_1}_{ji}T^{a_{n+1}}_{lk}\left(\prod_{j=1}^{n} f_{a_ja_{j+1}b_j}\right)T^{c_1}_{ji}T^{c_{n+1}}_{lk}. \tag{3.85}$$

We proceed as before, sharing the contribution with the u-channel:

$$\frac{1}{2}(-1)^n\left(\prod_{i=1}^{n} f_{a_ia_{i+1}b_i}\right)\left(\prod_{j=1}^{n} f_{c_jc_{j+1}b_j}\right)(T^{c_1}T^{a_1})_{ji}\left[(T^{c_{n+1+1}}T^{a_{n+1}})_{lk}-(T^{a_{n+1}}T^{c_{n+1}})_{lk}\right]. \tag{3.86}$$

After some manipulations and applying the Jacobi identity we can form a recurrence relation, such that the above is $N/2$ times the $n-1$ case. We know that in the $n=0$ case the colour factor is given by equation . Thus in the end we obtain

$$\left(\frac{N}{2}\right)^n\frac{N}{4}T^a_{ji}T^a_{lk}. \tag{3.87}$$

Performing the contractions in equation (3.82), we get

$$\begin{aligned}\mathrm{Im}\big(\mathcal{A}(s,t)\big) = \sum_{n=0}^{\infty}\Bigg\{\sum_f\int d\Pi_f\frac{N}{4}\mathcal{A}^{(0)}(s,t)(-N)^n\frac{g^2s\mathbf{q}_\perp}{\mathbf{k}^2_{1\perp}(\mathbf{k}_{1\perp}-\mathbf{q}^2_\perp)^2}\left(\frac{1}{\rho_1}\right)^{\epsilon_g(k_1^2)+\epsilon_g((k_1-q)^2)} \\ \times\Bigg[\prod_{i=1}^{n}\frac{g^2}{\mathbf{k}^2_{i+1\perp}(\mathbf{k}_{i+1\perp}-\mathbf{q}_\perp)^2}\left(\mathbf{q}^2_\perp-\frac{\mathbf{k}^2_{i\perp}(\mathbf{k}_{i+1\perp}-\mathbf{q}_\perp)^2+(\mathbf{k}_{i\perp}-\mathbf{q}_\perp)^2\mathbf{k}^2_{i+1\perp}}{(\mathbf{k}_{i\perp}-\mathbf{k}_{i+1\perp})^2}\right) \\ \times\left(\frac{\rho_i}{\rho_{i+1}}\right)^{\epsilon_g(k^2_{i+1})+\epsilon_g((k_{i+1}-q)^2)}\Bigg]\Bigg\}.\end{aligned} \tag{3.88}$$

(with the product in the second line replaced by 1 in the $n=0$ case). Up to the Reggeisation factors, one can check that the $n=0$ and $n=1$ cases correspond to equations (3.26) and (3.59), respectively.

Again, we wish to unravel the nested ρ integrals. To do so, we make use of the convolution formula given in equation (D.11). Thus, we define:

$$\int\left(\frac{\mathrm{Im}\big(\mathcal{A}(s,t)\big)}{\mathcal{A}^{(0)}(s,t)}\right)\left(\frac{s}{\mathbf{k}^2_\perp}\right)^{-\omega-1}d\left(\frac{s}{\mathbf{k}^2_\perp}\right)=\int\frac{d^2\mathbf{k}_\perp}{\mathbf{k}^2_\perp(\mathbf{k}_\perp-\mathbf{q}_\perp)^2}\mathcal{F}(\omega,\mathbf{k}_\perp,\mathbf{q}_\perp). \tag{3.89}$$

Performing the Mellin transform and integrating over ρ_i, we are left with:

$$\begin{aligned}\mathcal{F}(\omega,\mathbf{k}_\perp,\mathbf{q}_\perp) = \sum_{n=0}^{\infty}\frac{\pi}{2}\left(\frac{\alpha_s N}{4\pi^2}\right)^{n+1}(-1)^n\frac{\mathbf{q}_\perp^2}{(\omega-\epsilon_g(-\mathbf{k}_\perp^2)-\epsilon_g(-(\mathbf{k}_\perp-\mathbf{q}_\perp)^2))}\int d^2\mathbf{k}_{n+1\perp}^2 \\ \times\prod_{i=1}^{n}\left[\int\frac{d^2\mathbf{k}_{i\perp}}{\mathbf{k}_{i\perp}^2(\mathbf{k}_{i\perp}-\mathbf{1}_\perp)^2}\frac{1}{(\omega-\epsilon_g(-\mathbf{k}_{i\perp}^2)-\epsilon_g(-(\mathbf{k}_{i\perp}-\mathbf{q}_\perp)^2)}\right. \\ \left.\times\left(\mathbf{q}_\perp^2-\frac{\mathbf{k}_{i\perp}^2(\mathbf{k}_{i+1\perp}-\mathbf{q}_\perp)^2+\mathbf{k}_{i+1\perp}^2(\mathbf{k}_{i\perp}-\mathbf{q}_\perp)^2}{(\mathbf{k}_{i\perp}-\mathbf{k}_{i+1\perp})^2}\right)\right]\delta^{(2)}(\mathbf{k}_\perp-\mathbf{k}_{n+1\perp}).\end{aligned} \tag{3.90}$$

The most convenient way to evaluate this infinite sum is to formulate it as an integral equation. We obtain:

$$\begin{aligned}\mathcal{F}(\omega,\mathbf{k}_\perp,\mathbf{q}_\perp) = \frac{\pi}{2}\frac{\alpha_s N}{4\pi^2}\frac{\mathbf{q}_\perp}{(\omega-\epsilon_g(-\mathbf{k}_\perp^2)-\epsilon_g(-(\mathbf{k}_\perp-\mathbf{q}_\perp)^2))} \\ -\frac{\alpha_s N}{4\pi^2}\int d^2\mathbf{k}'\frac{\mathcal{F}(\omega,\mathbf{k}',\mathbf{q}_\perp)}{(\omega-\epsilon_g(-\mathbf{k}_\perp^2)-\epsilon_g(-(\mathbf{k}_\perp-\mathbf{q}_\perp)^2))} \\ \times\frac{1}{\mathbf{k}'^2(\mathbf{k}'-\mathbf{q}_\perp)^2}\left(\mathbf{q}_\perp^2-\frac{\mathbf{k}_\perp^2(\mathbf{k}'-\mathbf{q}_\perp)^2+\mathbf{k}'^2(\mathbf{k}_\perp-\mathbf{q}_\perp)^2}{(\mathbf{k}_\perp-\mathbf{k}')^2}\right).\end{aligned} \tag{3.91}$$

In analogy with the scalar field theory case, the integral equation has a solution for $\mathcal{F}(\omega,\mathbf{k}_\perp,\mathbf{q}_\perp)$ that is independent of $\mathbf{k}_\perp$. Multiplying by a factor of $(\omega-\epsilon_g(-\mathbf{k}_\perp^2)-\epsilon_g(-(\mathbf{k}_\perp-\mathbf{q}_\perp)^2))$ on both sides, we get:

$$\begin{aligned}(\omega-\epsilon_g(-\mathbf{k}_\perp^2)-\epsilon_g(-(\mathbf{k}_\perp-\mathbf{q}_\perp)^2))\mathcal{F}(\omega,\mathbf{q}_\perp) = \frac{\pi}{2}\frac{\alpha_s N\mathbf{q}_\perp^2}{4\pi^2}-\frac{\alpha_s N}{4\pi^2}\mathcal{F}(\omega,\mathbf{q}_\perp)\int d^2\mathbf{k}' \\ \times\left(\frac{\mathbf{q}_\perp^2}{\mathbf{k}'^2(\mathbf{k}'-\mathbf{q}_\perp)^2}-\frac{\mathbf{k}_\perp^2}{\mathbf{k}'^2(\mathbf{k}_\perp-\mathbf{k}')^2}-\frac{(\mathbf{k}_\perp-\mathbf{q}_\perp)^2}{(\mathbf{k}'-\mathbf{q}_\perp)^2(\mathbf{k}_\perp-\mathbf{k}')^2}\right).\end{aligned} \tag{3.92}$$

Then, noticing that

$$\begin{aligned}\epsilon_g(-\mathbf{k}^2) = -\frac{\alpha_s N}{4\pi^2}\int d^2\mathbf{k}'\frac{\mathbf{k}^2}{\mathbf{k}'^2(\mathbf{k}-\mathbf{k}')^2}, \\ \epsilon_g(-(\mathbf{k}-\mathbf{q}_\perp)^2) = -\frac{\alpha_s N}{4\pi^2}\int d^2\mathbf{k}'\frac{(\mathbf{k}-\mathbf{q}_\perp)^2}{(\mathbf{k}'-\mathbf{q}_\perp)^2(\mathbf{k}-\mathbf{k}')^2},\end{aligned} \tag{3.93}$$

we can write equation (3.92) as

$$\begin{aligned}\big(\omega-\epsilon_g(-\mathbf{k}_\perp^2)-\epsilon_g(-(\mathbf{k}_\perp-\mathbf{q}_\perp)^2)\big)\mathcal{F}(\omega,\mathbf{q}_\perp) \\ = \frac{\pi}{2}\frac{\alpha_s N}{4\pi^2}+\big(\epsilon_g(-\mathbf{q}_\perp^2)-\epsilon_g(-\mathbf{k}_\perp^2)-\epsilon_g(-(\mathbf{k}_\perp-\mathbf{q}_\perp)^2)\big)\mathcal{F}(\omega,\mathbf{q}_\perp).\end{aligned} \tag{3.94}$$

We can see that a remarkable cancellation occurs, and the solution is simply

$$\mathcal{F}(\omega, \mathbf{k}_\perp, \mathbf{q}) = \frac{\pi}{2}\frac{\alpha_s N}{4\pi^2}\frac{\mathbf{q}_\perp^2}{(\omega - \epsilon_g(-\mathbf{q}_\perp^2))}. \tag{3.95}$$

So the imaginary part of the amplitude is given by:

$$\mathrm{Im}\big(\mathcal{A}(s,t)\big) = -\frac{\pi}{2}\epsilon_g(t)\left(\frac{s}{\mathbf{k}_\perp^2}\right)^{\epsilon_g(t)}\mathcal{A}^{(0)}(s,t), \tag{3.96}$$

which is the imaginary part of:

$$\mathcal{A}(s,t) = \frac{1}{2}\left(\frac{-s}{\mathbf{k}_\perp^2}\right)^{\epsilon_g(t)}\mathcal{A}^{(0)}(s,t). \tag{3.97}$$

Adding the contribution from the u-channel using $s \leftrightarrow u$ and $s \approx -u$, and noting that we have already incorporated its relative minus sign in the colour factor, we obtain:

$$\begin{aligned}\mathcal{A}(s,t) &= \frac{1}{2}\mathcal{A}^{(0)}(s,t)\left[\left(\frac{-s}{\mathbf{k}_\perp^2}\right)^{\epsilon_g(t)} + \left(\frac{s}{\mathbf{k}_\perp^2}\right)^{\epsilon_g(t)}\right] \\ &= \mathcal{A}^{(0)}(s,t)\left(\frac{s}{\mathbf{k}_\perp^2}\right)^{\epsilon_g(t)}\frac{\left[e^{-i\pi\epsilon_g(t)}+1\right]}{2}.\end{aligned} \tag{3.98}$$

Since $\epsilon_g(t) \sim \mathcal{O}(\alpha_s)$, we therefore have to LL order:

$$\boxed{\mathcal{A}(s,t) = \mathcal{A}^{(0)}(s,t)\left(\frac{s}{\mathbf{k}_\perp^2}\right)^{\epsilon_g(t)},} \tag{3.99}$$

which is exactly equation (3.69). Note that we have been careful to use the correct pole prescription for s, i.e. $(-s - i\epsilon)^{\epsilon_g(t)} = e^{-i\pi\epsilon_g(t)}|s|^{\epsilon_g(t)}$.

In view of the notation that we will use in the next section, we define

$$\epsilon_g(t) \equiv \frac{\alpha_s}{4\pi}\alpha_g^{(1)}(t) = \frac{\alpha_s N}{4\pi^2}\int d^2\mathbf{k}\frac{t}{\mathbf{k}^2(\mathbf{q}_\perp - \mathbf{k})^2} \qquad (t = -\mathbf{q}_\perp^2), \tag{3.100}$$

where $\alpha_g^{(1)}(t)$ is known as the leading-order gluon *Regge trajectory*, with $\epsilon_g(t)$ as given by equation (3.35).

We also note that here we worked with a "typical" transverse momentum $\mathbf{k}_\perp$, but since $-\mathbf{k}_\perp^2 \sim t$, we should replace $\mathbf{k}_\perp^2 \to -t$ such that our amplitude is well-defined and expressed in terms of our Lorentz invariants. The only effect of this replacement is to change the dimensionless variable in the large logarithm from $\ln(s/\mathbf{k}_\perp^2)$ to $\ln(-s/t)$.

4 Regge factorisation at higher loops

We will now briefly discuss how the LL behaviour of the elastic $2 \to 2$ scattering amplitudes, that we have derived in detail from first principles, fits into the framework of *Regge theory*. We have already seen that the resummation of the logarithms into an exponent is a result of a simple pole in Mellin space – this is known as a *Regge pole*. There are also cut singularities, *Regge cuts*, that appear at higher logarithmic orders. We will introduce these concepts in section 4.1, so that we can investigate the consequences of these singularities on the structure of the scattering amplitude.

When only a simple Regge pole contributes, the amplitude factorises. This allows us, in turn, to study the high-energy behaviour of the recent exact results up to three loops for $2 \to 2$ elastic scattering in QCD [4, 11, 12]. Up to NLL, only a single pole contributes [3]. By studying the $gg \to gg$ amplitude to this order, we confirm the result of equation (3.35) for the LO gluon Regge trajectory, and extract its NLO generalisation. We also extract the gluon NLO *impact factor*, i.e. the NLL correction to the external gluon-Reggeon vertex. We do this in section 4.3. At NNLL, we find that a factorisation result only based on the exchange of a single Reggeon fails to reproduce the fixed-order result, as expected [5–8]. Indeed, at this order Regge cuts start contributing [5–8]. In section 4.4, we then develop a colour formalism that helps disentangle the two contributions. As a first application, we isolate the contribution associated to the cut and extract the leading-colour (LC) part of the three-loop Regge trajectory.

4.1 Signature and Regge limit for $2 \to 2$ scattering amplitudes

We now revisit the analyticity properties of the S-matrix [6]. Recall the dispersion relation from section 2.2.1:

$$\mathcal{A}(s,t) = \frac{1}{\pi}\int_0^\infty \frac{d\hat{s}}{\hat{s}-s-i\epsilon}\Delta_s(\hat{s},t) + \frac{1}{\pi}\int_0^\infty \frac{d\hat{u}}{\hat{u}+s+t-i\epsilon}\Delta_u(\hat{u},t), \tag{4.1}$$

where Δ_s and Δ_u are the discontinuities of the branch cut associated with the s- and u-channels, respectively:

$$\begin{aligned}\Delta_s(s,t) &= \frac{1}{2i}\lim_{\epsilon\to 0}\left(\mathcal{A}(s+i\epsilon,t) - \mathcal{A}(s-i\epsilon,t)\right),\\ \Delta_u(u,t) &= \frac{1}{2i}\lim_{\epsilon\to 0}\left(\mathcal{A}(u+i\epsilon,t) - \mathcal{A}(u-i\epsilon,t)\right).\end{aligned} \tag{4.2}$$

Note that $\Delta_{s,u} \in \mathbb{R}$. Consider the Mellin transform of the discontinuities:

$$\begin{aligned}a_j^s(t) &= \frac{1}{\pi}\int_0^\infty \frac{d\hat{s}}{\hat{s}}\Delta_s(\hat{s},t)\left(\frac{\hat{s}}{-t}\right)^{-j},\\ \Delta_s(s,t) &= \frac{1}{2i}\int_{\gamma-i\infty}^{\gamma+i\infty} dj\, a_j^s(t)\left(\frac{s}{-t}\right)^{j},\end{aligned} \tag{4.3}$$

and similarly for a_j^u and Δ_u. We note that we can interpret these Mellin transforms as a sum over power laws.

Since $\Delta_{s,u} \in \mathbb{R}$, we have

$$(a_{j^*}^{s,u}(t))^* = a_j^{s,u}(t). \tag{4.4}$$

Substituting for $\Delta_{s,u}$ in (4.1) and swapping the order of integration, we get

$$\mathcal{A} = -\frac{1}{2i}\int_{\gamma-i\infty}^{\gamma+i\infty} \frac{dj}{\sin(\pi j)} \left(a_j^s(t) \left(\frac{-s-i\epsilon}{-t}\right)^j + a_j^u(t) \left(\frac{s+t-i\epsilon}{-t}\right)^j \right), \tag{4.5}$$

where we used

$$\int_0^\infty \frac{d\hat{s}}{\hat{s}-s-i\epsilon}\left(\frac{\hat{s}}{-t}\right)^j = -\frac{\pi}{\sin(\pi j)}\left(\frac{-s-i\epsilon}{-t}\right)^j.$$

Next we project the amplitude onto eigenstates under the crossing symmetry $s \leftrightarrow u$. This leads to amplitudes of odd and even *signature*.

$$\mathcal{A}^{(\pm)}(s,t) = \frac{1}{2}\left(\mathcal{A}(s,t) \pm \mathcal{A}(-s-t,t)\right). \tag{4.6}$$

The reason for doing so is the following. Since the full amplitude must be symmetric under gluon exchange, the even and odd signatures can only receive contributions from symmetric and antisymmetric colour exchanges, respectively. As we have seen in the previous section, a single Reggeon is an antisymmetric colour-octet state. Hence, to study the contribution of the Regge pole one can focus on the odd-signature only. We now show how unitarity allows one to simply extract this component from the full result.

If we work in the region $s > 0$ and in the Regge limit, and remember that $(-s-i\epsilon)^j = e^{-i\pi j}|s|^j$, we obtain

$$\begin{aligned}
\mathcal{A}^{(+)} &= i\int_{\gamma-i\infty}^{\gamma+i\infty} \frac{dj}{\sin(\pi j)} \cos\left(\frac{\pi j}{2}\right) a_j^{(+)}(t) e^{jL}, \\
\mathcal{A}^{(-)} &= \int_{\gamma-i\infty}^{\gamma+i\infty} \frac{dj}{\sin(\pi j)} \sin\left(\frac{\pi j}{2}\right) a_j^{(-)}(t) e^{jL},
\end{aligned} \tag{4.7}$$

where we have defined

$$a_j^{(\pm)}(t) = \frac{1}{2}(a_j^s(t) \pm a_j^u(t)), \tag{4.8}$$

and the signature-even logarithm

$$L = \ln|s/t| - i\frac{\pi}{2}. \tag{4.9}$$

By virtue of equation (4.4), we have that $a_j^{s,u}(t) \in \mathbb{R}$ for $j \in \mathbb{R}$. As a result, the coefficients of the expansion in L are purely imaginary and purely real for $\mathcal{A}^{(+)}$ and

$\mathcal{A}^{(-)}$ respectively. This implies that one can single out the odd and even signatures just by taking the real and imaginary part of the high-energy result, *provided* that the latter is expressed in terms of L in equation (4.9) and not 'just' the large logarithm $\ln|s/t|$.

If the asymptotic behaviour of a scattering amplitude is a power law, this must correspond to a simple pole in Mellin space. If this is the case, we can write

$$a_j^{(-)}(t) = \frac{1}{j-1-\alpha(t)}. \tag{4.10}$$

Such a pole is known as a *Regge pole*. Then $\mathcal{A}^{(-)}$ is

$$\mathcal{A}^{(-)}(s,t)|_{\text{Regge pole}} = \int_{\gamma-i\infty}^{\gamma+i\infty} \frac{dj}{\sin(\pi j)} \sin\left(\frac{\pi j}{2}\right) \frac{1}{j-1-\alpha(t)} e^{jL}. \tag{4.11}$$

Picking up the residue from the Regge pole, we obtain

$$\mathcal{A}^{(-)}(s,t)|_{\text{Regge pole}} = \frac{\pi}{\sin\left(\frac{\pi\alpha(t)}{2}\right)} \frac{s}{t} e^{L\alpha(t)} + \text{sub-leading}. \tag{4.12}$$

In analogy with what we did in the previous section define $\alpha(t) \equiv \alpha_g(t)$ as the *Regge trajectory* of the gluon.

In general, there are not just Regge poles but also *Regge cuts* from Fourier coefficients of the form

$$a_j^{(-)}(t) = \frac{1}{[j-1-\alpha(t)]^{1+\beta(t)}}, \tag{4.13}$$

which has a branch cut along $[-\infty, 1+\alpha(t)]$. Integration along the discontinuity leads to

$$\mathcal{A}^{(-)}(s,t)|_{\text{Regge cut}} = \frac{\pi}{\sin\left(\frac{\pi\alpha(t)}{2}\right)} \frac{s}{t} \frac{1}{\Gamma(1+\beta(t))} L^{\beta(t)} e^{L\alpha(t)} + \text{sub-leading}. \tag{4.14}$$

In the next section, we will apply these results in the context of perturbation theory. In particular, we have seen (and derived, from first principles) that the LL behaviour of $2 \to 2$ elastic scattering in the Regge limit can be described by a single Regge pole, as the sum of logarithms exponentiates into a power. Under the assumption that this structure is preserved for higher-order corrections, one can constrain the functional form of the scattering amplitude – this is known as *Regge factorisation*. We will see that, indeed, this picture of a single Regge pole can be consistently interpreted up to NLL level. We will also observe how Regge factorisation breaks down at NNLL.

4.2 Application to perturbation theory

We will write the perturbative expansion for the $2 \to 2$ scattering amplitude as[4]:

$$\mathcal{A}(s,t) = 4\pi\alpha_s \sum_{n=0}^{\infty} \left(\frac{\alpha_s}{4\pi}\right)^n \mathcal{A}^{(n)}(s,t). \tag{4.15}$$

[4]Note that this notation is slightly different from the one we used in the previous sections. We adopt it here to closely follow [6].

In the previous section we saw that we can write this as a sum of even- and odd-signature amplitudes

$$\mathcal{A}(s,t) = \mathcal{A}^{(+)}(s,t) + \mathcal{A}^{(-)}(s,t), \tag{4.16}$$

where $\mathcal{A}^{(\pm)}(s,t)$ have been defined according to equation (4.6). It was shown that, when expanded in terms of L (crucially!), the odd and even signature correspond to the real and imaginary part of the full amplitude $\mathcal{A}(s,t)$ respectively. Their expansions can therefore be written as

$$\mathcal{A}^{(\pm)}(s,t) = 4\pi\alpha_s \sum_{l,m} \left(\frac{\alpha_s}{4\pi}\right)^l L^m \mathcal{A}^{(\pm,l,m)}, \tag{4.17}$$

with $\mathcal{A}^{(-,l,m)}$ purely real and $\mathcal{A}^{(+,l,m)}$ purely imaginary.

As we have said, the Regge limit the general tree-level scattering amplitude seen in equation (3.21) (but repeated below) has odd-signature. Thus

$$\mathcal{A}^{(0)}_{ij\to ij} = \mathcal{A}^{(-,0)}_{ij\to ij} = \frac{2s}{t}(T^b_i)_{a_3a_1}(T^b_j)_{a_4a_2}\delta_{\lambda_1\lambda_3}\delta_{\lambda_2\lambda_4}, \qquad \mathcal{A}^{(+,0)}_{ij\to ij} = 0. \tag{4.18}$$

At higher orders in the LL approximations, we had derived from first principles that

$$\mathcal{A}_{ij\to ij}|_{\text{LL}} = \mathcal{A}^{(-)}_{ij\to ij}|_{\text{LL}} = \left(\frac{-s}{t}\right)^{\frac{\alpha_s}{4\pi}\alpha_g^{(1)}(t)} 4\pi\alpha_s\mathcal{A}^{(0)}_{ij\to ij}. \tag{4.19}$$

Notice how this is precisely the behaviour expected from a single Regge pole, as per equation (4.12). We interpret $\alpha_g^{(1)}(t)$ as the leading order contribution to the gluon Regge trajectory, which we expand as:

$$\alpha_g(t) = \sum_{n=0}^{\infty} \left(\frac{\alpha_s}{4\pi}\right)^n \alpha_g^{(n)}(t). \tag{4.20}$$

Next, we want to consider what happens under higher-order corrections. If we assume that we only have a single Regge pole (i.e. we consider corrections only to the exchange of a single Reggeised gluon), then there are only two types of sub-leading corrections we can have. Firstly, so-called *impact factors* are $\mathcal{O}(\alpha_s)$ modifications to the external parton and Reggeon vertex. We denote them by $C_{i/j}(t)$. Secondly, we have corrections to the gluon trajectory. Together, these corrections enter the amplitude as follows:

$$\mathcal{A}^{(-)}_{ij\to ij} = 4\pi\alpha_s\mathcal{A}^{(0)}_{ij\to ij}e^{\alpha_g(t)L}C_i(t)C_j(t) \tag{4.21}$$

This form is shown schematically in figure 20, where the impact factor and correction to the trajectory are represented as a grey blob. If we also have contributions to the amplitude coming from Regge cuts, then the factorisation above is broken. An example of such a situation is shown in figure 20b.

Figure 20: (a) Impact factors and corrections to the Regge trajectory, preserving the single Regge pole, and (b) a correction involving Regge cuts.

Analogously to the trajectory, in perturbation theory we can write the impact factors as an expansion in the strong coupling constant.

$$C_{i/j}(t) = 1 + \sum_{n=1}^{\infty} \left(\frac{\alpha_s}{4\pi}\right)^n C_{i/j}^{(n)}(t) \tag{4.22}$$

where we have set $C_{i/j}^{(0)}(t) = 1$ in accordance with the result at LL order.

Before concluding this section, it is worth mentioning that the odd-signature amplitude is more interesting from the perspective of perturbation theory. FIrst, at LL the positive signature vanishes. Also, consider

$$|\mathcal{A}|^2 = (4\pi\alpha_s)^2 \left[|\mathcal{A}^{(0)}|^2 + \left(\frac{\alpha_s}{4\pi}\right)^2 2\mathrm{Re}\left(\mathcal{A}^{(0)}\mathcal{A}^{(1)*}\right) + \mathcal{O}(\alpha_s^4)\right] \tag{4.23}$$

Since $\mathcal{A}^{(0)} = \mathcal{A}^{(-,0)}$, from the reality properties of the odd- and even-signature amplitude we must have

$$2\mathrm{Re}\left(\mathcal{A}^{(0)}\mathcal{A}^{(1)*}\right) = 2\mathcal{A}^{(-,0)}\mathcal{A}^{(-,1)}. \tag{4.24}$$

This means that for computing cross-sections, the even-signature amplitude only enters at next-to-next-to-leading order and beyond.

If we substitute the expansions (4.22) and (4.20) into the factorised amplitude in equation (4.21), we can see how the corrections enter at each logarithmic order. Taking the high-energy limit of the odd-signature $gg \to gg$ amplitudes, and isolating the LL, NLL, and NNLL parts at each loop-level, we will be able to extract the gluon Regge trajectory and impact factor up to next-to-leading order. This is the goal of the next section. We will use our results to perform consistency checks to show that

Regge factorisation indeed works for the odd-signature amplitude up to NLL, and observe that it completely breaks at NNLL order.[5]

4.3 Extracting Regge trajectories and impact factors

Our starting point is the unrenormalised QCD amplitudes for $gg \to gg$ up to three loops, that we extract from [4]. In this reference, *dimensional regularisation* is used to regulate all UV and IR divergences, with loop momenta taken to be $d = 4 - 2\epsilon$ dimensional [10]. UV divergences are removed by expressing amplitudes in terms of the renormalised strong coupling in the $\overline{\text{MS}}$-scheme:

$$\bar{\alpha}_{s,b}\mu_0^{2\epsilon} = \bar{\alpha}_s(\mu)\mu^{2\epsilon} Z\left[\bar{\alpha}_s(\mu)\right] \tag{4.25}$$

where $\bar{\alpha}_s(\mu) = \alpha_s(\mu)/4\pi$, μ is the renormalisation scale, and $Z\left[\bar{\alpha}_s(\mu)\right]$ given by equation (16) in reference [4]. We renormalise, for convenience, at the momentum-transfer scale $\mu^2 = -t$.

Let us explicitly expand the amplitude up to three loops, as per equation (4.15):

$$\mathcal{A} = 4\pi\alpha_s \left[\mathcal{A}^{(0)} + \frac{\alpha_s}{4\pi}\mathcal{A}^{(1)} + \left(\frac{\alpha_s}{4\pi}\right)^2 \mathcal{A}^{(2)} + \left(\frac{\alpha_s}{4\pi}\right)^3 \mathcal{A}^{(3)} + \dots\right]. \tag{4.26}$$

Now we make use of the reality properties of equation (4.17). Expressing the amplitude in terms of L, and taking the real part, we can extract the odd-signature amplitude. Assuming that Regge factorisation in equation (4.21) holds, we can write the odd-signature amplitude in the following form, where we have expanded the impact factor and Regge trajectory up to three loops:

$$\begin{aligned}\mathcal{A}^{(-)} = 4\pi\alpha_s \mathcal{A}^{(0)} e^{\left(\alpha_g^{(0)} + \frac{\alpha_s}{4\pi}\alpha_g^{(1)} + \left(\frac{\alpha_s}{4\pi}\right)^2 \alpha_g^{(2)} + \left(\frac{\alpha_s}{4\pi}\right)^3 \alpha_g^{(3)} + \dots\right) L} \\ \times \left[1 + \frac{\alpha_s}{4\pi}C^{(1)} + \left(\frac{\alpha_s}{4\pi}\right)^2 C^{(2)} + \left(\frac{\alpha_s}{4\pi}\right)^3 C^{(3)} + \dots\right] \\ \times \left[1 + \frac{\alpha_s}{4\pi}C^{(1)} + \left(\frac{\alpha_s}{4\pi}\right)^2 C^{(2)} + \left(\frac{\alpha_s}{4\pi}\right)^3 C^{(3)} + \dots\right].\end{aligned} \tag{4.27}$$

We have set $C_i(t) = C_j(t) = C(t)$, since in the gluonic channel $gg \to gg$ the impact factors are the same for the upper and lower gluon line.

Multiplying out equation (4.27), we have at one-loop:

$$\mathcal{A}^{(-,1)} = \mathcal{A}^{(0)}\left[\underbrace{2C^{(1)}}_{\text{NLL}} + \underbrace{\alpha_g^{(1)} L}_{\text{LL}}\right], \tag{4.28}$$

at two loops:

$$\mathcal{A}^{(-,2)} = \mathcal{A}^{(0)}\left[\underbrace{{C^{(1)}}^2 + 2C^{(2)}}_{\text{NNLL}} + \underbrace{L(\alpha_g^{(2)} + 2\alpha_g^{(1)}C^{(1)})}_{\text{NLL}} + \underbrace{\frac{{\alpha_g^{(1)}}^2 L^2}{2}}_{\text{LL}}\right], \tag{4.29}$$

[5] Were we to consider the even signature amplitude, we would notice that in this case the Regge factorisation is broken at NLL [7, 8].

and finally, at three loops:

$$\mathcal{A}^{(-,3)} = \mathcal{A}^{(0)}\Bigg[\underbrace{2C^{(1)}C^{(2)} + 2C^{(3)}}_{\text{NNNLL}} + \underbrace{L\left(\alpha_g^{(3)} + \alpha_g^{(1)}{C^{(1)}}^2 + 2\alpha_g^{(2)}C^{(1)} + 2\alpha_g^{(1)}C^{(2)}\right)}_{\text{NNLL}} + \underbrace{L^2\left(\alpha_g^{(1)}\alpha_g^{(2)} + {\alpha_g^{(1)}}^2 C^{(1)}\right)}_{\text{NLL}} + \underbrace{\frac{{\alpha_g^{(1)}}^3 L^3}{6}}_{\text{LL}}\Bigg]. \tag{4.30}$$

To check the predictions of equations (4.28), (4.29), and (4.30), and to extract the impact factors and Regge trajectories, we need to take the high-energy limit of the $gg \to gg$ amplitudes. After this, we match the results at each loop level. The amplitudes are given by a class of functions known as *Harmonic Polylogarithms* (HPLs). In order to take the high energy limit, we need to obtain their small x expansions. We refer the reader to appendix F for a systematic way of doing this, as well as a brief account of their definition and properties.

Isolating the LL contribution to the one-loop odd-signature amplitude, we obtain using equation (4.28) the leading-order Regge trajectory:

$$\boxed{\begin{aligned}\alpha_g^{(1)}(t) = \frac{2N}{\epsilon} - \frac{N\pi^2}{6}\epsilon - \frac{14N\zeta_3}{3}\epsilon^2 - \frac{47N\pi^4}{720}\epsilon^3 \\ + \frac{1}{90}\left[35N\pi^2\zeta_3 - 1116N\zeta_5\right]\epsilon^4 + \mathcal{O}(\epsilon^5).\end{aligned}} \tag{4.31}$$

We note that this agrees with the result in equation (3.35) in the previous section, as it should. We also stress that the right hand side does not depend on t because we are setting $\mu^2 = -t$. Were we to use a different scale, explicit $\ln(-\mu^2/t)$ terms would appear, as seen in equation (3.35).

As a sanity check, we can see if equation (4.31) correctly predicts the LL behaviour at two and three loops. We found this to be the case. This serves as a verification that Regge factorisation works at LL level up to three loops. Of course, we know it holds up to arbitrary loop-order, since we derived this from first principles.

Next, sticking with equation (4.28), we consider the behaviour of the one-loop amplitude at NLL order. Using our result for $\alpha_g^{(1)}(t)$, we can extract the impact

factor:

$$
\begin{aligned}
C^{(1)}(t) = &-\frac{2N}{\epsilon^2} + \frac{1}{\epsilon}\left[-\frac{1}{3}(11N) + \frac{2n_f}{3}\right] + \frac{5n_f}{9} + N\left(-\frac{67}{18} + \frac{2\pi^2}{3}\right) \\
&+ \epsilon\left[n_f\left(\frac{28}{27} - \frac{\pi^2}{36}\right) + N\left(-\frac{202}{27} + \frac{11\pi^2}{72} + \frac{17\zeta_3}{3}\right)\right] \\
&+ \epsilon^2\left[n_f\left(\frac{164}{81} - \frac{5\pi^2}{108} - \frac{7\zeta_3}{9}\right) + N\left(-\frac{1214}{81} + \frac{67\pi^2}{216}\right.\right. \\
&\left.\left. + \frac{41\pi^4}{720} + \frac{77\zeta_3}{18}\right)\right] + \epsilon^3\left[n_f\left(\frac{976}{243} - \frac{7\pi^2}{81} - \frac{47\pi^4}{4320} - \frac{35\zeta_3}{27}\right)\right. \\
&\left. + N\left(-\frac{7288}{243} + \frac{101\pi^2}{162} + \frac{517\pi^4}{8640} + \frac{469\zeta_3}{54} - \frac{59\pi^2\zeta_3}{36} + \frac{67\zeta_5}{5}\right)\right] \\
&+ \epsilon^4\left[n_f\left(\frac{5840}{729} - \frac{41\pi^2}{243} - \frac{47\pi^4}{2592} - \frac{196\zeta_3}{81} + \frac{7\pi^2\zeta_3}{108} - \frac{31\zeta_5}{15}\right)\right. \\
&+ N\left(-\frac{43736}{729} + \frac{607\pi^2}{486} + \frac{3149\pi^4}{25920} - \frac{\pi^6}{4320} + \frac{1414\zeta_3}{81}\right. \\
&\left.\left. - \frac{77\pi^2\zeta_3}{216} - \frac{70\zeta_3^2}{9} + \frac{341\zeta_5}{30}\right)\right] + \mathcal{O}(\epsilon^5).
\end{aligned}
\tag{4.32}
$$

Inspecting equation (4.29), if we take the NLL contribution to the two-loop amplitudes and use our results for $\alpha_g^{(1)}(t)$ and $C^{(1)}(t)$, we can extract the NLO trajectory. Our result is shown in equation (4.33)

$$
\begin{aligned}
\alpha_g^{(2)}(t) = &\frac{56Nn_f}{27} + \frac{1}{\epsilon^2}\left[\frac{11N^2}{3} - \frac{2Nn_f}{3}\right] \\
&+ \frac{1}{\epsilon}\left[\frac{10Nn_f}{9} + N^2\left(-\frac{67}{9} + \frac{\pi^2}{3}\right)\right] + N^2\left(-\frac{404}{27} + 2\zeta_3\right) \\
&+ \epsilon\left[Nn_f\left(\frac{328}{81} - \frac{5\pi^2}{27} - 12\zeta_3\right) + N^2\left(-\frac{2428}{81} + \frac{67\pi^2}{54}\right.\right. \\
&\left.\left. + \frac{\pi^4}{30} + 66\zeta_3\right)\right] + \epsilon^2\left[Nn_f\left(\frac{1952}{243} - \frac{28\pi^2}{81} - \frac{211\pi^4}{1080}\right.\right. \\
&\left.\left. - \frac{680\zeta_3}{27}\right) + N^2\left(-\frac{14576}{243} + \frac{202\pi^2}{81} + \frac{2321\pi^4}{2160}\right.\right. \\
&\left.\left. + \frac{4556\zeta_3}{27} - \frac{71\pi^2\zeta_3}{9} - 82\zeta_5\right)\right] + \mathcal{O}(\epsilon^3)
\end{aligned}
\tag{4.33}
$$

Notice from equation (4.30) that we have found all the terms necessary to predict the NLL behaviour of the three loops. Again, we find the prediction and the exact result taken from the amplitude in the high-energy limit to be in complete agreement. We have therefore verified that Regge factorisation at NLL order works up to at least

three loops. This is expected, as Regge factorisation is known to hold at NLL at arbitrary loop order [3].

To make further progress, we extract the NNLL behaviour at two and three loops. However, in doing so, we immediately run into a problem – the colour structures that appear are no longer just that of the antisymmetric colour octet, i.e. the colour factor at tree level. In other words, the NNLL limit of the fixed-order result does not factorise on the tree-level. This indicates that the Regge factorisation is broken. The NNLL parts of the amplitudes are, in general, quite difficult to disentangle, partially due to the choice of the so-called *colour basis*. In the following section, our goal is to construct a more convenient colour basis for the purpose of Regge theory, consisting of projectors to irreducible representations of SU(N). Changing the results to this (orthogonal) projector basis will allow us to isolate the antisymmetric colour octet part of the NNLL amplitude, and attempt to extract the gluon Regge trajectory at next-to-next-to-leading order ($\alpha_g^{(3)}(t)$). While work on this is still in progress, initial analysis has proven fruitful.

While in this dissertation we consider just the exact results in the gluonic channel, the more long term goal is to repeat the analysis for the remaining cases of elastic $2 \to 2$ scattering. For these, exact results also exist [11, 12]. As such, we will construct a projector basis not just for $gg \to gg$, but for the general case of elastic $2 \to 2$ scattering in QCD.

4.4 Colour decomposition

Scattering amplitudes can be viewed as vectors in colour space. The colour decomposition of a scattering amplitude $\mathcal{A}$ takes the schematic form:

$$\mathcal{A} = \sum_i \mathcal{A}^{[i]} \mathcal{C}_i, \tag{4.34}$$

where the $\{\mathcal{C}_i\}$ are known as the *colour basis*, containing all the colour information. The $\{\mathcal{A}^{[i]}\}$ are known as colour-ordered *partial amplitudes*, which only depend on the space-time degrees of freedom and not on colour. We consider the general case of elastic $2 \to 2$ scattering, in which case the amplitudes can exhibit the colour-index structures shown in figure 21.

While we work with general SU(N), we label the irreducible representations of the colour degrees of freedom using their dimensions in the $N = 3$ case; hence, quark colour indices transform under the $\mathbf{3}$, and gluons under the $\mathbf{8}$. We can view the amplitudes above as acting on the tensor product of the representation vector spaces of the incoming two particles. Thus 21a acts on $\mathbf{8} \otimes \mathbf{8}$, 21b acts on $\mathbf{3} \otimes \mathbf{3}$, 21c acts on $\mathbf{3} \otimes \overline{\mathbf{3}}$, and finally 21d acts on $\mathbf{3} \otimes \mathbf{8}$. Note that the remaining cases $\bar{q}\bar{q} \to \bar{q}\bar{q}$ and $\bar{q}g \to \bar{q}g$ scattering can be obtained by complex conjugation of 21b and 21d, respectively.

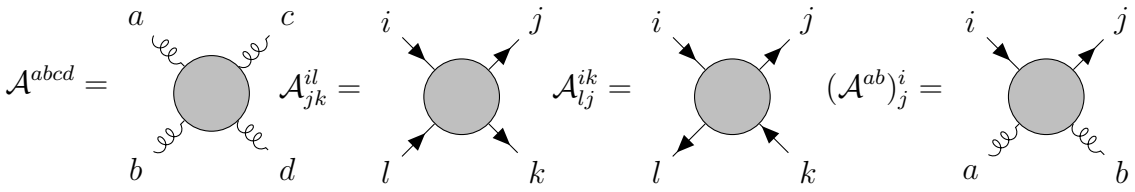

(a) $gg \to gg$ (b) $qq \to qq$ (c) $q\bar{q} \to q\bar{q}$ (d) $qg \to qg$

Figure 21: Colour index structure of general elastic $2 \to 2$ scattering amplitudes.

Our goal is to construct a particularly convenient colour basis for the purpose of Regge theory. This is an orthonormal basis $\{\mathcal{C}_i\}$ constructed out of projectors to the irreducible representations within the tensor product space. This essentially amounts to block-diagonalising the amplitude, with each block acting on the representation vector space of an irreducible representation. Our approach in performing these decompositions borrows from [13] and [14]. This consists of identifying the *primitive invariant tensors* of the symmetry group and using them to construct *invariant matrices* that act on the tensor product spaces. We can then construct projection operators to reduced representations from characteristic equations for the invariant matrices.

It will be useful to recall, without proof, some properties of projector operators. Consider a hermitian matrix M. By virtue of it being hermitian, it is diagonalisable. Let λ_i be its ith distinct eigenvalue. Then the operator:

$$P_i = \prod_{j \neq i} \frac{M - \lambda_j \mathbf{1}}{\lambda_i - \lambda_j}, \tag{4.35}$$

acts like the identity on the eigenspace of λ_i, and zero elsewhere. They are projectors

$$P_i^2 = P_i, \tag{4.36}$$

and satisfy completeness and orthonormality relations

$$\begin{aligned} \sum_i P_i &= \mathbf{1} \\ P_i P_j &= \delta_{ij} P_j \quad \text{(no sum)}. \end{aligned} \tag{4.37}$$

Finally, the dimension of the eigenspace of λ_i is the trace of the corresponding projector operator:

$$d_i \equiv \dim(\text{Eig}(\lambda_i)) = \text{Tr}(P_i). \tag{4.38}$$

Before proceeding, we note that conventions for colour algebra are listed in appendix B. We normalise the SU(N) fundamental generators such that $T_F = \frac{1}{2}$ and

$C_F = \frac{N^2-1}{2N}$. We will also make use of the *Fierz identity*:

$$(T^a)_{ij}(T^a)_{kl} = \frac{1}{2}\delta_{il}\delta_{jk} - \frac{1}{2N}\delta_{ij}\delta_{kl}, \tag{4.39}$$

from which we can derive the following helpful relations:

$$\begin{aligned} \mathrm{Tr}(AT^a)\mathrm{Tr}(BT^a) &= \frac{1}{2}\mathrm{Tr}(AB) - \frac{1}{2N}\mathrm{Tr}(A)\mathrm{Tr}(B), \\ \mathrm{Tr}(AT^aBT^a) &= \frac{1}{2}\mathrm{Tr}(A)\mathrm{Tr}(B) - \frac{1}{2N}\mathrm{Tr}(AB). \end{aligned} \tag{4.40}$$

The above relations are especially useful as a computational aid if one first systematically converts expressions into traces using

$$\begin{aligned} f^{abc} &= -2i\,\mathrm{Tr}\left([T^a, T^b]T^c\right) \\ d^{abc} &= 2\,\mathrm{Tr}\left(\left\{T^a, T^b\right\}T^c\right). \end{aligned} \tag{4.41}$$

4.4.1 $gg \to gg$

We begin with the gluonic channel, as this is the projector basis we have used to extract the gluon Regge trajectories and impact factors. Applying the Littlewood-Richardson rule (see e.g. [13]), we can perform a Clebsch-Gordan decomposition in general SU(N). We combine two colour octets, and obtain:

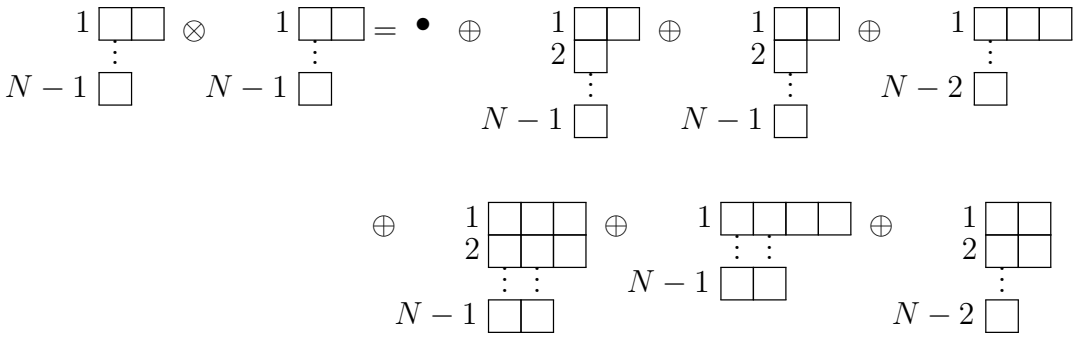

(4.42)

They correspond to the following irreducible representations, respectively:

$$\mathbf{8} \otimes \mathbf{8} = \mathbf{1} \oplus \mathbf{8}_a \oplus \mathbf{8}_s \oplus \mathbf{10} \oplus \overline{\mathbf{10}} \oplus \mathbf{27} \oplus \mathbf{0} \tag{4.43}$$

From the Young tableaux, we can also work out the dimensions of these irreducible representations in general SU(N):

$$\begin{aligned} d_{\mathbf{1}} &= 1 \\ d_{\mathbf{8}_a} &= N^2 - 1 \\ d_{\mathbf{8}_s} &= N^2 - 1 \\ d_{\mathbf{10}} &= \frac{1}{4}(N-2)(N-1)(N+1)(N+2) \\ d_{\overline{\mathbf{10}}} &= \frac{1}{4}(N-2)(N-1)(N+1)(N+2) \\ d_{\mathbf{27}} &= \frac{1}{4}(N-1)N^2(N+3) \\ d_{\mathbf{0}} &= \frac{1}{4}(N-3)N^2(N+1) \end{aligned} \tag{4.44}$$

which all satisfy the sanity check $N = 3$. Note that the last one vanishes for $N = 3$, where it has dimension "**0**".

The primitive invariant tensors at our disposal are δ_{ab}, f_{abc}, and d_{abc}. Using these, we can write down the following invariant matrices:

$$\delta_{ab}\delta_{cd} = \tag{4.45}$$

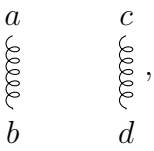

$$\frac{1}{2}\left(\delta_{ac}\delta_{bd} \pm \delta_{ad}\delta_{bc}\right) = \frac{1}{2}\left(\quad \pm \quad \right) \equiv \begin{cases} S_{abcd} & (+) \\ A_{abcd} & (-) \end{cases}, \tag{4.46}$$

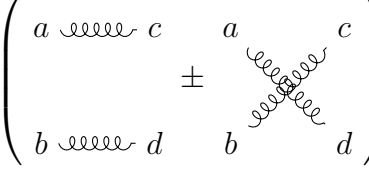

$$f_{abe}f_{ecd} = \tag{4.47}$$

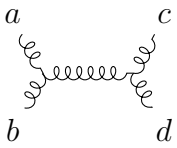

$$d_{abe}d_{ecd} = \tag{4.48}$$

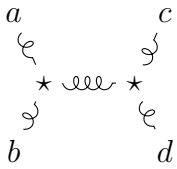

A convenient choice to complete the basis turns out to be:

$$(W_-)_{abcd} \equiv \mathrm{Tr}(T^aT^dT^bT^c) = \tag{4.49}$$

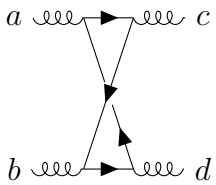

$$(W_+)_{abcd} \equiv \mathrm{Tr}(T^aT^cT^bT^d) = \tag{4.50}$$

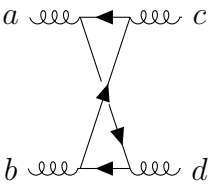

The trace operator (4.45) corresponds to the projector to the singlet:

$$P_{\mathbf{1}} = \frac{1}{N^2-1}\delta_{ab}\delta_{cd}, \tag{4.51}$$

and we can identify equations (4.47) and (4.48) as the projectors to the antisymmetric $\mathbf{8}_a$ and symmetric $\mathbf{8}_s$, respectively:

$$P_{\mathbf{8}_a} = \frac{1}{N}f_{abe}f_{ecd}, \tag{4.52}$$

$$P_{\mathbf{8}_s} = \frac{N}{N^2-4} d_{abe} d_{ecd}. \tag{4.53}$$

It is straightforward to check that these are indeed projectors (see equation (4.36)), and that the trace yields what is expected from equation (4.44).

Next, we observe that operators S and A in equation (4.46) project to the (reducible) symmetric and antisymmetric subspaces, respectively. Using equation (4.44) and noting that

$$\mathrm{Tr}(S) = \frac{N^2(N^2-1)}{2}, \qquad \mathrm{Tr}(A) = \frac{(N^2-1)(N^2-2)}{2},$$

the only option we have is:

$$\begin{aligned} S &= P_{\mathbf{1}} + P_{\mathbf{8}_s} + P_{\mathbf{27}} + P_{\mathbf{0}}, \\ A &= P_{\mathbf{8}_a} + P_{\mathbf{10}} + P_{\overline{\mathbf{10}}}. \end{aligned} \tag{4.54}$$

Our task now is to decompose the spaces:

$$\begin{aligned} S_\perp &\equiv S - P_{\mathbf{1}} + P_{\mathbf{8}_s} = P_{\mathbf{27}} + P_{\mathbf{0}}, \\ A_\perp &\equiv A - P_{\mathbf{8}_a} = P_{\mathbf{10}} + P_{\overline{\mathbf{10}}}. \end{aligned} \tag{4.55}$$

We can accomplish this by using the projector formalism introduced earlier. Consider the operator $Q \equiv 4W_- = 4\mathrm{Tr}(T^a T^d T^b T^c)$. Using the relations in equation (4.40), we can show that:

$$Q^2 = \mathbf{1} - \frac{N^2-1}{N} P_{\mathbf{1}} - \frac{N^2-4}{N^2} P_{\mathbf{8}_s} - P_{\mathbf{8}_a}. \tag{4.56}$$

It is then quick to spot from orthonormality of the projectors (4.37) that this acts like the identity on the subspaces (4.55):

$$Q^2 S_\perp = S_\perp, \qquad Q^2 A_\perp = A_\perp. \tag{4.57}$$

This tells us that Q has eigenvalues ± 1 when acting on each of $S_\perp$ and $A_\perp$. Using equation (4.35) we can now construct four projectors:

$$\left(\frac{\mathbf{1} \pm Q}{2}\right) S_\perp, \qquad \left(\frac{\mathbf{1} \pm Q}{2}\right) A_\perp. \tag{4.58}$$

After some work, and checking the dimensions of the resulting subspaces to identify the irreducible representations, this yields the remaining projectors:

$$P_{\mathbf{10}} = \frac{1}{2}(A_{abcd} - P_{\mathbf{8}_a\, abcd}) + W_{+abcd} - W_{-abcd}, \tag{4.59}$$

$$P_{\overline{\mathbf{10}}} = \frac{1}{2}(A_{abcd} - P_{\mathbf{8}_a\, abcd}) - (W_{+abcd} - W_{-abcd}), \tag{4.60}$$

$$P_{\mathbf{27}} = -\frac{(N-1)}{2N} P_{\mathbf{1}abcd} - \frac{(N-2)}{2N} P_{\mathbf{8}_s abcd} + \frac{1}{2} S_{abcd} + W_{-abcd} + W_{+abcd}, \tag{4.61}$$

$$P_{\mathbf{0}} = -\frac{(N+1)}{2N} P_{\mathbf{1}abcd} - \frac{(N+2)}{2N} P_{\mathbf{8}_s abcd} + \frac{1}{2} S_{abcd} - (W_{+abcd} + W_{-abcd}). \tag{4.62}$$

This completes the decomposition in the gluonic channel. For our purposes, this suffices – however, as mentioned, the more long-term intention is to extract the high-energy behaviour for all cases of $2 \to 2$ scattering in QCD. We thus present the remaining colour compositions below.

4.4.2 $qq \to qq$

For the case of elastic scattering of two quarks, the colour decomposition is more straightforward. Using the Littlewood-Richardson rule, we can perform the Clebsch-Gordan decomposition:

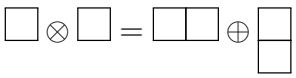

$$\mathbf{3} \otimes \mathbf{3} = \mathbf{6} \oplus \bar{\mathbf{3}} \tag{4.63}$$

In general, the amplitude has to be a linear combination of the two *invariant matrices* shown in figure (4.64).

$$\mathbf{1}^{il}_{jk} \equiv \delta^i_j \delta^l_k = \quad , \qquad \sigma_{(12)}{}^{il}_{jk} \equiv \delta^i_k \delta^l_j = \quad . \tag{4.64}$$

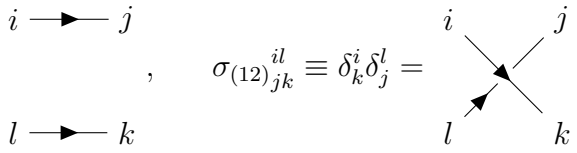

When acting on a tensor $\phi^{jk} \in \mathbf{3} \otimes \mathbf{3}$, the operator $\sigma_{(12)}$ permutes the two indices, while $\mathbf{1}$ leaves them unchanged. Inspecting the Young tableaux, the $\mathbf{6}$ irreducible representation is fully symmetric with respect to $j \leftrightarrow k$, whereas the $\bar{\mathbf{3}}$ is fully antisymmetric. We can thus split up a general tensor ϕ^{jk} into (anti)symmetric parts that transform under the corresponding irreducible representation:

$$\phi^{jk} = \underbrace{\frac{1}{2}(\phi^{jk} + \phi^{kj})}_{\mathbf{6}} + \underbrace{\frac{1}{2}(\phi^{jk} - \phi^{kj})}_{\bar{\mathbf{3}}}. \tag{4.65}$$

Evidently, the projectors to the irreducible representations are given by:

$$\begin{aligned} P_{\mathbf{6}} &= \frac{1}{2}(\mathbf{1} + \sigma_{(12)}), \\ P_{\bar{\mathbf{3}}} &= \frac{1}{2}(\mathbf{1} - \sigma_{(12)}), \end{aligned} \tag{4.66}$$

with dimensions:

$$\begin{aligned} d_{\mathbf{6}} &= \mathrm{Tr}(P_{\mathbf{6}}) = \frac{N(N+1)}{2}, \\ d_{\bar{\mathbf{3}}} &= \mathrm{Tr}(P_{\bar{\mathbf{3}}}) = \frac{N(N-1)}{2}. \end{aligned} \tag{4.67}$$

The dimensions can also quickly be verified from the Young tableaux.

4.4.3 $q\bar{q} \to q\bar{q}$

The decomposition of $\mathbf{3} \otimes \bar{\mathbf{3}}$ contains the adjoint representation and the singlet:

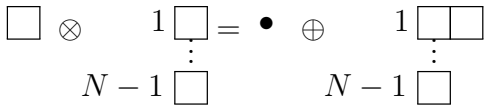

(4.68)

$$\mathbf{3} \otimes \bar{\mathbf{3}} = \mathbf{1} \oplus \mathbf{8}$$

We can write down the invariant matrices, corresponding to an identity operator and a trace operator:

$$\mathbf{1}^{ik}_{lj} \equiv \delta^i_j \delta^k_l =$$

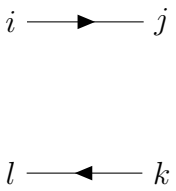

$$, \qquad T^{ik}_{lj} \equiv \delta^i_l \delta^k_j =$$

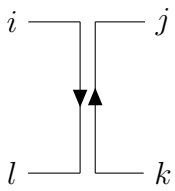

. (4.69)

Consider T acting on the entire representation vector space, twice:

$$T^{im}_{ln} T^{nk}_{mj} = \delta^i_l \delta^m_n \delta^n_m \delta^k_j = N T^{ik}_{lj}. \tag{4.70}$$

We observe that the eigenvalues of T are 0 and N. Now we can construct the projectors to the irreducible representations using equation (4.35), which yields:

$$\begin{aligned} (P_{\mathbf{8}})^{ik}_{jl} &= \delta^i_j \delta^k_l - \frac{1}{N} \delta^i_l \delta^k_j, \\ (P_{\mathbf{1}})^{ik}_{jl} &= \frac{1}{N} \delta^i_l \delta^k_j. \end{aligned} \tag{4.71}$$

The dimensions are what we would expect of the adjoint and the singlet:

$$\begin{aligned} d_{\mathbf{8}} &= \mathrm{Tr}(P_{\mathbf{8}}) = N^2 - 1, \\ d_{\mathbf{1}} &= \mathrm{Tr}(P_{\mathbf{1}}) = 1. \end{aligned} \tag{4.72}$$

4.4.4 $qg \to qg$

For the remaining case, we will quickly sketch how to get to the result. It is very similar to the $gg \to gg$ case but slightly less involved. The decomposition is:

$$\mathbf{8} \otimes \mathbf{3} = \mathbf{15} \oplus \mathbf{3} \oplus \bar{\mathbf{6}}. \tag{4.73}$$

The projector to the $\mathbf{3}$ corresponds to an s-channel quark:

$$P_{\mathbf{3}} = \frac{2N}{N^2-1} \left(T^a T^b\right)^i_j . \tag{4.74}$$

Then, we notice that the operator $2\left(T^b T^a\right)^i_j$ acts like the identity on the leftover part of the space $\mathbf{1} - P_{\mathbf{3}}$, allowing us to construct the two remaining projectors:

$$\begin{aligned} P_{\mathbf{15}} &= \frac{1}{2}\delta_{ab}\delta^i_j - \frac{1}{N+1}\left(T^a T^b\right)^i_j + \left(T^b T^a\right)^i_j , \\ P_{\bar{\mathbf{6}}} &= \frac{1}{2}\delta_{ab}\delta^i_j - \frac{1}{N-1}\left(T^a T^b\right)^i_j - \left(T^b T^a\right)^i_j . \end{aligned} \tag{4.75}$$

Their traces are:

$$\begin{aligned} d_{\mathbf{15}} &= \mathrm{Tr}\left(P_{\mathbf{15}}\right) = \frac{1}{2}(N-1)N(N+2), \\ d_{\mathbf{3}} &= \mathrm{Tr}\left(P_{\mathbf{3}}\right) = N, \\ d_{\bar{\mathbf{6}}} &= \mathrm{Tr}\left(P_{\bar{\mathbf{6}}}\right) = \frac{1}{2}(N-2)N(N+1). \end{aligned} \tag{4.76}$$

4.5 Leading-colour gluon Regge trajectory at three loops

As advertised, we will now use the colour formalism we have just developed to attempt to extract the trajectory $\alpha_g^{(3)}(t)$ from the NNLL parts of the two- and three-loop amplitudes, where we have observed Regge factorisation to break down. We are still investigating this, but are able to present a subset of the result here – namely the leading-colour (LC) part.

First, we note that the $gg \to gg$ amplitudes are given in reference [4] in the following colour basis:

$$\begin{aligned} C_1 &= \mathrm{Tr}(T^{a_1}T^{a_2}T^{a_3}T^{a_4}) + \mathrm{Tr}(T^{a_1}T^{a_4}T^{a_3}T^{a_2}), \\ C_2 &= \mathrm{Tr}(T^{a_1}T^{a_2}T^{a_4}T^{a_3}) + \mathrm{Tr}(T^{a_1}T^{a_3}T^{a_4}T^{a_2}), \\ C_3 &= \mathrm{Tr}(T^{a_1}T^{a_3}T^{a_2}T^{a_4}) + \mathrm{Tr}(T^{a_1}T^{a_4}T^{a_2}T^{a_3}), \\ C_4 &= \mathrm{Tr}(T^{a_1}T^{a_2})\mathrm{Tr}(T^{a_3}T^{a_4}), \\ C_5 &= \mathrm{Tr}(T^{a_1}T^{a_3})\mathrm{Tr}(T^{a_2}T^{a_4}), \\ C_6 &= \mathrm{Tr}(T^{a_1}T^{a_4})\mathrm{Tr}(T^{a_2}T^{a_3}). \end{aligned} \tag{4.77}$$

It is convenient to construct a change-of-basis matrix to convert the above basis into a basis spanned by the projectors $\{P_i\}$ defined in section 4.4.1. To do so, we write:

$$\mathcal{A} = \sum_i \mathcal{A}^{[i]} C_i = \sum_i \mathcal{A}'^{[i]} P_i, \tag{4.78}$$

and construct a change of basis matrix M such that

$$\mathcal{A}'^{[i]} = M_{ij}\mathcal{A}^{[j]} \tag{4.79}$$

For definiteness, we order the projectors as $\{P_{\mathbf{1}}, P_{\mathbf{8}_a}, P_{\mathbf{8}_s}, P_{\mathbf{10}}, P_{\overline{\mathbf{10}}}, P_{\mathbf{27}}, P_{\mathbf{0}}\}$. Note that the basis in equation (4.77) is not complete, so M will not be invertible.

We now describe how to obtain M. This is made computationally easier by first converting all the projectors to traces using equations (4.41) – then, one can use equations (4.40) to take inner products between the projectors and the basis elements above. Doing this, one obtains:

$$M = \begin{pmatrix} -\frac{1}{2N} & \frac{N^2-1}{2N} & \frac{N^2-1}{2N} & \frac{1}{4} & \frac{N^3-N}{4N} & \frac{1}{4} \\ 0 & \frac{N}{4} & -\frac{N}{4} & \frac{1}{4} & 0 & -\frac{1}{4} \\ -\frac{1}{N} & \frac{N^2-4}{4N} & \frac{N^2-4}{4N} & \frac{1}{4} & 0 & \frac{1}{4} \\ 0 & 0 & 0 & \frac{1}{4} & 0 & -\frac{1}{4} \\ 0 & 0 & 0 & \frac{1}{4} & 0 & -\frac{1}{4} \\ \frac{1}{2} & 0 & 0 & \frac{1}{4} & 0 & \frac{1}{4} \\ -\frac{1}{2} & 0 & 0 & \frac{1}{4} & 0 & \frac{1}{4} \end{pmatrix} \tag{4.80}$$

We proceed by making the assumption that the antisymmetric colour octet, i.e. the part of the amplitude proportional to $P_{\mathbf{8}_a}$, is not 'polluted' by contributions from Regge cuts at least to leading-colour. This allows us to use the Regge-factorised form (4.21) for this contribution. Working in the projector basis, taking the NNLL part of equation (4.29) and isolating the antisymmetric colour octet, we can obtain $C^{(2)}(t)$. This allows us to extract $\alpha_g^{(3)}(t)$ from the NNLL part of equation (4.30), again only keeping the term proportional to $P_{\mathbf{8}_a}$.

We obtain the following for the renormalised leading-colour gluon Regge trajectory at 3-loops.

$$\begin{aligned} \alpha_g^{(3)}(t) = N^3 \Bigg[& -\frac{242}{27\epsilon^3} + \frac{1}{\epsilon^2}\left(\frac{2086}{81} - \frac{22\pi^2}{27}\right) + \frac{1}{\epsilon}\Bigg(-\frac{44\zeta_3}{9} + \frac{268\pi^2}{81} - \frac{245}{9} \\ & - \frac{22\pi^4}{135}\Bigg) - \frac{20\pi^2\zeta_3}{9} + \frac{6664\zeta_3}{27} - 16\zeta_5 + \frac{77\pi^4}{270} + \frac{1598\pi^2}{243} - \frac{297029}{1458}\Bigg] \\ & \times \left(1 + \mathcal{O}\left(\frac{1}{N^2}\right)\right) \end{aligned} \tag{4.81}$$

We stress once again that the right-hand side does not depend on t because we are setting $\mu^2 = -t$. Were we to keep μ general, $\ln(-\mu^2/t)$ terms would appear.

We now comment on our result (4.81). First, we note that the leading-colour gluon Regge trajectory that we have found agrees with [4], where it was extracted via a different formalism. Interestingly, we also note that the colour structure proportional to n_f agrees with the result in [4], even at sub-leading colour. The sub-leading colour part for pure gluodynamics $n_f = 0$ still needs to be investigated.

Of course, this analysis has relied on the assumption that the antisymmetric colour octet is not polluted by contributions from Regge cuts. So it is interesting to note that indeed any such contribution does not seem to enter at the LC level, and neither does it seem to enter the fermionic part at the SLC level.

5 Conclusion

In this dissertation, we have studied the high-energy limit of QCD, particularly in the case of elastic $2 \to 2$ scattering. We re-derived from first principles the all-order result at the leading-logarithmic level. We have done this first in a simpler scalar field theory, and then in full QCD. By matching against results for the one- and two-loop $gg \to gg$ scattering amplitudes, we have extracted the leading-order and next-to-leading-order gluon Regge trajectory and impact factor. Using these results and comparing the Regge prediction against the three-loop $gg \to gg$ scattering amplitudes [4], we have verified that Regge factorisation works at NLL level up to at least three loops.

We observed that Regge factorisation completely breaks down at NNLL, where Regge cuts start playing a role. However, their colour structure is different from the one of the Regge pole [7, 8]. Thus, one should be able to disentangle the contributions from the Regge poles and Regge cuts by carefully analysing the colour structure of the result. We then studied a colour formalism that may help in doing so. Using this formalism, we have been able to isolate the contribution of the Regge pole at NNLL, although, for the time being, only at the leading-colour level. As a consequence, we have been able to extract the leading-colour Regge trajectory at 3-loops, and found perfect agreement with the findings of [4], where it was extracted via a different formalism. Interestingly, for the matter content (i.e. terms proportional to the number of flavours n_f), our result agrees with [4], even at the sub-leading colour level.

There are several lines of investigation that are interesting to pursue. First, one should repeat this analysis for the $qq \to qq$ [12] and $qg \to qg$ [11] processes, and check the consistency of Regge factorisations across different channels. Also, it would be interesting to study the contribution of the Regge cuts to both the odd- and even-signature amplitudes. We leave this for future investigations.

References

[1] E. A. Kuraev, L. N. Lipatov and V. S. Fadin, *The Pomeranchuk Singularity in Nonabelian Gauge Theories*, *Sov. Phys. JETP* **45** (1977) 199–204.

[2] J. R. Forshaw and D. A. Ross, *Quantum chromodynamics and the pomeron*, vol. 9. Cambridge University Press, 1, 2011.

[3] V. S. Fadin and L. N. Lipatov, *BFKL pomeron in the next-to-leading approximation*, *Phys. Lett. B* **429** (1998) 127–134, [hep-ph/9802290].

[4] F. Caola, A. Chakraborty, G. Gambuti, A. von Manteuffel and L. Tancredi, *Three-loop gluon scattering in QCD and the gluon Regge trajectory*, 2112.11097.

[5] S. Caron-Huot, *When does the gluon reggeize?*, *JHEP* **05** (2015) 093, [1309.6521].

[6] S. Caron-Huot, E. Gardi and L. Vernazza, *Two-parton scattering in the high-energy limit*, *JHEP* **06** (2017) 016, [1701.05241].

[7] V. S. Fadin, *Particularities of the NNLLA BFKL*, *AIP Conf. Proc.* **1819** (2017) 060003, [1612.04481].

[8] V. S. Fadin and L. N. Lipatov, *Reggeon cuts in QCD amplitudes with negative signature*, *Eur. Phys. J. C* **78** (2018) 439, [1712.09805].

[9] Y. V. Kovchegov and E. Levin, *Quantum chromodynamics at high energy*, vol. 33. Cambridge University Press, 8, 2012. 10.1017/CBO9781139022187.

[10] G. 't Hooft and M. J. G. Veltman, *Regularization and Renormalization of Gauge Fields*, *Nucl. Phys. B* **44** (1972) 189–213.

[11] F. Caola, A. Chakraborty, G. Gambuti, A. von Manteuffel and L. Tancredi, *To appear*, 22XX.XXXXX.

[12] F. Caola, A. Chakraborty, G. Gambuti, A. von Manteuffel and L. Tancredi, *Three-loop helicity amplitudes for four-quark scattering in massless QCD*, *JHEP* **10** (2021) 206, [2108.00055].

[13] P. Cvitanovic, *Group theory: Birdtracks, Lie's and exceptional groups*. 2008.

[14] Y. L. Dokshitzer and G. Marchesini, *Soft gluons at large angles in hadron collisions*, *JHEP* **01** (2006) 007, [hep-ph/0509078].

[15] R. E. Cutkosky, *Singularities and discontinuities of Feynman amplitudes*, *J. Math. Phys.* **1** (1960) 429–433.

[16] M. E. Peskin and D. V. Schroeder, *An Introduction to quantum field theory*. Addison-Wesley, Reading, USA, 1995.

[17] R. D. Ball and S. Forte, *Asymptotic freedom at small x*, *AIP Conf. Proc.* **407** (1997) 937, [hep-ph/9706459].

Appendices

A Feynman rules

We write matrix elements obtained from the Feynman rules as $i\mathcal{A}$, such that $\mathcal{A}$ is part of the T matrix.

A.1 Feynman rules for the scalar field theory

- Gluon propagator:
$$\frac{i}{p^2 - m^2 + i\epsilon}$$
- Quark propagator:
$$\frac{i}{p^2 + i\epsilon}$$
- $q\bar{q}g$ vertex:
$$-igm(T^a)_i^j(T^r)_l^m$$
- ggg-vertex:
$$-igmf_{abc}f_{rst}$$

A.2 Feynman rules for QCD

- Gluon propagator (set $\xi = 1$ for Feynman gauge):
$$-i\frac{g^{\mu\nu} - (1-\xi)\frac{p^\mu p^\nu}{p^2}}{p^2 + i\epsilon}\delta^{ab}$$
- Fermion propagator:
$$i\frac{\not{p} + m}{p^2 - m^2 + i\epsilon}\delta_{ij}$$
- ggg vertex:
$$gf^{abc}\left[g^{\mu\nu}(k-p)^\rho + g^{\nu\rho}(p-q)^\mu + g^{\rho\mu}(q-k)^\nu\right]$$
- $g\psi\bar{\psi}$ vertex:
$$ig\gamma^\mu T^a_{ji}$$
- $gc\bar{c}$ vertex:
$$-gf^{abc}p^\mu$$
- Ghost propagator:
$$\frac{i\delta^{ab}}{p^2 + i\epsilon}$$

B Colour conventions

T^a are the generators of the fundamental representation of SU(N), and f^{abc} are the structure constants satisfying the commutation relation

$$[T^a, T^b] = if^{abc}T^c.$$

The structure constants satisfy the *Jacobi identity*:

$$f^{abe}f^{bcd} + f^{bde}f^{cad} + f^{cde}f^{abd} = 0. \tag{B.1}$$

Let T_R and C_R denote the index and quadratic Casimir of a representation R of SU(N). In the fundamental representation, we normalise the generators such that

$$\begin{aligned}\mathrm{Tr}(T^aT^b) &= T_F\delta^{ab} = \frac{\delta^{ab}}{2},\\ (T^aT^a)_{ij} &= C_F\delta_{ij} = \frac{N^2-1}{2N}\delta_{ij}.\end{aligned}$$

The generators of the adjoint representation of SU(N) are given by:

$$(T^a_{\mathrm{adj}})_{bc} = -if^{abc},$$

with the Casimirs being

$$\begin{aligned}\mathrm{Tr}(T^a_{\mathrm{adj}}T^b_{\mathrm{adj}}) &= T_A\delta^{ab} = N\delta^{ab},\\ (T^a_{\mathrm{adj}}T^a_{\mathrm{adj}})_{bc} &= C_A\delta_{bc} = N\delta_{bc}.\end{aligned}$$

C Optical theorem

We start with the unitarity of the S-matrix:

$$S^\dagger S = \mathbf{1}, \tag{C.1}$$

which implies the following for the T-matrix, the non-trivial part of the S-matrix ($S = \mathbf{1} + iT$):

$$T^\dagger T = -i(T - T^\dagger). \tag{C.2}$$

Next, consider the scattering of an initial state $|p_1, p_2\rangle$ to a final state $|p_3, p_4\rangle$:

$$\langle p_3, p_4| \, T^\dagger T \, |p_1, p_2\rangle = -i \left(\langle p_3, p_4| \, T \, |p_1,\, p_2\rangle - \langle p_3, p_4| \, T^\dagger \, |p_1,\, p_2\rangle \right). \tag{C.3}$$

Inserting a complete set of final states on the left-hand side:

$$\mathbf{1} = \sum_n \left(\prod_{i=1}^n \int \frac{d^3k_i}{(2\pi)^4} \frac{1}{2E_i} \right) |\{k_i\}\rangle \, \langle \{k_i\}| \,, \tag{C.4}$$

and defining the scattering amplitude $\mathcal{A}$ as:

$$\langle p_3, p_4| \, T \, |p_1, p_2\rangle \equiv (2\pi)^4 \delta^{(4)}\big(p_1 + p_2 - (p_3 + p_4)\big) \mathcal{A}\left(p_1, p_2 \to p_3, p_4\right), \tag{C.5}$$

we obtain the optical theorem:

$$\mathrm{Im}\big(\mathcal{A}(p_1, p_2 \to p_3, p_4)\big) = \frac{1}{2} \sum_f \int d\Pi_f \mathcal{A}^*(p_3, p_4 \to \{k_i\}) \mathcal{A}(p_1, p_2 \to \{k_i\}). \tag{C.6}$$

The integral over intermediate states is given by:

$$\sum_f \int d\Pi_f = \sum_n \left(\prod_{i=1}^n \int \frac{d^3\mathbf{k}_i}{(2\pi)^4} \frac{1}{2E_i} \right) (2\pi)^4 \delta^{(4)}\big(p_1 + p_2 - \sum_i k_i\big). \tag{C.7}$$

The optical theorem can be applied to individual orders in perturbation theory. In fact, it can be applied to the level of individual Feynman diagrams. A systematic way of doing this is given by a set of Cutkosky *cutting rules*. We will simply state them here, but for more details see e.g. [15] or [16]. The imaginary part of any Feynman diagram can be extracted as follows:

1. Cut through the diagram in all possible ways such that the cut propagators can simultaneously be put on shell.

2. Replace each cut propagator with an on-shell condition $2\pi\delta(p^2 - m^2)$, then perform the integral over the phase space of intermediate states.

3. Sum the contributions of all possible cuts.

D Mellin transform

It is useful to introduce a technique that can be used to unravel the nested integrals over the Sudakov variables ρ_i in section 2.5. This is an integral transform known as the *Mellin transform*, and it is closely related to the Laplace transform.

D.1 Definition from Laplace transform

Consider the one-sided Laplace transform $\mathcal{L}$ of a function f:

$$\mathcal{L}\{f\}(\omega) := \int_0^\infty dt\, f(t) e^{-\omega t}. \tag{D.1}$$

Changing variables $x = e^t$, we get:

$$\mathcal{L}\{f\}(\omega) = \int_1^\infty dx\, x^{-\omega-1} f(\ln x). \tag{D.2}$$

We can then define the Mellin transform $\mathcal{M}$ of a function $f(x)$ as:

$$\mathcal{F}(\omega) \equiv \mathcal{M}\{f\}(\omega) := \int_1^\infty dx\, x^{-\omega-1} f(x). \tag{D.3}$$

Evidently, it is related to the Laplace transform via $\mathcal{M}\{f(\ln x)\}(\omega) = \mathcal{L}\{f(x)\}(\omega)$.

In our case, we will be taking the Laplace transform of a function $f(s)$. To keep a dimensionless integration variable, we normalise s by the square of a typical transverse momentum $\mathbf{k}_\perp^2$. We obtain:

$$\mathcal{F}(\omega) = \int_1^\infty d\left(\frac{s}{\mathbf{k}_\perp^2}\right)\left(\frac{s}{\mathbf{k}_\perp^2}\right)^{-\omega-1} f(s). \tag{D.4}$$

The inverse transform is given by:

$$f(s) = \frac{1}{2\pi i}\int_{\mathcal{C}} d\omega \left(\frac{s}{\mathbf{k}_\perp^2}\right)^{\omega} \mathcal{F}(\omega), \tag{D.5}$$

where $\mathcal{C}$ is a contour to the right of all the singularities of $\mathcal{F}(\omega)$ on the ω-plane.

D.2 Properties

A useful example for our purposes is the Mellin transform of a function $f(s)$ that is of the form:

$$f(s) = (\ln s)^r s^\alpha, \tag{D.6}$$

then its Mellin transform is given by

$$\mathcal{F}(\omega) = (\mathbf{k}_\perp^2)^\alpha \frac{\Gamma(r+1)}{(\omega-\alpha)^{r+1}}. \tag{D.7}$$

We observe that if our function is a pure power law $f(s) \propto s^\alpha$, then we get a simple pole at $\omega = \alpha$. For non-integer r, the Mellin transform has a cut singularity. In general, to deduce behaviour in the Regge limit, we are interested in the nature and position of the ω-plane singularities.

A very important property of the Mellin transform, and the reason we introduce it in the first place, is its ability to unravel nested integrals. Let $f(s)$ be given by a convolution of n-functions $f_i(s/\mathbf{k}_\perp^2)$, such that

$$f(s) = \mathbf{k}_\perp^2 \prod_{i=1}^{n} \int_{\rho_{i+1}}^{1} \frac{d\rho_i}{\rho_i} f_i\left(\frac{\rho_{i-1}}{\rho_i}\right) \delta(\rho_n s - \mathbf{k}_\perp^2), \tag{D.8}$$

(where $\rho_0 = 1$ and $\rho_{n+1} = 0$). Then the Mellin transform is

$$\mathcal{F}(\omega) = \prod_{i=1}^{n} \int_{\rho_{i+1}}^{1} \frac{d\rho_i}{\rho_i} f_i\left(\frac{\rho_{i-1}}{\rho_i}\right) \rho_n^\omega. \tag{D.9}$$

Following section 2.5, we find it convenient to perform the change of variables from ρ_i to τ_i

$$\tau_i = \frac{\rho_i}{\rho_{i-1}}, \tag{D.10}$$

such that $\rho_n = \tau_1\tau_2\ldots\tau_n$. The Jacobian of this transformation is $\rho_1\rho_2\ldots\rho_{n-1}$. Equation (D.9) can then be written as

$$\mathcal{F}(\omega) = \prod_{i=1}^{n} \int_0^1 d\tau_i \tau_i^{\omega-1} f_i\left(\frac{1}{\tau_i}\right) = \prod_{i=1}^{n} \mathcal{F}_i(\omega). \tag{D.11}$$

We see that convolutions translate to multiplication in Mellin space.

E Suppressed diagrams at LL order

E.1 The scalar field theory case

The goal of this section is to show that in the scalar field theory that was introduced in section 2, any diagram that is not an uncrossed ladder diagram is suppressed in the LL approximation.

Crossed ladder diagrams

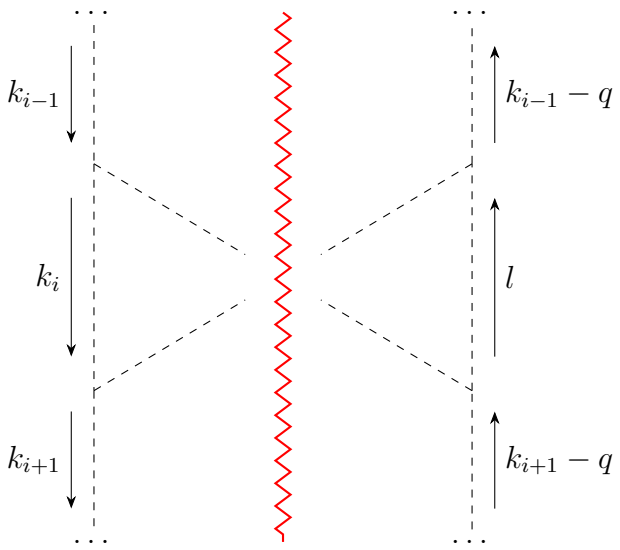

Figure 22: Crossed section of a ladder diagram.

The momentum labelled l to the right of the cut is given by:

$$l = k_{i-1} + k_{i+1} - k_i - q. \tag{E.1}$$

In the strongly ordered limit, we have $\rho_{i-1} \gg \rho_i \gg \rho_{i+1}$ and $|\lambda_{i+1}| \gg |\lambda_i| \gg |\lambda_{i-1}|$. The denominator of the propagator is of the order:

$$l^2 \approx s\lambda_{i+1}\rho_{i-1}. \tag{E.2}$$

Since $s\lambda_{i+1} \sim \mathbf{k}_\perp^2 \rho_i$, we have

$$l^2 \sim \frac{\rho_{i-1}}{\rho_i}\mathbf{k}_\perp^2 \gg \mathbf{k}_\perp^2. \tag{E.3}$$

Thus this diagram is suppressed.

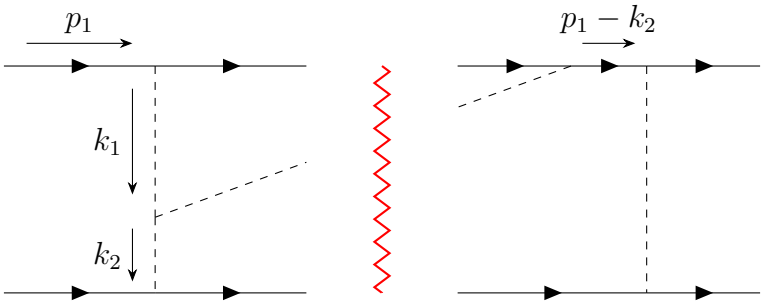

Figure 23: Cut vertex correction graph.

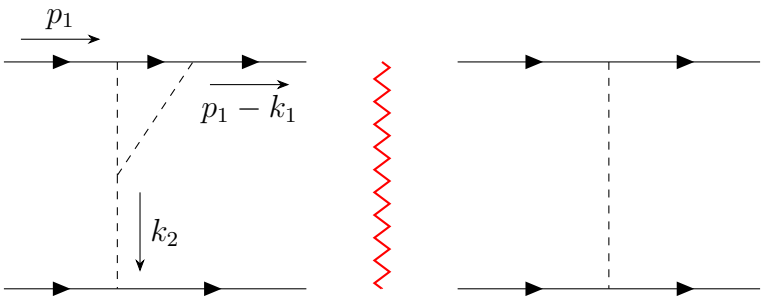

Figure 24: Vertex correction graph.

Vertex correction diagrams

Consider a vertex correction diagram. For illustrative purposes, we look at the two-loop case. First, one where the cut also goes through the intermediate gluon, and one where the cut passes through two quark lines.

For diagram 23, we have a fermion propagator on the right side of the cut that contributes a denominator $(p_1 - k_2)^2 \sim |\lambda_2| s \gg \mathbf{k}_\perp^2$. This is in contrast to the uncrossed ladder diagram where all denominators are of order $\sim \mathbf{k}_\perp^2$. Next, consider diagram 24. The reasoning is identical to the one described for diagram 5a. The Lorentz invariants constructed from the momenta flowing into the vertex cannot generate any s-dependence, and such the integral over loop momenta cannot generate a large logarithm.

Self-energy corrections

Self-energy insertions are suppressed for identical reasons described for diagram 5b. Lorentz invariants constructed momenta flowing into the self-energy insertion, whether this be on the quark line or an intermediate gluon, cannot generate a large logarithm, as they are independent of s.

Three (or more) gluon exchange diagrams

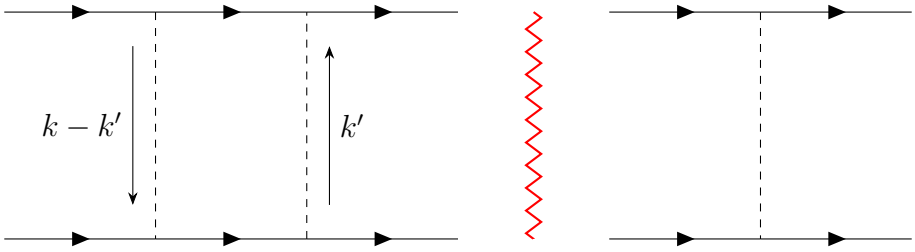

Figure 25: Three gluon exchange graphs.

Consider a triple gluon exchange diagram in the t-channel, such as the one in figure 25. When the denominators of the virtual gluons are small $\sim \mathbf{k}_\perp^2$, this heavily restricts the phase space of intermediate states. This results in the amplitude being suppressed by a power of m^2/s compared to two-gluon exchange graphs. The suppression is even greater if we consider four-gluon exchange graphs, and so forth.

E.2 The QCD case

In this section we show, using the gauge technique used in section 3.4.1, that the diagrams that are not of the form of uncrossed ladders are suppressed, i.e. contribute only sub-leading logarithmic terms. This amounts to suppressions by at least one factor of ρ_i/ρ_{i-1} with respect to the uncrossed ladder diagram. To begin with, we consider an uncrossed ladder section shown in figure 26. The contribution of an

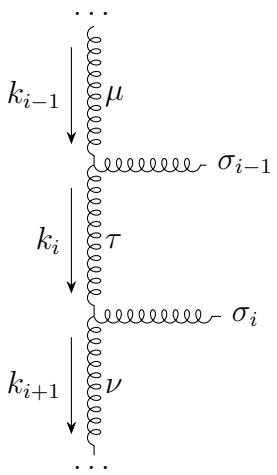

Figure 26: Uncrossed ladder section.

uncrossed ladder section is proportional to two effective vertices:

$$\Gamma_{\mu\tau}^{\sigma_{i-1}}\Gamma_{\nu}^{\tau\sigma_i}. \tag{E.4}$$

Performing the contraction over τ, the dominant contribution proportional to $p_1^{\sigma_{i-1}} p_2^{\sigma_i}$ is

$$\sim \frac{2p_{2\mu}p_{1\nu}}{s}\rho_{i-1}\lambda_{i+1}p_1^{\sigma_{i-1}}p_2^{\sigma_i}, \tag{E.5}$$

and the dominant contribution proportional to $k_{i-1\perp}^{\sigma_{i-1}} k_{i+1\perp}^{\sigma_i}$ is

$$\sim \frac{2p_{2\mu}p_{1\nu}}{s}k_{i-1\perp}^{\sigma_{i-1}}k_{i+1\perp}^{\sigma_i}. \tag{E.6}$$

We want to show suppression of other diagrams with respect to these contributions.

Crossed ladder diagrams

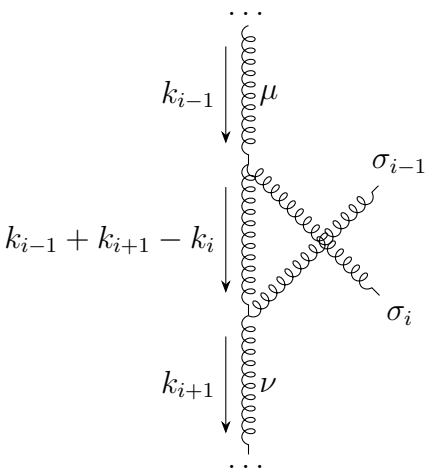

Figure 27: Crossed ladder section.

Consider a section of a crossed ladder diagram, shown in figure 27. We first need to adjust equation (3.78) for when we have a momentum k_i^μ entering the vertex from the top, and k_j^μ from the bottom. We obtain

$$\begin{aligned}
&\frac{2k_{i\perp}^\mu k_{j\perp}^\nu}{\rho_i\lambda_j s}\Big[-g_{\mu\nu}(k_i+k_j)^\sigma + g_\mu^\sigma(2k_i-k_j)_\nu + g_\nu^\sigma(2k_j-k_i)_\mu\Big] \\
&\sim \frac{2}{\rho_i\lambda_j s}\mathbf{k}_\perp^2\left[\rho_i p_1^\sigma + \lambda_j p_2^\sigma + (k_i+k_j)_\perp^\sigma\right] \\
&\sim 2\frac{\rho_{j-1}s}{\rho_i}\left[\rho_i p_1^\sigma + \lambda_j p_2^\sigma + (k_i+k_j)_\perp^\sigma\right],
\end{aligned} \tag{E.7}$$

where in the last step we used the fact that $\rho_{j-1}\lambda_j \sim \mathbf{k}_\perp^2/s$ from the on-shell condition of the jth outgoing gluon.

Now, inspecting the section of the crossed ladder, the middle vertical line has momentum $k_{i-1} + k_{i+1} - k_i$, so the propagator has a denominator of $\sim \rho_{i-1}\lambda_{i+1}s$.

Together, the part of the contribution from the two vertices that is proportional to $p_1^{\sigma_{i-1}} p_2^{\sigma_i}$ is of the order

$$\sim \left(\frac{\rho_i}{\rho_{i-1}}\right)^2 \frac{2p_2^\mu p_1^\nu}{s} \rho_{i-1}\lambda_{i+1} p_1^{\sigma_{i-1}} p_2^{\sigma_i}. \tag{E.8}$$

The ρ_i factors come from the fact that $\lambda_j \approx \lambda_{i+1}$, which is true due to the strong ordering. From the on-shell conditions we can also replace ρ_{j-1} by ρ_i.

Since $\rho_i \ll \rho_{i-1}$, the diagram is suppressed. Further, the propagator from the middle vertical gluon of the crossed ladder diagram contributes a denominator that is much greater than the $\mathbf{k}_{i\perp}^2$ denominator from the uncrossed ladder. As such, there is double suppression, and even greater suppression if more rungs are crossed.

Diagrams with a triple gluon vertex on the horizontal rung

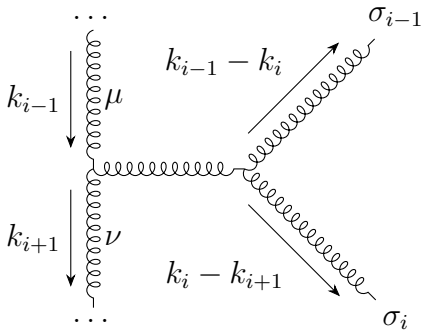

Figure 28: Ladder section with triple gluon vertex on horizontal rung.

Consider now diagram 28, a section of a graph where the horizontal rung splits up into two gluons. Firstly, contracting the triple gluon vertex on the left side with $k_{i-1\perp}^\mu k_{i+1\perp}^\nu$, we obtain a term

$$\sim \frac{2p_1^\mu p_2^\nu}{s} \mathbf{k}_\perp^2 \rho_{i-1}\lambda_{i+1} s k_{i-1\perp}^{\sigma_{i-1}} k_{i\perp}^{\sigma_i}. \tag{E.9}$$

Then, using $\mathbf{k}_\perp^2 \sim s\rho_i\lambda_{i+1}$, we get

$$\sim \frac{2p_1^\mu p_2^\nu}{s} \frac{\rho_i}{\rho_{i-1}} k_{i-1\perp}^{\sigma_{i-1}} k_{i\perp}^{\sigma_i}. \tag{E.10}$$

This is suppressed with respect to the uncrossed ladder by a factor of ρ_i/ρ_{i-1}. Secondly, the horizontal gluon propagator has a momentum that is much larger than $\mathbf{k}_\perp^2$. We thus get double suppression with respect to the uncrossed ladder.[6]

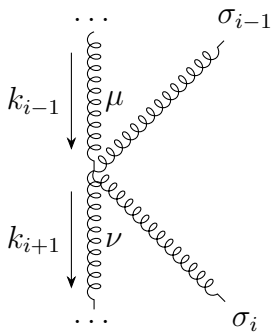

Figure 29: Ladder section with four-point gluon vertex.

Diagrams with a four-point gluon vertex

Next, we have diagram 29, a section of a ladder with a four-point gluon vertex. The four-point gluon vertex carries no momentum dependence. As a result, the diagram contributes a term proportional to:

$$\frac{1}{\rho_{i-1}\lambda_{i+1}s}k_{i-1\perp}^{\sigma_{i-1}}k_{i\perp}^{\sigma_i}. \tag{E.11}$$

The lack of an ith vertical gluon contributing a $\mathbf{k}_{i\perp}^2$ to the denominator of the propagator means that we have suppression with respect to the uncrossed ladder by a factor $\sim \rho_i/\rho_{i-1}$. Looking at other terms, e.g. those proportional to $p_1^{\sigma_{i-1}}p_2^{\sigma_i}$, we find similar suppression factors.

Fermion loops

Technically, when we consider two quarks scattering to two quarks and n gluons at tree level, we should also consider the case where there are fermion-antifermion pairs in the final state. Figure 30 shows three possible sections of the ladder where a fermion-antifermion pair is produced. Very crudely, the fermion exchanged in the t-channel contributes a lower s dependence compared to the gluon, by virtue of it being spin-1/2.

Consider diagram 30a. Using the propagator prescription from our gauge technique, we find that this diagram contributes a term

$$\sim \frac{1}{\rho_{i-1}\lambda_{i+1}s}\bar{u}(k_{i-1}-k_i)\gamma\cdot k_{i-1\perp}\gamma\cdot k_i\gamma\cdot k_{i+1\perp}u(k_{i+1}-k_i), \tag{E.12}$$

which is of the order

$$\frac{\mathbf{k}_\perp^2}{\rho_{i-1}\lambda_{i+1}s}\left(k_i\cdot k_{i-1}, k_i\cdot k_{i+t}, k_i^2\right). \tag{E.13}$$

The term on the left of the brackets is of the order ρ_i/ρ_{i-1}, whereas the scalar products inside the brackets are of the order $\sim \mathbf{k}_\perp^2$. Thus we have a suppression

[6] This is not true in axial gauges, see e.g. [17]

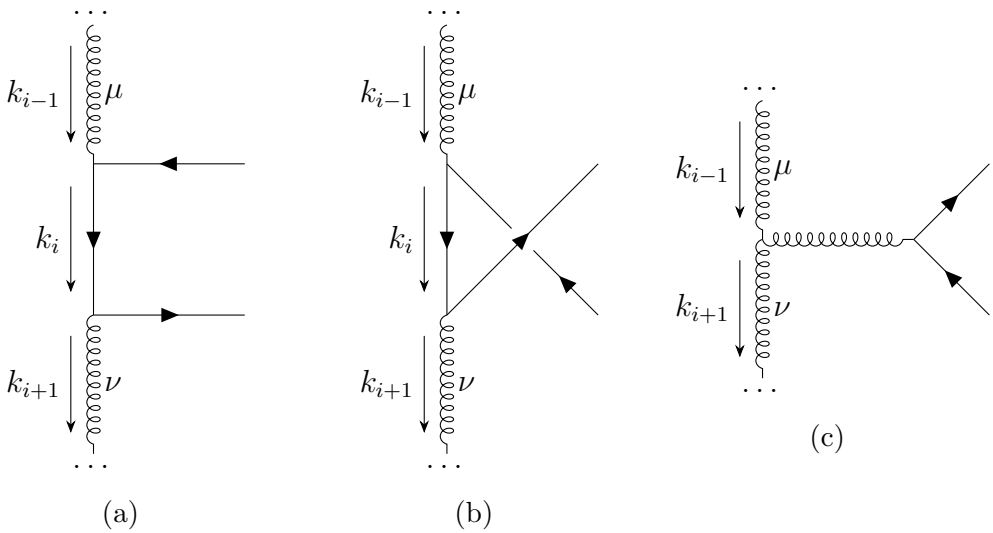

Figure 30: Fermion loops in ladder section.

ρ_i/ρ_{i-1} compared to the uncrossed gluon ladder. Examining 30a and 30c yields similar suppression factors due to the hard fermion- or gluon-propagator. We can thus neglect fermion loops, correct to LL order.

Vertex corrections and self-energy insertions

The argument is identical to that of the scalar field theory case. However, note that this is true for the Feynman gauge. In Coulomb or axial gauges, where external vectors are introduced, we could get terms proportional to s. Consider e.g. vertex corrections to the upper quark line, which has momentum p_1. The external vector (which can have a component proportional to p_2) could then generate an s through a scalar product.

F Harmonic polylogarithms

The multi-loop results in [4, 11, 12] are expressed in terms of *harmonic polylogarithms* (HPLs), and to be able to manipulate them it is useful to recount their definitions and some of their properties. Our goal is to be able to project the amplitudes onto even and odd signature, and to expand them for small x. For the former we need to know how they behave under the mapping $x \to \frac{x}{x-1}$. However, this is not necessary to do if we exploit their properties discussed in section 4 – i.e. expanding in terms of L, we can take the real and imaginary part of the full amplitude to obtain the odd and even signature amplitudes, respectively.

For our purposes, the HPL is recursively defined as follows

$$G_{a\mathbf{b}} = \int_0^x \frac{dx'}{x'-a} G_{\mathbf{b}}(x'), \tag{F.1}$$

where $a \in \{0,1\}$ and $\mathbf{b}$ is a string of 0's and 1's. The number of indices carried by G is known as the *weight* of the HPL, denoted by ω. The $\omega = 1$ polylogarithms are defined as

$$\begin{aligned} G_0(x) &= \ln(x), \\ G_1(x) &= \ln(1-x). \end{aligned} \tag{F.2}$$

which starts the recursion. Also,

$$G_{\mathbf{0}_\omega} \equiv \frac{1}{\omega!} \ln^\omega x, \tag{F.3}$$

where $\mathbf{a}_\omega$ is a string of ω a's. Through repeated integration we can then see that

$$G_{\mathbf{1}_\omega} = \frac{1}{\omega!} \ln^\omega(1-x). \tag{F.4}$$

Next, we want to formulate expansions of the HPLs for small x. This can be done by expanding the integrand in the definition (F.1) as a power series in x, and integrating term by term. For weight $\omega = 1$, this is straightforward.

$$\begin{aligned} &G_0(x) \approx \ln(x), \\ &G_1(x) = \int_0^x \frac{dx}{x-1} \approx -x - \frac{x^2}{2} - \frac{x^3}{3} - \frac{x^4}{4} - \frac{x^5}{5} - \frac{x^6}{6} + \mathcal{O}\left(x^7\right). \end{aligned} \tag{F.5}$$

We will show how to get the expansions up to weight $\omega = 2$. In the case of $G_{01}(x)$, we have:

$$\begin{aligned} G_{01}(x) &= \int_0^x \frac{dx'}{x'-a} \ln(1-x) \\ &= \int_0^x dx' \left[-1 - \frac{x}{2} - \frac{x^2}{3} - \frac{x^3}{4} - \frac{x^4}{5} - \frac{x^5}{6} - \frac{x^6}{7} + \mathcal{O}\left(x^7\right)\right] \\ &= -x - \frac{x^2}{4} - \frac{x^3}{9} - \frac{x^4}{16} - \frac{x^5}{25} - \frac{x^6}{36} + \mathcal{O}\left(x^7\right). \end{aligned} \tag{F.6}$$

Then, for $G_{10}(x)$ we can do the same, or use a *shuffle identity* to write it in terms of HPLs for which we already know the expansions[7]:

$$G_{10}(x) = G_1(x)G_0(x) - G_{01}(x). \tag{F.7}$$

We thus obtain

$$\begin{aligned} G_{10}(x) = {} & x + \frac{x^2}{4} + \frac{x^3}{9} + \frac{x^4}{16} + \frac{x^5}{25} + \frac{x^6}{36} + \mathcal{O}(x^7) \\ & + \left(-x - \frac{x^2}{2} - \frac{x^3}{3} - \frac{x^4}{4} - \frac{x^5}{5} - \frac{x^6}{6} + \mathcal{O}(x^7)\right) \ln(x) \end{aligned} \tag{F.8}$$

A combination of term by term integration and appropriate shuffle identities allows us to iteratively generate the small x expansions for higher weights as well.

[7] It is straightforward to prove this relation from the definition (F.1).